Characterizing and dissociating sensory attenuation in State estimation and Gating.

Dissertation

zur Erlangung des Grades eines
Doktors der Naturwissenschaften

der Mathematisch-Naturwissenschaftlichen Fakultät
und
der Medizinischen Fakultät
der Eberhard-Karls-Universität Tübingen

vorgelegt
von

Kalpana Gupta
aus Roorkee, India

October 2023

Tag der mündlichen Prüfung: 24.04.2024

Dekan der Math.-Nat. Fakultät: Prof. Dr. Thilo Stehle
Dekan der Medizinischen Fakultät: Prof. Dr. Bernd Pichler

1. Berichterstatter: Prof. Dr. Cornelius Schwarz

2. Berichterstatter: Prof. Dr. Jan Benda

Prüfungskommission: Prof. Dr. Cornelius Schwarz

Prof. Dr. Jan Benda

Prof. Dr. Ziad Hafed

Prof. Dr. Andrea Burgalossi

Erklärung / Declaration:

Ich erkläre, dass ich die zur Promotion eingereichte Arbeit mit dem Titel:

"Characterizing and dissociating sensory attenuation in State estimation and Gating",

selbständig verfasst, nur die angegebenen Quellen und Hilfsmittel benutzt und wörtlich oder inhaltlich übernommene Stellen als solche gekennzeichnet habe. Ich versichere an Eides statt, dass diese Angaben wahr sind und dass ich nichts verschwiegen habe. Mir ist bekannt, dass die falsche Abgabe einer Versicherung an Eides statt mit Freiheitsstrafe bis zu drei Jahren oder mit Geldstrafe bestraft wird.

I hereby declare that I have produced the work entitled:

"Characterizing and dissociating sensory attenuation in State estimation and Gating",

submitted for the award of a doctorate, on my own (without external help), have used only the sources and aids indicated and have marked passages included from other works, whether verbatim or in content, as such. I swear upon oath that these statements are true and that I have not concealed anything. I am aware that making a false declaration under oath is punishable by a term of imprisonment of up to three years or by a fine.

Iowa City, den .....5 July 2024. .....

Datum / Date Unterschrift /Signature

Contents

1. Summary

The state estimation (SE) theory is the modern instantiation of a classic sensorimotor theory called the reafferent principle (Von Holst and Mittelstaedt, 1950). It estimates the body's or its limbs' kinematic state based on optimal integration of the internal model's predictive signals (based on an efference copy and other contextual signals) and external sensory signals. It generates the so-called sensory prediction error that can be used to estimate the state, optimize movement and perception, as well as to train the internal model. State estimation gives rise to the sensory prediction that is employed to cancel the reafference inputs or the sensory consequences of self-motion to enhance the information from more relevant stimuli. Sensory gating (SG), a process that modifies the sensory signal as well, attenuates external sensory responses that occur during the movements (Hentschke et al. (2006), (Seki et al., 2003, Chapman et al., 1987b, Chapman et al., 1988, Rushton et al., 1981, Ghez and Pisa, 1972, Chapman et al., 1987a). It is currently not known whether attenuation caused by SE and SG is the expression of the same or different functional (behavioral) systems, and whether it is based on the same or different neuronal circuits. In fact, many studies studying SG discussed their results in the framework of SE. Others that meant to study SE show phenomena better assigned to SG.

Here, I established an experimental paradigm in mice with the aim to separate the two processes. To this end I used and extended the open loop approach first pioneered by Curtis Bell (1982) in weakly electric fish. This method records the neuronal motor command while blocking its motor outcome. Introduction of an artificial sensory consequence after the onset of a motor command then allows to probe the neuronal prediction signal by omitting the sensory consequence. My first extension was to realize the open loop approach in a mammal - in the tactile whisker-related system of head-fixed mice, trained to generate a whisker reaching movement. This was required, as SG has been described so far only in mammals. The second extension was to add rare test stimuli that deliberately varied the delay of a sensory consequence after learning the sensory consequence at a fixed delay. It turned out that SG is active throughout the movement

while SE is active only at the time point of the predicted sensory consequence, a major difference between the processes, and the reason for my success to separate them.
The experimental setup included the chronic implantation of a micro-electrode in the facial nucleus to extracellularly measure the whisker motor command, and multi-electrode devices in the somatosensory cortex to record the tactile sensory signals. The reafferent loop was opened by surgically disrupting two branches of the distal facial motor nerve, which innervate the intrinsic whisker muscles, and thus, paralyzing whisker movements. Artificial sensory consequences of an intended reach were realized by deflecting the immobilized whisker using a Piezo actuator. In a different, closed-loop approach, I left the movement intact and electrically stimulated the trigeminal nucleus to mimic the sensory consequence of the intended whisker movement. The artificial sensory consequence was presented at the trained (predicted) delay. In rare test trials it was shifted to other times during the movement, to times between intended movements, or was omitted. The tactile responses were recorded in the primary somatosensory cortex (S1) and consistently were found to be strongest in between movements, significantly attenuated at a medium level with shifted stimuli, and attenuated significantly stronger at predicted delays (12 mice studied in open loop and 3 mice studied in closed loop). Somatosensory attenuation due to SE turned out to be adaptable to a new delay within a few hundred trials and acting at a temporal precision of tens of milliseconds. It could be trained at delays up to 200-300ms from motor command onset. In contrast, SG was observed independently of learning the sensory consequence. It was present at all times up to 500ms after the motor command onset. Using a linear array of 16 electrodes distributed across the six neocortical layers, I could show that the neuronal reflections of SE and SG are distributed across all layers of S1.

The significance of my work is that for the first time two neuronal functional systems could be disentangled that act as movement-dependent attenuators of sensory signal flow. SE is highly likely predictive of detailed sensory consequences of movement. One speculation close at hand is that it may be dependent on cerebellar function. Whether SG-mediated attenuation is of predictive nature needs to be studied in the future. In view

of its known dependence on neocortical circuits (Chakrabarti and Schwarz, 2018), it may well be related to higher functions like attentional processes or reward predictions.

2. Introduction

Sensory and motor functions are crucial aspects of brain function that allow us to perceive and interact with the world around us. These functions involve the processing of sensory information and the generation of appropriate motor responses. The sensory function involves the reception and interpretation of sensory stimuli from the external environment and the body's internal state. Motor function refers to the ability of the brain to generate and control voluntary and involuntary movements. It involves the coordination of muscles, and other structures to execute precise movements. The brain plays a central role in coordinating and integrating sensory input and motor output through complex neural networks by a fundamental process known as sensorimotor integration. This integration allows us to effectively sense the ever-changing surrounding world and adapt our actions accordingly. Some key aspects of sensorimotor integration include perception, sensory processing, motor planning, motor execution, and feedback mechanism. Understanding the intricate mechanisms of sensory and motor functions in the brain is essential for advancing our knowledge of neurological disorders, developing effective therapies, and enhancing our overall understanding of human cognition and behavior.

Our sensory systems detect the changes in our body and the environment whenever we move, speak, or act. Normally, we recognize these sensations as the outcome of our actions and differentiate them from similar sensations generated externally. Our ability to perceive our actions as distinct from other people is crucial to our functioning as social beings. Imagine being in a state in which your brain is unable to distinguish the sensory signals generated by your body from those coming from external events, objects, and actions. This peculiar circumstance would cause the world to seem to shift constantly whenever you shift your gaze or move your eyes; you would perpetually question if someone is speaking with you whenever you speak. Furthermore, every time you touch

your own body, you would endure a sensation of tickling. To prevent such a scenario, the brain uses a strategy to suppress the perception of self-generated information and enhance the differentiation between it and externally generated information. To achieve that, the brain predicts the sensory consequences of self-generated actions and dissociate them from the ones externally generated.

We possess the remarkable capacity to control our movements across a wide range of activities, whether it be executing basic limb motions or engaging in complex tasks like dribbling a basketball, throwing a baseball, or juggling. We often admire the remarkable skills of athletes, yet even the ability to perform simple eye and arm movements accurately is truly extraordinary when viewed from a theoretical standpoint. Our proficiency in producing a lifetime of precise movements does not stem from having a fixed set of actuators, flawless sensors, or rapid transmission lines from birth. Instead, it arises from the fact that we are equipped with an adaptable nervous system that continually compensates for these inherent limitations. Without such compensation, these inherent constraints could result in consistent errors in our movements.

There are several motor control theories, each providing a unique perspective on how the nervous system coordinates and controls the complex movements of the human body (Cano-de-la-Cuerda et al., 2015). These theories explain how the brain deals with this complex integration of sensorimotor information to generate predictions related to sensory consequences that lead via appropriate state estimation, to stable perception and motor adaptation. These theories continue to evolve and refine our understanding of the complex mechanisms underlying perception and motor control.

2.1. The Reafference principle.

In a typical sensorimotor integration pathway, sensory information from the environment flows through the sensor to the higher sensory centers, and in response, the higher motor centers send a motor command to the effector to perform an action. The motor act in itself also elicits sensory inputs from its own receptors. These self-induced sensory inputs were

termed **reafference signals** (Von Holst and Mittelstaedt, 1950). Reafferent input is informative about the enacted movement and can be used in modifying the motor act itself. However, in many circumstances, the reafference input (sensory consequence) generated from one's own actions can also interfere with the sensing of external stimuli, triggering inappropriate responses. The two groups (Sperry, 1950, Von Holst and Mittelstaedt, 1950) were concerned with the problem caused by reference signals and performed behavioral experiments inferring that the brain solves the problem of unwanted reafference by generating a signal from motor command centers that nullifies the unwanted effect of the reafference. These signals were termed **efference copy** by Von Holst and Mittelstaedt and corollary discharge by Sperry. Both studies suggested that the efference copy could help to strip the reafference from the afference, the incoming sensory signal, and generate the exafference, containing only sensory signals about movements of the world, a process called **reafference principle**.

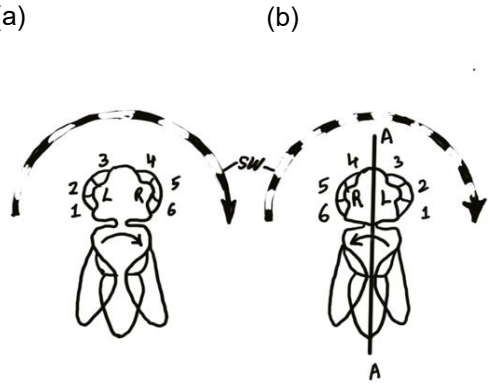

Figure 1. Von Holst's example.
The behavior of the insect Eristalis, when a striped cylinder SW is rotated past the eyes from left to right.
a) Normal insect, b) following rotation of the head by 180 degrees, about the axis A-A. R=right eye, L=left eye. Ommatidium is numbered. The arrow on the thorax indicates the direction of active turning.

The reafference principle has been supported by electrophysiological studies in model systems since the 1950s. Examples of these studies include experiments conducted on the auditory system of the cricket (Heiligenberg, 1969) and the mechanosensory system of the crayfish (Wiersma, 1947), which have shown that removing reafferent sensory stimulation is necessary for correctly interpreting and emphasizing external stimuli.

In their original experiment (Fig.1), Von Holst and Mittelstaedt presented a scenario where a fly tries to maintain its visual field as a moving object passes by (Von Holst and Mittelstaedt, 1950). It was originally thought they achieve this by inhibiting the optokinetic reflex during voluntary movement. However, experiments showed that the reflex inhibition hypothesis is wrong and that movement across the retina influences locomotion, even

during voluntary movement. In fact, changing the position of the eyes by turning the head by 180 degrees causes the insect to turn continuously in the same direction, and any attempt to move in the opposite direction only makes it worse, a spiraling loss of control. They suggested two potential explanations for how the CNS anticipates the type of retinal image motion: the CNS either stores information about the efference sent to the limbs and compares it with subsequent retinal changes, or it relies on reafference from the receptors of the moving limbs to calculate body motion and compare it with retinal reafference.

In addition, an apparent paradox was observed by them. It was previously believed that postural reflexes corrected any deviations from normal to maintain "normal postures." However, von Holst noticed that fish and other creatures could maintain abnormal postures, such as a fish positioning itself vertically or on its side. Moreover, when disturbances cause deviations from the abnormal posture, the muscles reflexively restore the abnormal posture instead of the normal one. This baffled everyone as to how a simple reflex could act in this manner. The reafference principle offered a solution to this problem by suggesting that the equilibrium is not adjusted according to an absolute norm, but relative to movement commands from higher centers.

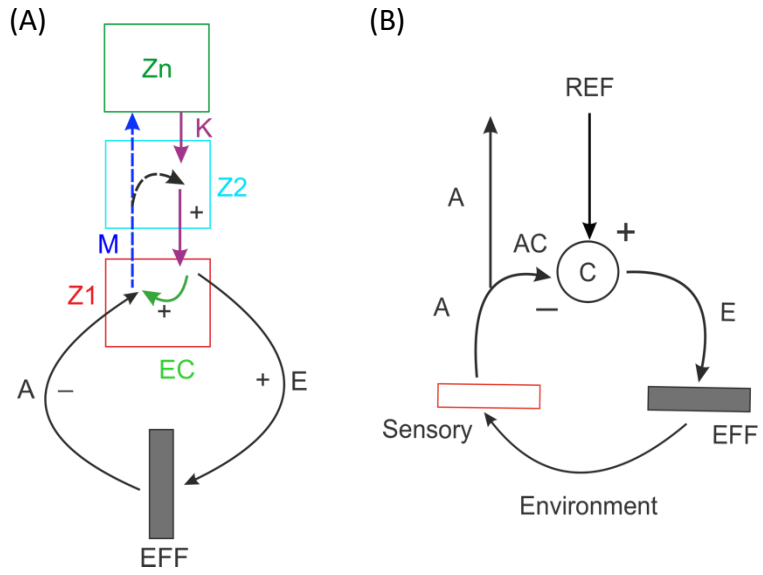

Figure 2. The reafference principle.
Zn=higher processing center; Z1, Z2= processing center; M= residual signal; K=motor command; A=afferent signal; E=efferent signal/error signal; EC=efference copy; EFF=effector; AC=afference copy; C=Comparator; REF=Reference signal.
(A) Schematic of reafference principle. adapted from (Von Holst and Mittelstaedt, 1950).
(B) Perceptual control theory, adapted from (Powers, 2022).

Despite their lack of familiarity with negative feedback control systems, von Holst and

Mittelstaedt endeavored to create a model that would explain their presence in the nervous system. This process brought him close to developing control theory, which in turn laid the groundwork for his concepts of efference copies, reafference, exafference, and a residual signal that was sent to higher systems after the subtraction of a reafference signal from an efference copy. Fig 2A depicts his model for the reafference principle, in which a command signal 'K' runs down a hierarchy of processing centers. In the lowest center Z1 it splits into two. The longer branch 'E' carries an efference signal to the effector 'EFF' which is moving, but also sensing, and could be a muscle, limb, whole body or a sensory organ. The shorter branch, the "efference copy," 'EC,' interacts inside Z1 with the afference 'A' caused by the effector in motion. The efference copy is then thought to strip the reafference from the afference, resulting in the exafference or residual signal 'M' which signals exclusively world movements to higher processing centers. In one of them (Z2) it may inform the descending motor command K about the remaining reafference and update/correct the descending motor command.

Von Holst and Mittelstaedt's diagram is close to a modern negative feedback system as is demonstrated by the perceptual control theory shown in Fig. 2B. The difference is that the efference signal is interpreted as an error signal originating from the comparison of an afference copy and a central reference signal (Powers, 2022). Spinal anatomy shows a nice reflection of the predicted split of the afference in the "bifurcation of the dorsal roots." The spinal cord motoneuron then compares the afference and a reference signal of a control system.

The reafference principle has also been explored through research on the weakly electric mormyrid fish, which has demonstrated that efference copy signals are sent directly to second-order principal cells to cancel out reafferent sensory information (Singla et al., 2017, Bell, 1982, Requarth and Sawtell, 2011). According to recent electrophysiological research, reafferent vestibular information is significantly repressed in both rodents and primates during the early stages of processing in the vestibular nuclei (Cullen, 2012), as well as subsequent stages in the vestibular cerebellum (Brooks and Cullen, 2013) and vestibular thalamus (Dale and Cullen, 2019). The principle of reafference has been used

to explain other perceptual studies, like why we cannot tickle ourselves (Claxton, 1975). There are modern formulations of this theory which are explained further.

2.2. State Estimation

A modern theory based on the reafference principle is called **state estimation** (Shadmehr and Mussa-Ivaldi, 2012). It explains how the brain uses a predictive model to compute a prediction about the sensory input that will ensue when taking a motor action in a certain context, based on past experiences and expectations. It proposes that the brain compares such internally generated predictions to the actual sensory feedback it receives from the environment. The difference to the classic reafference principle is that SE is assumed to be a mechanism that computes Bayesian inference (Körding and Wolpert, 2004). Together with a related theory called **predictive coding** or **free energy principle,** which traces back to ideas of von Helmholtz (1962) (Dayan et al., 1995, Friston, 2010), state estimation and reafference principle is an influential theory in the field of computational neuroscience. An important field of application is engineering and robotics, where the mechanisms of state estimation go under the name of “forward model control”.

The ability to move and perceive in a robust and adaptive manner relies on the accuracy of estimating the movement state of the body and limbs. Bayesian theory (Körding and Wolpert, 2004) suggests that the optimal estimate can be obtained by combining information about the distribution of kinematic variables, which is called the prior, with evidence from sensory feedback. When you are playing for example, at dusk or during rain or fog, and there is an increase in uncertainty, the system should rely more on prior knowledge. In order to use a Bayesian strategy, the brain must be able to represent both the prior distribution and the level of uncertainty in the sensory feedback. In a study, it is demonstrated that individuals are able to internally represent the statistical distribution of a task and their level of sensory uncertainty and that they integrate this information in a way that aligns with a Bayesian process for optimizing performance (Hillis et al., 2002, Cox, 1946). These findings suggest that the central nervous system uses probabilistic models during sensorimotor learning (Körding and Wolpert, 2004). The fundamental

notion that arises is that our estimate of the state of the world is a merging of two types of information: our predictions and our observations. The principle of processes of generating predictions about the sensory consequences and comparing those predictions with the actual sensory feedback are explained in the following.

2.2.1. Internal predictions regarding sensory consequences of motor action.

Modern theory of motor control (Fig. 3) states that the integration of the reafference involves an **forward model** that formulates the predictions by using the efference copy and other contextual parameters (Jordan and Rumelhart, 1992, Wolpert, 1996). The internal forward models are suggested to be located in the cerebellum (Daniel M. Wolpert, 1998, Shadmehr and Krakauer, 2008, Shadmehr et al., 2010, Therrien and Bastian, 2019). While computing predictions is the fundamental function of forward models, they in addition guarantee that motor commands and other context variables (from sensory via cognitive to motor variables) are readily translated into sensory outcomes, and such can be compared with the actual sensory feedback. There are delays at various points within the sensorimotor system from the time it takes to receive sensory input (afferent information) to the time required for our muscles to respond to motor commands (efferent instructions). Sensory feedback from our surroundings and the outcomes of our action's experiences delays due to receptor dynamics, nerve fiber conduction times, and synaptic relays. These delays can result in errors and unstable movements. Hence, the clear advantage of making sensory predictions is that the brain does not have to wait for the sensory feedback to arrive.

Forward model-generated predictions have several proposed applications in sensory and motor systems. The prediction of how a motor command will alter the state of the body and the environment is believed to underlie anticipatory motor control, such as maintaining posture (Gahery et al., 1981, Massion, 1992) and generating appropriate grip forces when manipulating objects (Johansson and Cole, 1992, Flanagan and Wing, 1997). Predictions of the resulting sensory feedback from a movement not only contribute

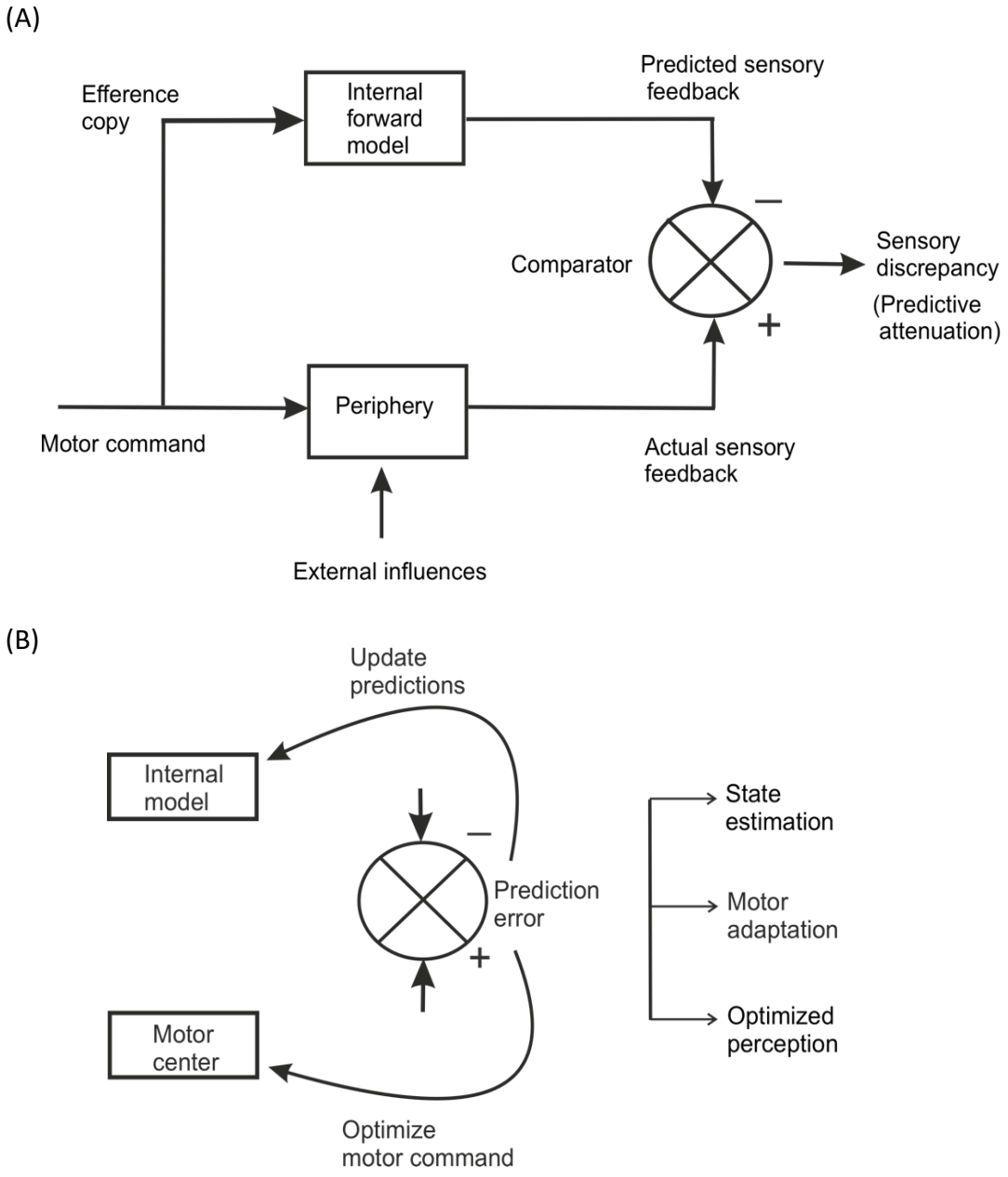

Figure 3. The modern theory of motor control.

(A) Dissociating self-generated from external sensory responses. By using efference copy, the internal forward model formulates the predicted sensory feedback. The actual sensory feedback reflects self-generated and externally generated sensory responses. The actual sensory feedback is compared/integrated with the predicted sensory feedback by the comparator to cancel or attenuate the self-generated sensory input and generate sensory discrepancy.

(B) Prediction error and implications. The disparity in predicted vs. actual sensory feedback generates prediction errors. Prediction error updates the internal model and motor center for modified predictions and optimized motor command, leading to state estimation, motor adaptation, and optimized perception.

to perceptual stability, as envisioned in Von Holst's model, but be utilized for improvement of motor programs, mental simulation, and state estimation (Davidson and Wolpert, 2005). As the cerebellum is suggested to be the site of internal models (Daniel M. Wolpert, 1998, Izawa et al., 2012, Lisberger, 2009, Miall et al., 2007, Nowak et al., 2007, Yavari et al., 2016), the neuroimaging studies on somatosensory attenuation disclosed reduced cerebellar activity, reduced activity in the secondary somatosensory cortex (Blakemore et al., 1998, Kilteni and Ehrsson, 2020, Shergill et al., 2013) and increased connectivity between the two areas (Blakemore et al., 1999, Kilteni and Ehrsson, 2020) when the self-generated touches were compared to the externally generated ones. Purkinje cells, which exhibit the highest convergence ratio in the brain (input divided by output fibers), are believed to compute these predictions. Afferent connections to Purkinje cells are formed through highly plastic synapses, potentially enabling a form of supervised learning (Gao et al., 2012, Raymond et al., 1996).

2.2.2. Comparing predictions with actual sensory feedback.

The discrepancies that occur during the comparison of internally generated predictions with actual sensory feedback generates **prediction errors**. These errors are useful to monitor and improve performance (perception and action). Further they update the predictive internal model to have modified predictions and optimized motor command, which ultimately leads to state predictions, motor adaptation, and sensory predictions to obtain optimized perception.

An example that displays the use of state predictions for optimal sensorimotor control is a waiter who carries a tray full of glasses (Fig. 4). When a customer picks up a glass, it can be difficult for the waiter to keep the tray perfectly steady and prevent the remaining glasses from spilling. However, when the waiter himself picks up the glass, the task becomes much easier. Why is it easier when the waiter does it himself? The explanation for this is- when the waiter picks up a glass, his/her brain predicts the exact moment when the weight will be removed from the tray and the exact mass of the glass and then reduces

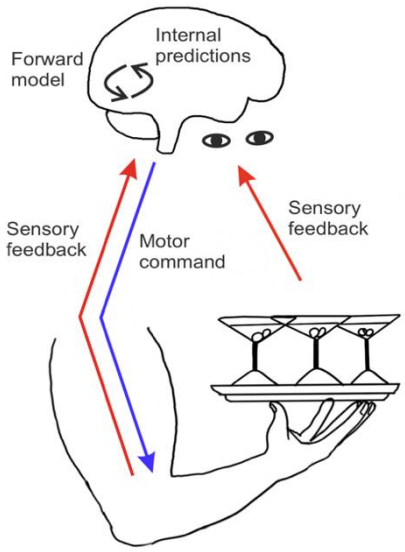

Figure 4. Example of state estimation.

When a waiter carries the tray in one hand, it has sensory feedback about the weight and state of the glass, which is used by the internal forward model to formulate predictions of the sensory consequences and future state. The brain then sends the motor command to the arm muscle to reduce the activity.

the activity in the muscles holding the tray. However, if someone else picks up a glass, the brain has to rely on sensory information (rather than predictions), which has a delay and causes the muscles to be late in reducing activity. Therefore, the brain compensates by predicting the consequences of lifting the glass and adjusting before receiving sensory feedback (Shadmehr and Mussa-Ivaldi, 2012). This is why we should let the waiter pick up the glass and hand it over. In this experiment, making sensory predictions has a clear advantage because the brain can shut off the muscles holding the glass without waiting for sensory measurements. The delay in these measurements can cause stability issues, but relying on predictions allows one to overcome this delay.

One of the various examples of motor adaptation include a well-studied paradigm of **visuomotor adaptation** in which the researcher introduces a perturbation that alters the visual outcomes of the motor commands while keeping the proprioceptive outcomes unaffected (Krakauer et al., 1999, Krakauer et al., 2000). Patients with cerebellar lesions, particularly in specific areas (inferior olive, posterior lobe), exhibit deficits in adapting to visuomotor perturbations like prism adaptation (Martin et al., 1996) (Baizer et al., 1999). This is due to the impairments in generating accurate sensory predictions that hinders the generation of sensory prediction errors, resulting in difficulties in motor learning and adaptation. Similar results were seen in the variant of the saccadic adaptation experiment in the context of eye movements (McLaughlin, 1967).

Sensory predictions that are derived from state predictions are not only used to compensate for the intrinsic delays in receiving sensory feedback (Davidson and Wolpert, 2005, Franklin and Wolpert, 2011, Kawato, 1999) but are also used to **attenuate the self-generated somatosensory signals** by means of comparative integration explained above, to increase the prominence of any externally generated tactile information (Bays and Wolpert, 2007, Blakemore et al., 2000). Numerous behavioral studies since the early 1970s have shown that the self-generated touch feels less intense than the externally applied touch (Shergill et al., 2003). This arises because the self-induced touch has been anticipated by the forward models using the efference copy, causing the somatosensory feedback to be suppressed, resulting in attenuation (Bays et al., 2005, Blakemore et al., 1998). An everyday example of such attenuation is the perception of tickle. It is a common experience that it is hard to tickle oneself, and empirical studies have confirmed that a self-generated tickle is perceived as less intense than an identical stimulus imposed externally (Weiskrantz et al., 1971, Claxton, 1975, Blakemore et al., 1998).

The phenomenon of sensory attenuation is not confined to humans and other animal species also use similar strategies. For example, the electro-sensory system of a weakly electric fish allows it to selectively respond to externally produced electrical discharges by attenuating its predicted electro-sensory feedback (Roy and Cullen, 2004, Sawtell, 2017). Mice exhibit attenuated auditory cortical responses to self-generated sounds, specifically for the tone frequencies that the animal has associated with its own locomotion. Conversely, this attenuation is absent when the same sounds are produced externally (Schneider et al., 2018, Audette et al., 2022). During active head movements in primates, the activity in the vestibular nucleus in response to vestibular reafference is attenuated compared to passive head movements. This reduction enables the animal to preserve its head and body posture and trigger vestibular-related reflexes as necessary (Brooks et al., 2015, Crapse and Sommer, 2008, Roy and Cullen, 2004). It has also been suggested that patients with auditory hallucinations have an abnormal predictive mechanism which may result in inaccurate predictions, leading to the erroneous attribution of self-generated actions to external sources (Feinberg, 1978, Frith, 1992, Frith et al., 2000). Individuals with Schizophrenia may exhibit such difficulties, experiencing

self-generated actions as originating from an external source, which may manifest as delusions of control or the misperception of self-generated speech as an auditory hallucination (Schneider, 1959).

Studies using functional neuroimaging have indicated that the somatosensory cortex and anterior cingulate cortex might be responsible for sensory attenuation. When a tactile stimulus is self-produced, these regions show less activation compared to when the same stimulus is externally produced (Blakemore et al., 2000). State estimation signals, incorporating predictions and sensory inputs, are hypothesized to be utilized by higher-level motor and perceptual structures to integrate the current state into ongoing motor commands or percepts. The regions of parietal cortex, including the somatosensory cortex (S1/S2) and neighboring areas such as the posterior parietal cortex (PPC), have been consistently implicated in hosting signals associated with state estimation (Mathis et al., 2017, Haarmeier et al., 1997, Lindner et al., 2006). These cortical areas receive cerebellar signals through a complex thalamocortical projection system. Despite the widespread acceptance of this theoretical framework, there is currently limited understanding of the neural mechanisms that underlie the predictive attenuation or state estimation phenomenon. This is partly due to the scarcity of neuro-imaging studies, conflicting results regarding the role and location of cerebellar activity, and the absence of behavioral measures to complement the neural findings. The evidence of comparative integration or state estimation is firmest at the cortical level; thus, it is my investigation site in the current project with objective to examine the neural signature of state estimation in attenuating predicted sensory consequences, its properties, and how it distinguishes itself from other processes that attenuate sensory flow.

2.3. State estimation vs. Sensory gating.

As described above, SE deals with the attenuation of sensory signals arising from self-generated movements, also called reafference signals. However, another line of research has revealed another type of sensory attenuation, which I will show in this thesis to be different and separable from SE, a process is known as sensory gating (SG)(Fig. 5)

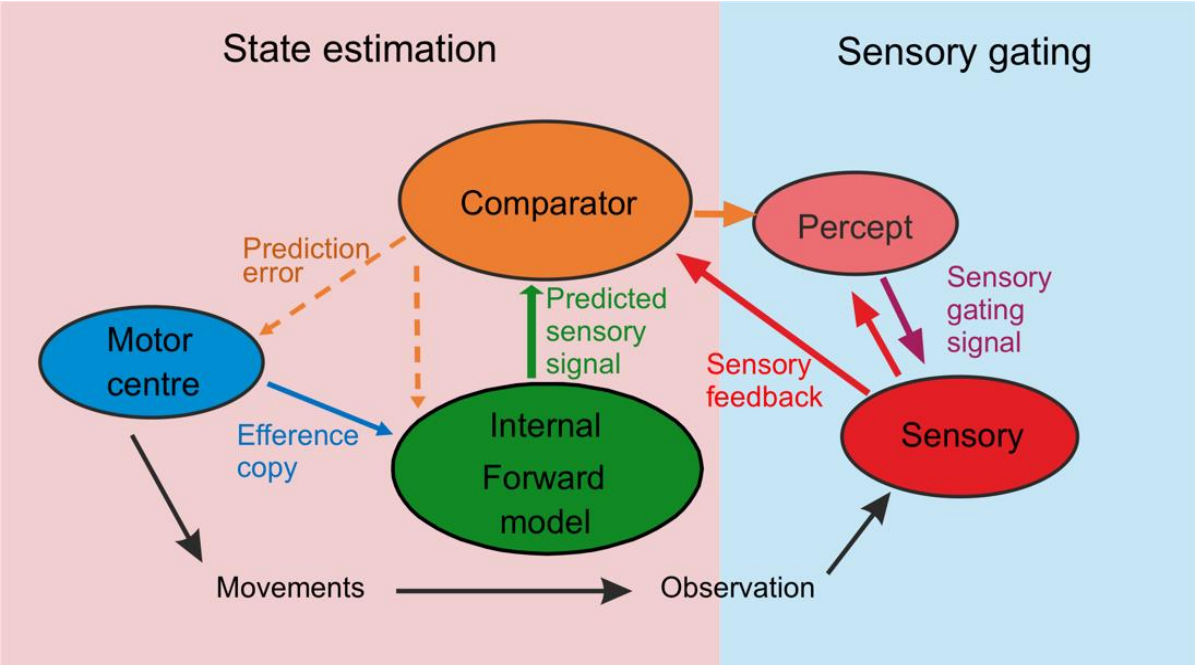

Figure 5. State estimation vs. Sensory gating.

The motor command generates movements and elicits sensory consequences observed by the periphery, and the information flows to sensory centers. The motor center also sends efference copy to the internal model. State estimation, hypothesized to take place in the higher sensory center, comparator, involves the comparison of predictions formulated by the internal forward model about the sensory consequences of an action with the actual sensory feedback to generate prediction errors to update an internal model and optimize motor command. Sensory gating attenuates sensory signals during movement and is a top-down process. The SG is recorded in lower sensory centers, input from higher centers/percept.

(Hentschke et al., 2006, Seki et al., 2003, Chapman et al., 1987b, Chapman et al., 1988, Rushton et al., 1981, Ghez and Pisa, 1972, Chapman et al., 1987a). In psychophysical research with humans, the phenomenon of tactile suppression or gating related to movement is demonstrated as an increase in the threshold of detection (Malenka et al., 1982, Chapman et al., 1987a, Fraser and Fiehler, 2018, Gertz et al., 2017, Voudouris et al., 2019), a decrease in the rate of detection (Malenka et al., 1982, Chapman et al., 1987a, Chapman and Beauchamp, 2006, Colino and Binsted, 2016, Cybulska-Klosowicz et al., 2011, Williams et al., 1998, Williams and Chapman, 2000), a decrease in the precision of detection (Colino et al., 2014, Gertz et al., 2017, Voudouris et al., 2019), and a decrease in the subjective intensity of externally generated stimuli (Papakostopoulos et

al., 1975, Williams and Chapman, 2000) when the stimulated body part moves compared with when it is at rest.

SG is observed in various species (Azim and Seki, 2019). For example, in cat medial lemniscus the nerve stimulation evoked responses are suppressed before and during limb movements (Ghez and Lenzi, 1971). Also, in monkeys, the attenuation of cutaneous afferent input during active movement has been documented in both the primary somatosensory cortex (Jiang et al., 1990, Jiang et al., 1991, Seki and Fetz, 2012) and the spinal cord (Seki and Fetz, 2012, Seki et al., 2003).

State estimation and sensory gating share two key conceptual similarities. Firstly, they both involve the modulation of the perception of cutaneous stimuli during movement, either in terms of magnitude or precision. Secondly, they seem to serve a similar functional role (Chapman and Beauchamp, 2006), which is to reduce the influx of afferent information that can be predicted from the motor command and enable the detection of external inputs that may be biologically significant, such as touches caused by predators (Blakemore et al., 2000, Brooks and Cullen, 2019, McNamee and Wolpert, 2019) or task-relevant sensory information for the ongoing or upcoming movement (Chapman, 1994, Collins et al., 1998, Rushton et al., 1981).

Importantly, however, there is one key difference between the two phenomena. State estimation or predictive attenuation of touch is associated with somatosensory reafference, which refers to tactile responses or touches caused by our own voluntary movement. In contrast, gating is related to somatosensory exafference, which pertains to external touches occurring during our voluntary movement. However, somatosensory research often considers the two phenomena as a unified strategy of suppression in the brain. In a recent study (Kilteni and Ehrsson, 2022), in a single experimental design, the perception of touches on the left hand was examined while manipulating the left arm's state of either movement or rest (left limb state). The origin of the touches was also manipulated, distinguishing between reafferent touches generated by the right hand and exafferent touches generated by an external source. The study demonstrated that

voluntary movement gates the precision of both self-generated and externally generated touch. However, there is a notable difference in the amplitude of self-generated touch, which is consistently attenuated compared to externally generated touch. Also, it can be concluded that the mechanisms of state estimation and gating operate independently and are not correlated, suggesting that they are separate perceptual phenomena.

The previous work in our lab has demonstrated the existence of a sensory gating effect in the trigeminal nuclei in the brainstem, which is the second neuronal station in the ascending whisker-related system in rodents (Chakrabarti and Schwarz, 2018). The lack of inputs from the cerebellum to trigeminal neurons (Teune et al., 2000) poses a challenge in reconciling it with the direct action of the internal model, which is believed to exist in the cerebellum. And state estimation or predictive attenuation, as we assume, uses the predictions formulated by the cerebellum (Daniel M. Wolpert, 1998, Izawa et al., 2012, Lisberger, 2009, Miall et al., 2007, Nowak et al., 2007, Yavari et al., 2016), thus, should be considered cerebellum dependent.

Additionally, gating signals in trigeminal nuclei and S1 have been found to be independent of detailed movement parameters and typically incorporate a temporally dispersed movement-related aspect (Chakrabarti and Schwarz, 2018, Hentschke et al., 2006, Seki et al., 2003), a fact that is difficult to align with the idea that state estimation is about precise predictions of sensory consequences of movement (Bell, 1982, Brooks et al., 2015, Singla et al., 2017). In my planned experiments, I will explicitly consider the possibility that sensory gating exists independently from state estimation.

The objective of this study was to investigate whether two different predictive systems exist that attenuate the tactile signal independently in movement-related fashion. After providing evidence of their existence, I will further demonstrate their separability, by reporting about the different working range and temporal precision of both processes.

2.4. Experimental setup

2.4.1. Bell's experiment in electric fish.

My experimental setup is inspired by Bell's experiment on electric fish (Bell, 1982). He demonstrated the existence of predictive signals, which, in adaptive ways, cancel the unwanted effect of reafference signals.

In his experiments the effects of the electric organ discharge (EOD) motor command were investigated (Fig. 6A). The reflection of the electrical field generated by EOD from invisible objects and conspecifics in turbid waters is normally used to perceive and explore the fish's vicinity. Curare, added to the water in the fish tank, blocks synaptic transmission of motoneurons onto the electric organ. It silences EOD and opens the sensorimotor loop. The brain's motor command, however, a synchronized volley in the afferents to the electromotor cells could still be recorded from the skin of the fish's tail and used to trigger artificial electrical pulses in the water to activate electroreceptors and thereby simulate certain aspects of the EOD. With this experimental setting, he was able to introduce varying latencies of the (artificial) sensory consequences of ego-motion (in this case, electromotor commands) and show that predictive signals in a cerebellum-like structure in the fish brainstem readily adapt through learning mechanisms to a wide variety of imposed sensory consequences of movement (Bell, 1982).

2.4.2. Our experimental setup.

Mice whisker system

The whisker system serves as a sensorimotor mechanism utilized by various animals, including rodents, to gather environmental information. During active exploration, mice move their whiskers back and forth at high frequencies (~10 Hz) to scan the nearby environment. This sensory action provides spatial and textural information about their surroundings (Ferezou et al., 2007, Diamond et al., 2008).

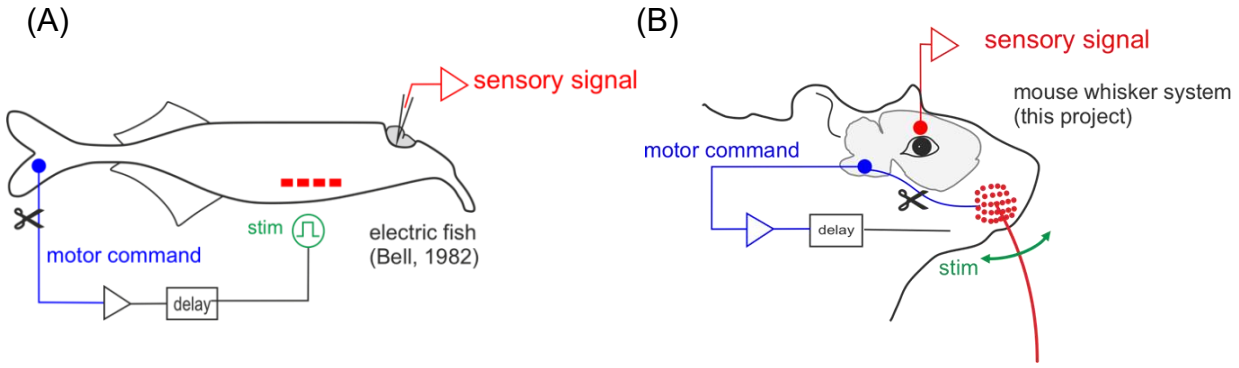

Figure 6. Translation of Bell's experiment in mice whisker system.

(A) Bell's experiment in electric fish. Fish was curarized, so there was no electric organ discharge (motor command). Stimulated the lateral line system after recording the motor command in the tail after introducing a delay. The sensory signals were recorded in sensory centers.
(B) Experimental strategy in mice whisker system. The reafferent loop is opened by cutting the facial nerve (scissors symbol, blocking all natural reafferent signals). Motor commands were recorded in the facial nucleus (FN), and the sensory consequences were mimicked by an artificial stimulator, the evoked sensory responses of which is then recorded in S1 barrel cortex.

The whiskers are moved by both intrinsic and extrinsic muscles which is located in the mystacial whisker pad (Dorfl, 1982, Haidarliu et al., 2010). These whisker muscles are innervated by cholinergic motor neurons in the lateral facial nucleus of brainstem which directly drive whisker movement. These large neurons, possess dendrites that extend beyond the facial nucleus (Friauf, 1986). The whisker motor neurons receive synaptic inputs from premotor neurons that determine when action potentials are fired. Premotor neurons are located in the brainstem, midbrain and neocortex.

The whisker primary somatosensory cortex (wS1) and whisker motor cortex (wM1) both play roles in whisker motor control (Petersen, 2014, Schwarz and Chakrabarti, 2015). Strong stimulation of wS1 causes rapid retraction of the contralateral whiskers, possibly through innervation of spinal trigeminal premotor neurons of extrinsic whisker-pad muscles (Matyas et al., 2010, Sreenivasan et al., 2015). Stimulation of wM1 evokes short-latency rhythmic whisker protraction (Gerdjikov et al., 2013), similar to exploratory whisking. These whisking movements might be driven by wM1 as it strongly innervates the facial whisker motor nucleus (Grinevich et al., 2005, Sreenivasan et al., 2015) and

brainstem reticular formation that contain premotor neurons, and a central pattern generator for whisking (Matyas et al., 2010, Takatoh et al., 2013, Sreenivasan et al., 2015). Both of these pathways play important functional roles in exploratory rhythmic whisking and whisker retraction.

Nerve endings within the whisker follicles translate the movement of the whiskers into action potentials, and this information is conveyed to the somatosensory cortex. Adopted from a review (Adibi, 2019), the distal axon of the trigeminal ganglion innervates the whisker follicles, and each ganglion innervates only one whisker follicle. Trigeminal nuclei neurons receive inputs from trigeminal ganglion cells and organize them into distinct clustered groups known as "barrelettes." These neurons primarily project to individual barreloids, which are grouped aggregations representing specific whiskers within the contralateral thalamus. The afferent fibers of VPM neurons from thalamic barreloids extend and branch within the corresponding neuronal aggregations, known as barrels, located in layer IV of the primary somatosensory cortex. This forms a direct and individual connection between the VPM barreloids and cortical barrels.

The self-generated whisking in mice could deform the whisker follicle and stimulate mechanoreceptors to generate reafferent sensory input. This reafference signal is important to localize objects in space and determine whisker position (Kleinfeld and Deschênes, 2011). In a study (Szwed et al., 2003), it was demonstrated that during whisking intervals, primary neurons in the trigeminal ganglion transmit two types of signals. One signal represents a reference signal that encodes the current position of the rat's vibrissae, while the other signal corresponds to a more conventional sensory signal that encodes the contact of the vibrissae with an object. However, there is evidence suggesting the presence of a modulatory efference copy at the cortical level, which could potentially affect the magnitude of whisking (Fee et al., 1997). This central information can be utilized to fine-tune feedback loops within the vibrissae sensorimotor system on a larger scale, aiming to optimize sensory processing (Ahissar and Kleinfeld, 2003). We took advantage of the mice whisker system to study the suppression of reafference signals generated by stimulated mechanoreceptors at the cortical level (Fig. 6B).

Open Reafference loop.

The basic principle of an open reafference loop (ORL) is to alter the default relationship between a given motor command and its sensory consequence. For example, a whisk in one direction would cause a sensation of whisker movement (e.g., by tactile neurons) in a given predictable direction. ORL violates this relationship (e.g., movement command does not lead to whisker movement) to investigate principles of prediction and state estimation. Back in the 1940s, the reafferent loop was not really "opened" in its entirety. However, a sign conversion was imposed on the reafferent signals, systematically biasing the function of the feedback branch of the loop. Von Holst and Mittelstedt turned the head of a fly by 180° and fixed it in place (Von Holst and Mittelstaedt, 1950). The same was done with the eyes of fish by Sperry (Sperry, 1950). Both manipulations turned the normally compensatory movements to ego-motion into dysfunctional and unstoppable circling movements since ego-motion, and resulting image motion were now aligned rather than opposite as before. Here, we will directly translate Bell's experiment to the whisker system of the operantly conditioned mouse (Figs 6B and 7A). We will cut the facial nerve such that movement commands to whiskers, which are generated in the brain, do not cause actual whisker movements. We will then replace the whisker movements with experimentally controlled whisker stimulations by an external device, with various delays. Thus, the relationship between whisker movement command and actual whisker movement will be under full experimental control. We used the motor commands, which we could still record in the facial nucleus of the brain stem, as the trigger for an actuator, which artificially moves (stimulates) the whisker, mimicking the sensory consequences of the whisking. The evoked sensory responses were then recorded in the whisker representation of primary somatosensory cortex (barrel cortex).

Closed Reafference loop.

We also employed control experiments using the closed reafference loop approach (Fig. 7B). Here we kept the reafference loop intact and provided the external stimulation on top of the reafference signal.

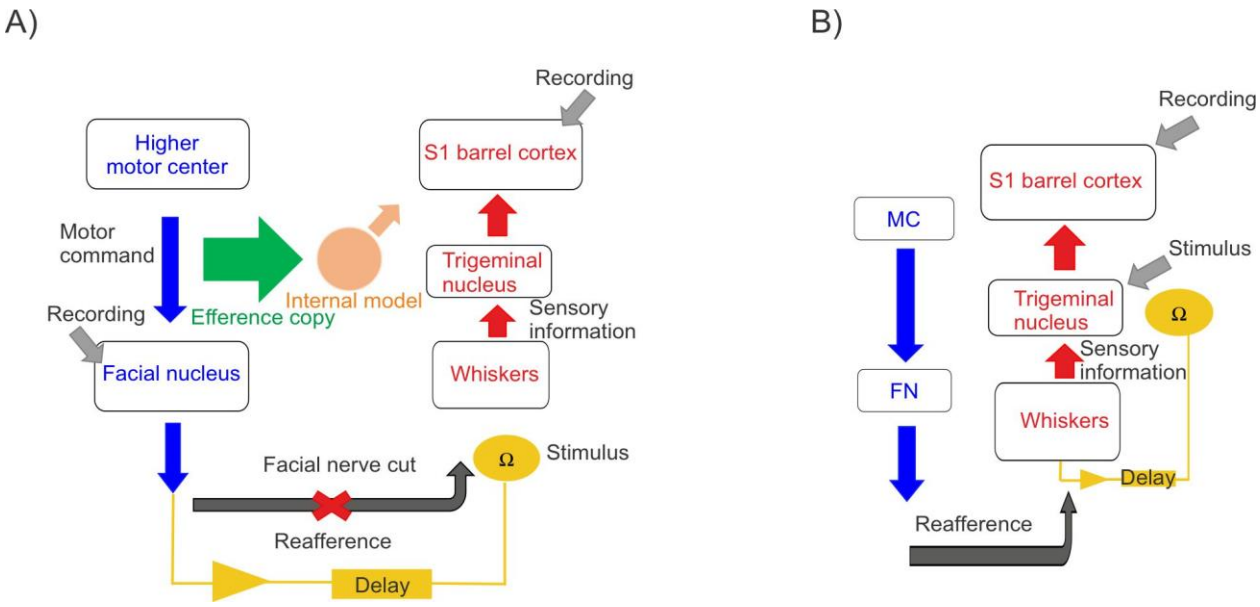

Figure 7. Experimental setup.

A) Open reafference loop (ORL). Mice are implanted with a single electrode in the facial nucleus of the brain stem to assess motor command and a multi-electrode array to record sensory signals related to state estimation in the S1 barrel cortex. The reafference loop is opened by cutting the facial nerve. The prediction of the internal model is then trained by pairing motor commands with external whisker stimulation. Delays are introduced at the time of stimulation from the movement start.
B) Close reafference loop (CRL). Mice are implanted with a single electrode in the trigeminal nucleus of the brain stem to stimulate and a multi-electrode array to record sensory signals related to state estimation in the S1 barrel cortex. The electrical stimulation in the trigeminal nucleus is triggered by a large whisker protraction after a delay.

This was done to support the results of the open loop approach where the facial nerve is cut, and there is a possibility of the existence of the unwanted effects of plasticity in the related brain areas and concomitant unnoticed changes in the behavior of the mouse. The ORL approach is irreversible and could have immediate and delayed effects, which include alterations in synaptic connections within the facial motor system. This can lead to changes in the neuronal circuitry and functional reorganization to compensate for innervation loss. In addition, non-facial nerve-mediated whisker movements exist, which arise from autonomic, cholinergic axons traveling within the infraorbital branch of the trigeminal nerve (ION). It has been shown that there is a modest and/or inconsistent increase in ION-mediated whisker movement amplitude starting about four weeks after the facial motor nerve transection (Heaton et al., 2014).

Contrary to fish, where electric discharges are generated automatically, mice have to be operantly conditioned to move a whisker. In CLR a protraction of the whisker across a target was used as the trigger for the sensory consequence, which in this case was an electrical stimulation in the whisker's representation within the brain stem trigeminal nucleus. The evoked responses were then recorded further up the ascending tactile pathway, in barrel cortex.

2.5 Hypothesis and Expectations.

My hypothesis (Fig. 8) states that state estimation and sensory gating are two different predictive systems that both result in sensory attenuation as already mentioned. The base assumptions incorporated in the hypothesis were, for one, that state estimation is specific to the sensory consequences of the body's own movements; hence it is thought to be temporally precise. Second, sensory gating is thought to attenuate the sensory signals before and during the movements and hence is thought to be temporally imprecise, i.e., being evoked within a larger interval starting at or shortly before the movement.

To capture the effect of these processes, we provided different stimuli (presented in pseudorandom sequence) in the experiment (Fig. 9). The stimuli were identical in terms of deflection trajectory. However, they were applied at different latencies after onset of the motor command (Fig.8).

1. Predicted trials (red in Fig. 8 and 9): these trials contained whisker movements at the trained latency. These trials were presented most frequently (10 out of 13 times in block-wise randomized sequence. These trials are hypothesized to capture the effect of both, SE and SG, because they mimic the learned sensory consequences.
2. Omitted trials: These trials omit stimulation after a motor command. They were presented rarely (1 in 13 trials). In absence of the stimulus, they were expected to reveal the predictive signal.

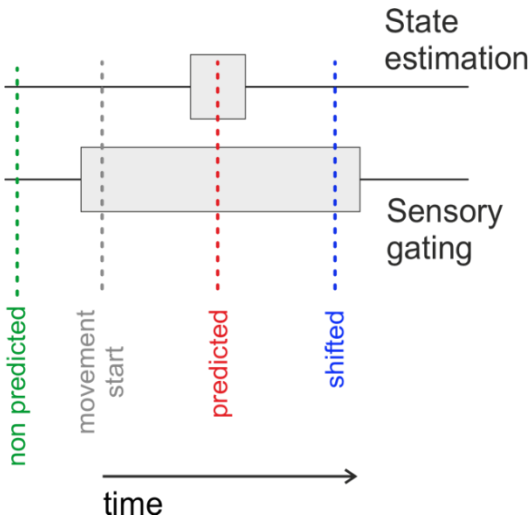

Figure 8. Hypothesis figure.

State estimation (SE) is precise and closer to movement start and sensory gating (SG) with a broader range. Red, predicted trials capture both SE and SG effects; blue, shifted trials capture only SG and green, non-predicted trials do not fall in the range of any attenuating effect.

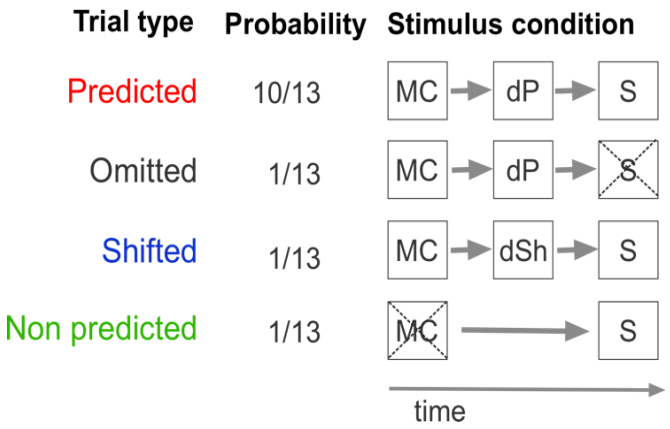

Figure 9. Stimulus conditions and trial types.

MC: Motor command; dP: predicted delay; S: stimulation; dSh: shifted delay. In predicted trials, stimulus comes after motor command with some time delay. In omitted trials, there is no stimulation. In shifted trials, stimulus came after motor command and shifted delay. In non-predicted trials, stimulus comes in the absence of motor command.

3. Shifted trials (blue in figs. 8 and 9): These were also rarely presented (1 in 13). They have a different delay than predicted trials and are hypothesized to capture only the SG effect. This is because the animal presumably did not learn that sensory consequence.
4. Non-predicted trials: Rarely presented (1 in 13), they present a whisker flick outside of a motor command. These represented tactile stimulation that is unpredicted, a pure exafference. It will fall outside the movement perimeter, and therefore, outside the possible effect of both motor-related attenuations.

The aim of this study is to demonstrate the existence of two sensory attenuation processes within the same experimental framework and to dissociate state estimation from sensory gating in the tactile system. My objective is to investigate the adaptability and potential learning involved in the state estimation process, as well as the speed at which animals can acquire this learning. Additionally, we explored the precision of state

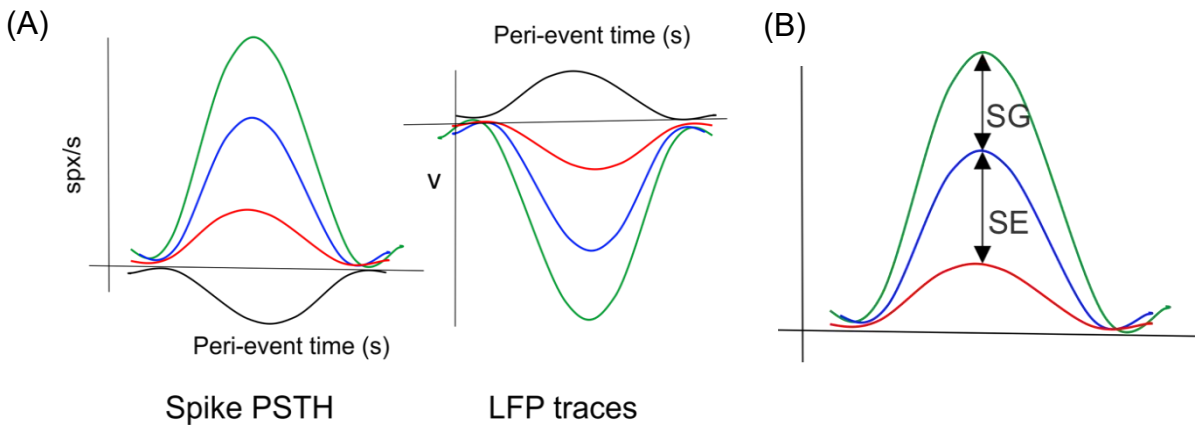

Figure 10. Depiction of expected results, PSTHs, and LFPs.

(A) Schematic of the expected effects of SE and SG on the neuronal response to different stimulus timings. Spike PSTH and LFP traces. The time of stimulation would be before (to the left of) the shown responses.
(B) Depiction of the two effects. Sensory gating (SG): Non-predicted vs shifted. State estimation (SE): Shifted vs predicted.

estimation. Finally, my objective also was to investigate the ranges at which SE and SG can be observed, the temporal precision, as well as the dynamics of potential learning involved in the state estimation process. In a subset of mice, I have also recorded the neural activity across all the layers of the S1 somatosensory cortex to check the presence of basic effects and speculate about the site of state estimation.

Under the working hypothesis, I expected the following outcome of the experiment (Fig. 10). Predicted trials (red) will show the effect of both state estimation and sensory gating and are the one which will be maximally attenuated (possible neuronal responses to the whisker deflection are plotted as spike rate and potential of LFP response). Shifted trials (blue) will exclusively capture the effect of sensory gating and therefore are expected to be less attenuated in comparison to predicted trials. Non-predicted trials (green), in turn, should carry the full tactile response and thus reveal the maximal response amplitude.

Finally, I hypothesize that the process of predictive attenuation is highly precise and has a smaller effective range as compared to sensory gating.

3. Materials and Methods

3.1. Materials

Animals:

All electrophysiological recordings during the experiments were performed on C57BL/6N mice, n=15 (12 for ORL and 3 for CRL) after implanting the electrodes in the desired brain area and training the animals for the behavioral task. Animals, male, aged 9-12 weeks, were obtained from Charles River Laboratory, and housed in individual cages to avoid any whisker plucking because of any stress due to transportation. They were provided running wheels and wooden blocks in the cage to enrich their environment. Animal cages were kept in a scantainer with regulated humidity of ~55%, ambient temperature of 25°C, and inverted 12h day/12h night cycle with food and water ad libitum before experiments. Water was restricted during the experiment with a minimum of 1ml/day of water compensated during the task or/and afterward as a water gel. Weekends were provided with free water and again taken off on Sunday evening. Animal experiments were conducted according to the German law, under a license issued by the local authorities (Regierungspräsidium Tübingen).

Electrodes:

Custom-made **tungsten wire electrodes** were pulled and ground in-house (Schwarz et al., 2010) and used for implantation in 7 animals. A single electrode of impedance- 1-3 MΩ and length 6-7mm was used to record from the facial nucleus, and a 2x2 array of 4 electrodes, impedance 1-3 MΩ and length 2mm, to record from primary somatosensory barrel cortex.

Silicon arrays, single shank, containing 16 electrodes of impedance 1 MΩ, were also used to implant in primary somatosensory barrel cortex in 5 animals. The length of the shank was 1500μm, and the distance between each electrode was 100μm (Product no.- E16-100-S1-L6 NT, Atlas Neuroengineering bvba, Belgium).

Additional **silver wire electrodes** were implanted on the cerebellum and prefrontal cortex as ground and reference electrodes, respectively, for a non-silicon array setup. The wire was made into a ball on one side so that it could sit on top of the brain without damaging the tissue. In case of silicon array setup, the ground and reference wires from the array were carefully implanted on top of prefrontal cortex.

Jumper cables (Omnetics connector, Minneapolis, USA) were used to connect the electrodes in the silicon array implanted in the primary somatosensory cortex and the single electrode implanted in FN to the head stage (micro preamplifier).

Surgical apparatus:

All surgeries were performed using stereotaxic apparatus and ear bars (Stoelting, USA, and Kopf, Tujunga, USA). The stereotaxic apparatus was used for the Micro-stimulation guided implantation in the facial nucleus and intrinsic optical imaging-guided implantation in the primary somatosensory cortex. Hydraulic micromanipulator (Kopf, Tujunga, USA) was used to advance and retract electrodes inside the brain.

Task controller:

The tasks for the motor training and experiment were designed in MATLAB Simulink state engine, running on a dedicated real-time machine and using an I/O interface of National instruments (Austin, USA).

Equipment controlling the behavioral task:

Restrainer: Animals were head fixed for the experiment using the restrainer box (Schwarz et al., 2010). We utilized a restrainer composed of black plastic, with a front plate constructed from anodized aluminum dyed black, as described by Welsh in 1998 (Welsh, 1998). The restrainer was designed to be narrow enough to prevent the animal from turning inside while still allowing for comfort. The box had a conical shape, with a wider opening at the back end for mouse entry and a narrower opening at the front end for head fixation and rat exit. The front shield, which held the head-fixation bracket, could be vertically adjusted to customize the height of the head in relation to the body. This

vertical positioning was crucial to ensure the mice assumed a comfortable posture and needed to be optimized for each individual. Additionally, the front end featured a foot plate that could be adjusted in height to provide a comfortable resting position for the forepaws while preventing limb extension towards the snout. At the back end, a door could be slid in and secured with a screw. This back door included an opening specifically designed to accommodate the mouse's tail.

Whisker tracking system: Whiskers were traced using a laser optical device (LOD) laser curtain. The whisker was extended by sliding it onto a slender polyimide tube (with a diameter of 0.3 mm and a length of 1.4-1.6 cm), which covers the hair from its base to its tip. For monitoring the whisking movements, a two-dimensional laser beam was projected onto a linear CCD array, and the shadow created by the tube was tracked using the LOD, Metra-Light system (San Mateo, CA, USA). The width of the Metra-light receiver array was 0.8cm.

Water and light delivery system: The water and light delivery system was acquired from Med Associates, St Albans, VT, USA. A TTL pulse that inputs from the Simulink real-time machine to the respective controller enables the light to turn on and off and opens a magnetic water valve for a determined time (1 ms) to generate a drop size amount for the animal to lick from the spout.

Piezo lick sensor: In electrophysiological recordings, the spout, typically crafted from a plastic venous catheter, is preferred over steel catheters due to the significant licking artifacts the latter generate. To the catheter, a miniature piezo element called a piezo sensor is securely attached using epoxy glue. The output voltage of the piezo element is amplified, subjected to high pass filtering, and digitized through a comparator circuit featuring an adjustable threshold. This setup allows for the detection of a lick. A digitized signal is then recorded and sent to Simulink real-time machine. The Piezo lick controller was built in house (Schwarz et al., 2010), and the sensors were obtained from PI (Physik Instrumente).

Piezo actuator: For whisker deflection we used ceramic bending actuators (PICMA®, PI), that contain multilayer bender elements with high reliability. The actuator has an operating voltage range of 0-60 V and a displacement of ±450 μm. A glass capillary tube was attached to the center of the piezo to stimulate the whisker of the animal that was inserted in the tube. We used 10 V to operate the actuator at 0.5cm from the whisker follicle to move the whisker 0.9mm (0.45mm in both directions).

Recording and data acquisition system:

For neural data acquisition, all the components were obtained from Multichannel systems (Reutlingen, Germany). **Miniature preamplifiers** for 8 channels amplified the signals to 4X, and some had the amplification of 10X. The 16 channels micro amplifiers used for silicon array recordings amplified the signal to 10X.

The output signal of the preamplifiers was duplicated and input into **two bandpass filters**; one copy was filtered through a bandpass filter for spikes (filters signals from 200-5000 Hz) and the other through a broadband filter (range 1-5000 Hz). Both filters also added amplification of 500X. The total amplification of individual spike and LFP signals up until here was 2000X (with 4X preamp) and 5000X (with 10X preamp). The signal from the bandpass filter entered the **breakout box** with output ports and was used to extract the spike signal from different channels. The output signal from the breakout box then entered the computer system with **a Multichannel system card** installed to receive signals into individual channels, 1-64 used for spikes and channels 65-128 for LFPs. The voltage traces were viewed in real-time on **MC rack software** from Multichannel systems. The traces were then recorded at the sampling rate of 40Khz with a gain of 2000X and 20Khz with a gain of 5000X in tungsten and silicon array animals, respectively. The digital signals from the equipment that control behavior (Water pump, light, lick sensor, whisker stimulator, and other behavior parameters) were recorded into the MC rack using the digital breakout box, which input the digital bits into the computer system with a digital card installed. Whisking signal from the LOD input into the additional analog input port in the MC card and was recorded in MC rack software.

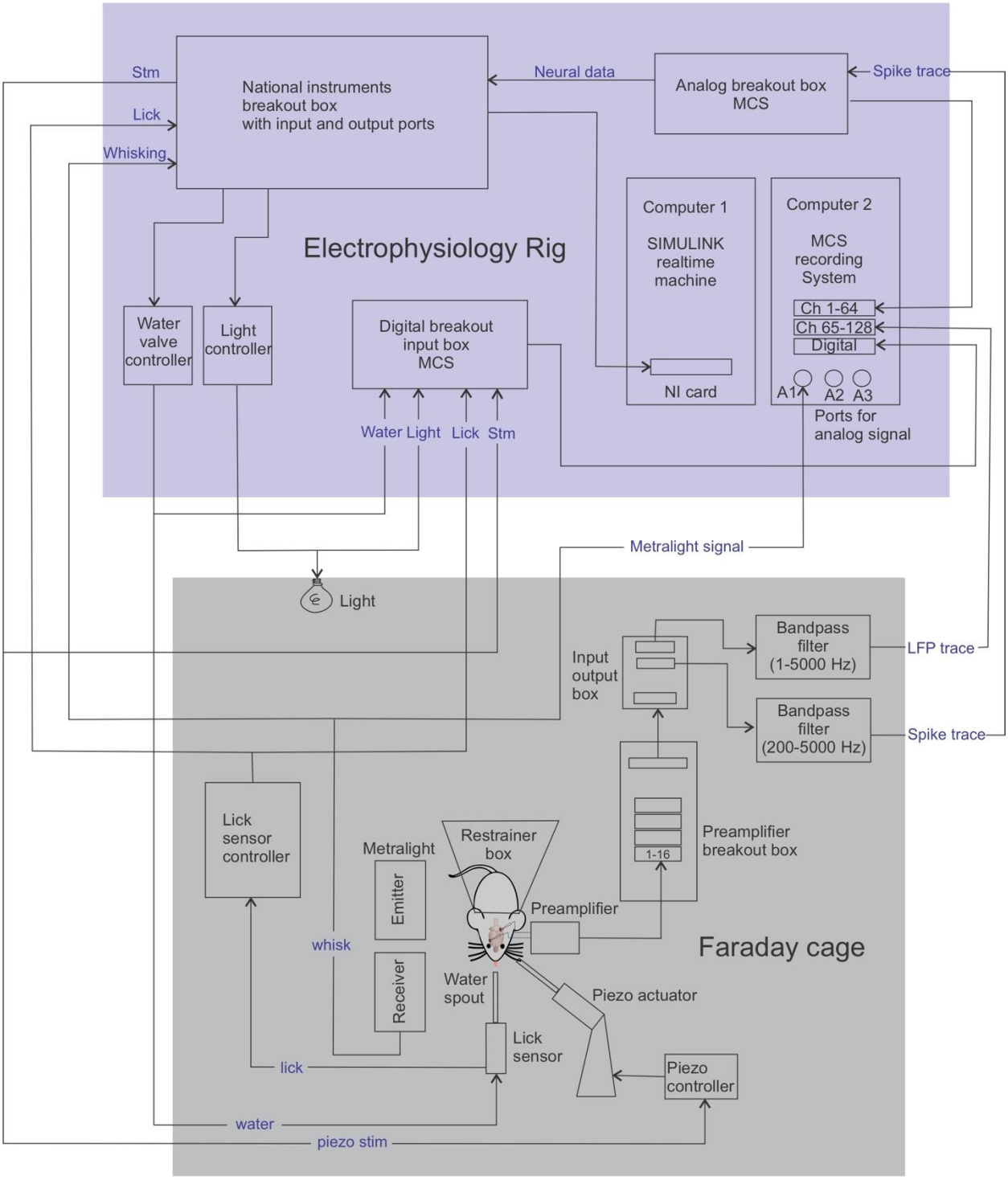

Figure 11. Schematic of the experimental setup. Components of behavior and electrophysiology.

Stimulus generator: A stimulus generator (STG, Multichannelsystems, Reutlingen, Germany) was used to generate electrical micro stimulation to guide electrode implantation into the facial nucleus. It was also used in the closed-loop experiment to provide electrical stimulation in the trigeminal brainstem nucleus.

Dip switch: An arrangement was made to split the signals recorded from implanted electrodes into two copies. Spikes were recorded through one preamplifier that referenced the signals through one of the electrodes to subtract movement related artifact and LFPs were recorded through another preamplifier that referenced the signal through the silver ball electrode implanted on top of the prefrontal cortex.

3.2. Experimental procedures.

The experimental setup included an electrophysiology rig and Faraday cage along with other above-mentioned components. Fig. 11 shows the detailed schematic of the experimental setup used for training the animals and performing experiments while collecting neural data. To implement the experimental procedures, a series of complex methods were established. Fig. 12 shows the timeline of procedures performed for the study.

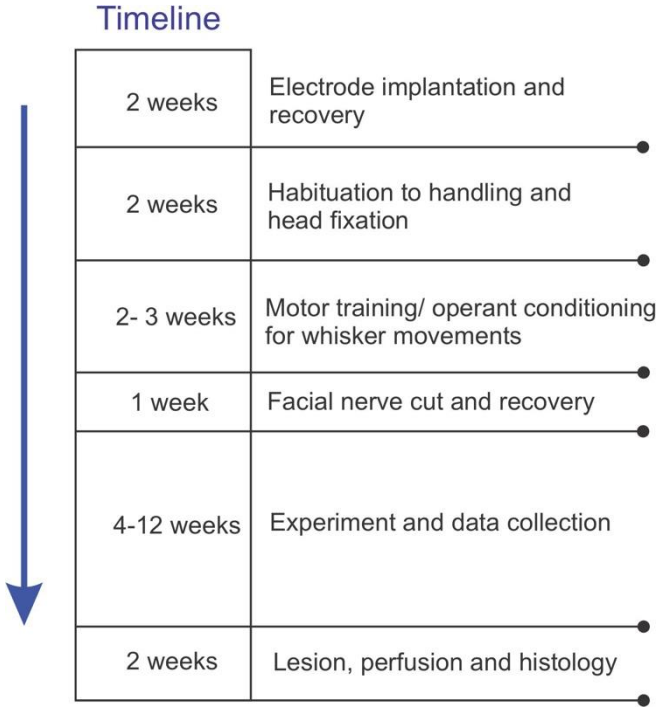

Figure 12. Timeline of the experimental procedure.

3.2.1. Implantation of electrodes and head post.

FN implantation: To begin with, mice were implanted with tungsten electrodes in the facial nucleus of the brainstem in the area that corresponds to whisker protraction (Fig. 13C). During the surgery, the animal was lightly anesthetized using an isoflurane

chamber at 2% with a flow of 120 ml/min. After the animal was in a deep sleep (checking the responses to tail pinches), the anesthesia was continued by an intraperitoneal (i.p.) injection of 3K (fentanyl 0.5 mg/kg, midazolam 12.5 mg/kg, and fluanisone 25 mg/kg, i.p.). The supplement doses of 33% of the initial dose were given after intervals of about 50 mins after checking the response to tail pinch. Hairs above the dorsal skull were shaved, and the mouse was transferred to the stereotaxic frame. The body temperature was monitored and controlled by a system with a rectal probe containing a temperature sensor and a heating pad that provides heat. The temperature was set to 35°C. After making an incision on the skin above the dorsal skull, it was prepared by cleaning all the connective tissue using hydrogen peroxide. Optibond was applied on the dry skull to make the contact of dental cement, which is used to embed the electrode later. Markings were made for craniotomies for implantation in FN (at 5.5mm rostrocaudal from bregma and 1.8 mediolateral from midline), and S1 (1.5mm rostrocaudal from bregma and 3.25mm mediolateral from midline). The area marked for FN was then drilled using a drill bit at 5000 rpm, and the skull was removed. The brain area was then mapped using a tungsten electrode and microstimulation with a short rectangular pulse of 5-10μA current while monitoring the whiskers. After locating the area, which gave rise to whisker movements upon microstimulation, the immobile electrode was implanted. The craniotomy was covered with Kwik seal, and the electrode was embedded using dental cement. The preparation was then closed, and the skin was sutured. The still anesthetized mice were first given the painkiller carprofen (5 mg/kg) followed by 3K antidote (naloxone 1.20 mg/kg, flumazenil 0.50 mg/kg, and atipamezole 2.50 mg/kg, i.p.), on which anesthesia was reversed within a few minutes. Everyday post-surgery care included the continuation of carprofen injection (two times a day for minimally 3 days) and, if needed, the administration of warmth and electrolytes. 12 animals were implanted in FN and performed an open loop experiment.

Trigeminal implantation: 3 animals were implanted in the trigeminal area of the brainstem in their first surgery. These animals performed a closed-loop experiment, a control for facial motor nerve cut. After making markings for the trigeminal nucleus, 5mm rostro-caudal from bregma and 0.8 mm mediolateral from the midline, a craniotomy was made.

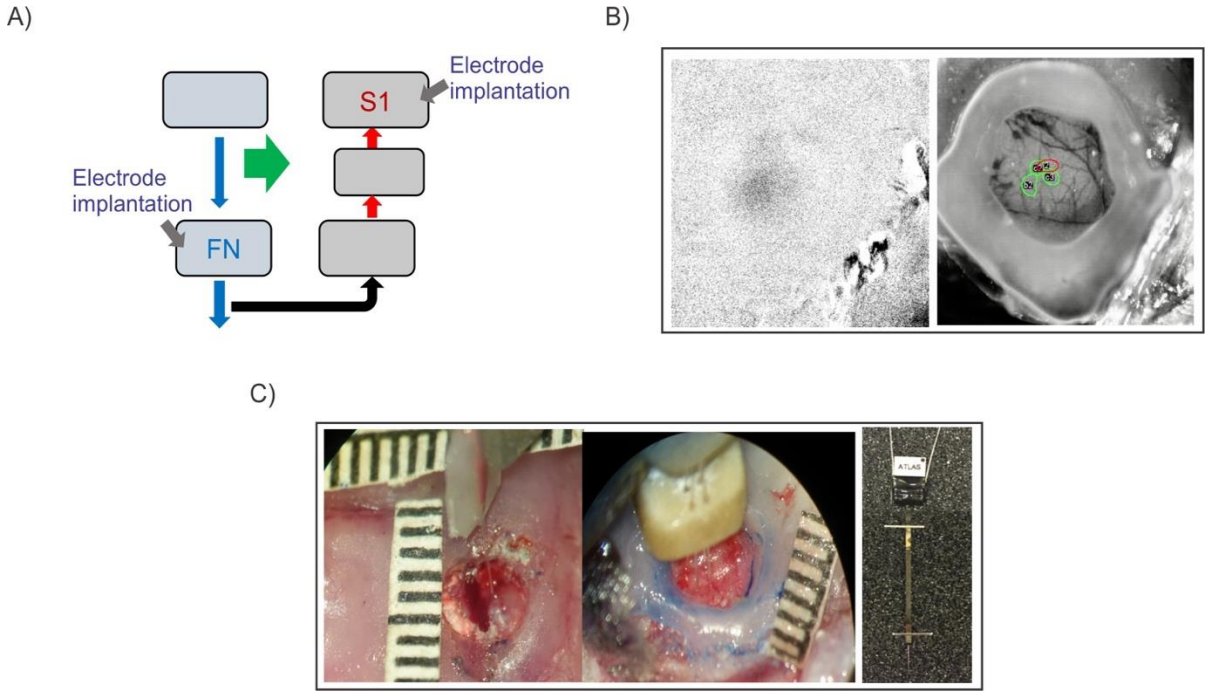

Figure 13. Surgical procedures.

A) Schematic showing electrode implantation in FN (facial nucleus) and S1 (somatosensory barrel cortex). B) Images from intrinsic imaging, dark blob corresponds to whisker barrel. The brain picture was then aligned to the blob, and electrodes were implanted accordingly. C) Electrode implantation in FN in the first image and S1 in the second image.

The area was mapped by recording the neural activity evoked by the manual whisker wiggling. The neuron firing was heard using the speaker and recorded using the MCRack software. When the nucleus specific to the C2 whisker was located, the electrode was implanted by covering the craniotomy with a Kwik seal and embedding and fixing the electrode using dental cement.

S1 implantation and preparation of head post: After implanting the electrode in the facial nucleus (n=12) and trigeminal nucleus (n=3), animals were recovered for a week, and another surgery was performed in all the animals where a mobile array of 4 electrodes (2x2) was implanted in S1 barrel cortex along with a head screw (Fig. 13B, C). All the initial procedures performed for anesthesia were the same as the first surgery. A specific barrel column (C2) was located with the guidance of optical intrinsic imaging. Intrinsic imaging allows the recording of neural activity non-invasively by measuring hemodynamic

changes in the brain (Joachimsthaler et al., 2015). Intrinsic optical imaging is a technique that takes advantage of the distinct absorption characteristics of oxygenated and deoxygenated hemoglobin (Hillman, 2007). When neural activity occurs, the response in the vicinity typically exhibits an initial rise in deoxygenated hemoglobin and blood flow, followed by an increase in oxygenated hemoglobin (Juavinett et al., 2017). To detect these changes, different wavelengths are employed for measuring total hemoglobin and blood flow (500-599nm), as well as deoxyhemoglobin (600-699nm) (Morone et al., 2017). Using the prior markings, the skull was thinned carefully using a drill bit at 1000 rpm. The intrinsic camera was compiled with Helioscan software (Langer et al., 2013), which was used to control the piezo stimulator for whisker stimulation and acquire images with and without stimulation. We used a red light of wavelength 620-750 nm to image layer 2/3 of the S1 barrel cortex to detect a whisker barrel, a blob of neurons with deoxyhemoglobin, while deflecting the corresponding whisker using a piezo actuator. After locating the whisker barrel, the electrode array was introduced into the brain and fixed using dental cement after covering the craniotomy with a Kwik seal. A head-post (M1 stainless steel screw, head-down) was placed on the back of the skull and embedded within the dental cement. The skin was then carefully sutured, and post-operative drugs were administered, like in the first surgery. Animals were monitored regularly to provide any care, if needed, for 3-5 days until they were fully recovered.

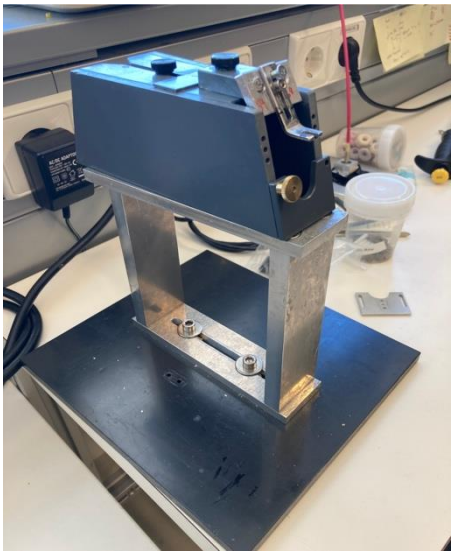

Figure 14. Restrainer box used for head fixation.

3.2.2. Habituation and training.

Head fixation:

After the mice recovered from the surgery, they were habituated to handling. The animals were also familiarized with the restrainer box by keeping the box in their cages for some time. Fruit loops were provided as a reward after each session. In a week time, when they were comfortable with handling, mice were trained to get their head fixed to a restrainer box (Fig.

14). Head fixation procedures and systematic desensitization protocols to minimize any stress were done as described elsewhere (Schwarz et al., 2010). When the animal was habituated to getting its head fixed and drinking from the waterspout during head fixation, its behavioral training was started.

Training to whisker reaching task:

In the training setup, designed using MATLAB Simulink, the water reward was given following a precise whisker protraction (Fig. 15A). The behavior was controlled by Simulink real-time machine with an NI card interface. The whisking signal from the laser optical device (LOD) and the lick detection is input into the state flow (shown in fig. 15B), which controls the output of water and light. A virtual baseline and threshold were set to control the placement of the tracked whisker before the movement and to track its movement across baseline and threshold as done in (Chakrabarti et al., 2021). A polyimide tube was put on a C2 whisker to make it thicker and easily detectable by LOD. To start the task, the animal had to retract his whiskers at a resting position so that the whisking voltage is less than the predetermined baseline. The house light was used to signal to the animal the possibility to start a trial (OFF means 'whisker retracted, trial start enabled; ON means 'whisker misplaced, trial not enabled; the light was also switched ON when a trial was aborted). The animal thus performed precise whisker protraction across baseline and threshold. The crossing of the threshold triggered a reward (drop of water) at a short delay of 200ms. A lick after movement and reward delay was counted as a successful trial (hit). Between task enablement and reward delivery licking at the spout aborted the trial, the light went on according to whisker position and the mouse had to start again (invalid trial). To monitor the learning and performance of the task, the waveform of the whisker trace, the score = hit trials per total trials, as well as licking behavior was tracked. Extracellular multiunit spike activity in the FN, presumably the motor command for whisker movements, was recorded (The FN motor command was later used as a proxy to whisker protraction after the facial nerve had been cut). To detect FN bursts that relate to whisker movements, two thresholds (X and Y) were set and continually optimized. FN activity without movements should stay below X, while Y should

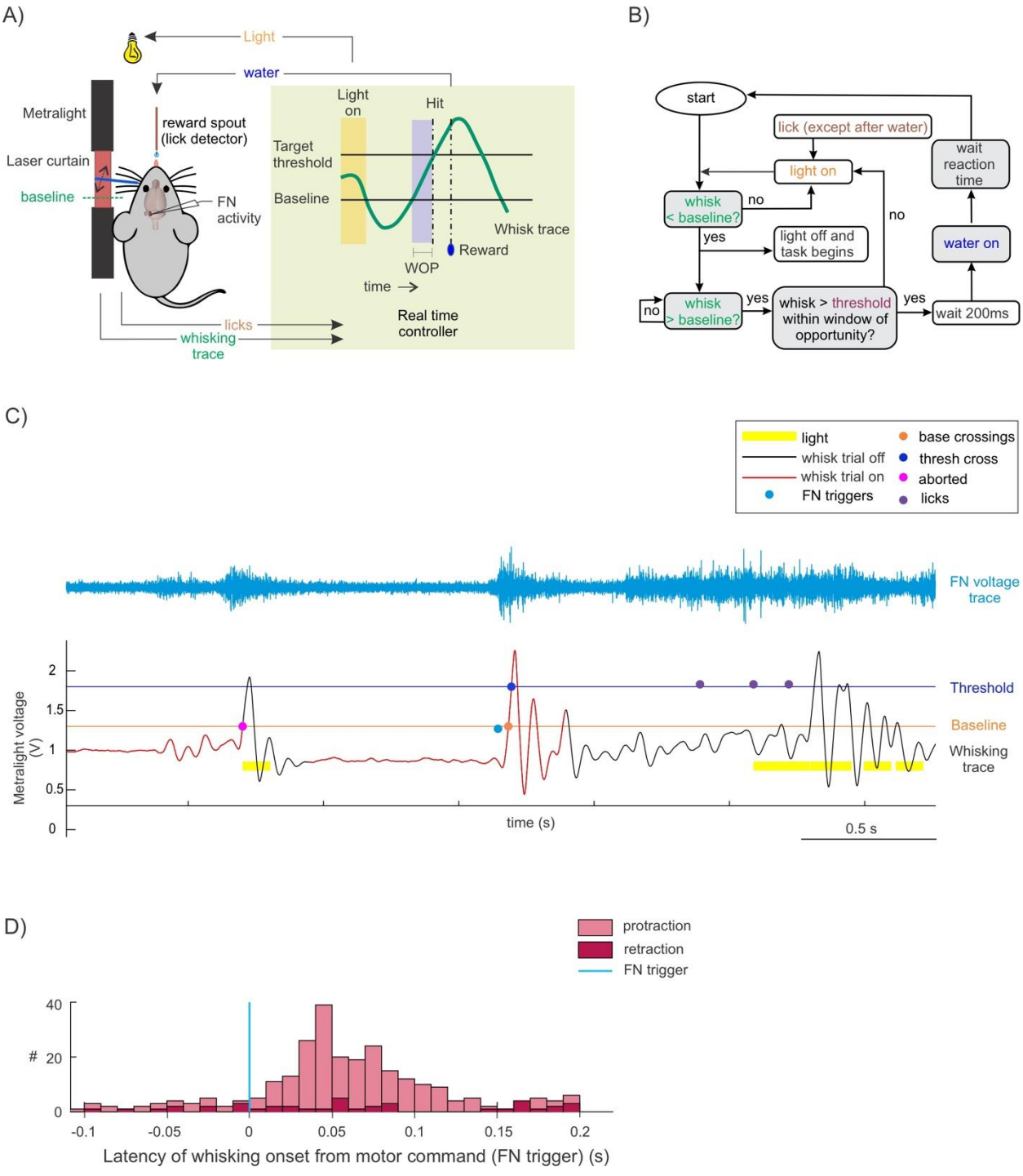
A)
Light
water
Metralight
reward spout
(lick detector)
Laser curtain
baseline
FN
activity
licks
whisking
trace
Light
on
Hit
Target
threshold
Baseline
Whisk trace
Reward
WOP
time
Real time
controller
B)
start
lick (except after water)
light on
wait
reaction
time
whisk
< baseline?
no
yes
light off and
task begins
no
water on
no
whisk
> baseline?
yes
whisk > threshold
within window of
opportunity?
yes
wait 200ms
C)
light
whisk trial off
whisk trial on
FN triggers
base crossings
thresh cross
aborted
licks
FN voltage
trace
Metralight voltage
(V)
2
1.5
1
0.5
0
Threshold
Baseline
Whisking
trace
time (s)
0.5 s
D)
protraction
retraction
FN trigger
40
#
20
0
-0.1
-0.05
0
0.05
0.1
0.15
0.2
Latency of whisking onset from motor command (FN trigger) (s)

Figure 15. Motor training.

A) Behavioral setup for the motor task, where the whisking trace was recorded by laser optical device (LOD), and sent to real-time controller. The task begins when the mouse brings its whisker below the baseline, and if the mouse protracts to cross the virtual baseline and threshold in the given window of opportunity (WOP), it gets a water reward. The delivery of water and light is controlled by Simulink's real-time controller. B) Flowchart of the task controlled by Simulink state engine or state flow. C) A snippet of an example session from animal 517-71. Whisking coincides with the FN activity. The red whisking trace shows the trial-on phase, and the black indicates trial-off. After FN trigger/motor command, there is a base crossing followed by a threshold cross. Water (not shown here) was rewarded after 200ms which was then followed by a lick. D) Latency of baseline crossings from the motor command.

be exceeded whenever a whisking movement was performed. All the behavioral parameters, along with the FN neural activity, were recorded using the MCRack software (Fig. 15C). After setting X and Y the latency of whisker movement upon a detected onset of a FN burst was monitored (Fig. 15D). At the end of the motor training, all mice were able to perform precise whisker reaches in air that were preceded by a discernible burst of FN activity. It took 2-3 weeks to train the animals to perform this motor task. Typically, mice were able to perform about 150 hit trials per session.

3.2.3. Facial motor nerve cut.

When the mice had learned the task and the conditions for the motor command were determined, a facial motor nerve was cut to open the reafference loop (Fig. 16) in the animals performing the ORL experiment (12 animals). Animals were anesthetized using the same procedure described above. The ipsilateral cheek area was shaved, and a vertical incision was made. Muscles were retracted to locate buccal and marginal nerves. A section from both buccal and marginal was dissected carefully and removed to reduce the chances of nerve regeneration. The skin was sutured back, and the animal was recovered using the antidots after injecting with a pain killer (carprofen). Loss of whisking was checked after the animal had recovered from the surgery. The nerve cut impeded any precise and large amplitude whisking movements across baseline and threshold. There were very low amplitude residuals of whisker movements generated passively by face movements.

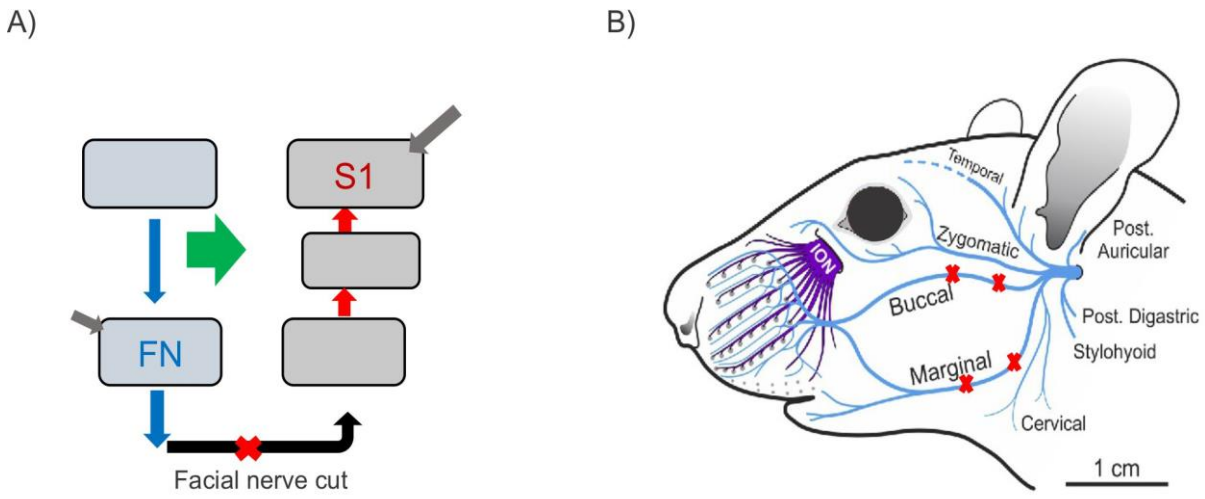

Figure 16. Facial nerve cut.

A) Schematic showing the opening of the reafference loop by cutting the facial motor nerve.
B) Mouse facial motor and sensory nerves. The buccal and Marginal motor nerves responsible for whisker movements were severed, and the part was removed.

3.2.4. Experiment and data collection.

Open reafference loop: Mice with interrupted facial nerve (Fig. 17) the presumed motor command in FN was used as a proxy for whisking (Fig 17A, B). FN activity was accepted as motor command if it fulfills the conditions set in the motor training (using thresholds X and Y). It triggered a whisker deflection via the piezo actuator after various delays. The experiment contained 4 kinds of stimuli (trial types). The most frequent one (10 out of a block of 13) delivered a stimulus after the onset of the motor command with the *predicted* delay (dP)). Rare trials (1/13) presented a whisker deflection *shifted* by a certain delay (dSh)). Further, in 1 out of 13 trials respectively, a *non-predicted* stimulus (without a motor command), and *omitted* stimulus (no stimulus after a detected motor command). Water reward was provided after all stimulus types except the non-predicted. A snippet from an example session is plotted in figure 17C, showing the stimulus types corresponding to motor command along with the spike and LFP responses evoked by the stimulus. The evoked neural responses to the whisker stimulation were recorded in the S1 barrel cortex using the implanted 2x2 electrode array in the specific barrel column. The array was

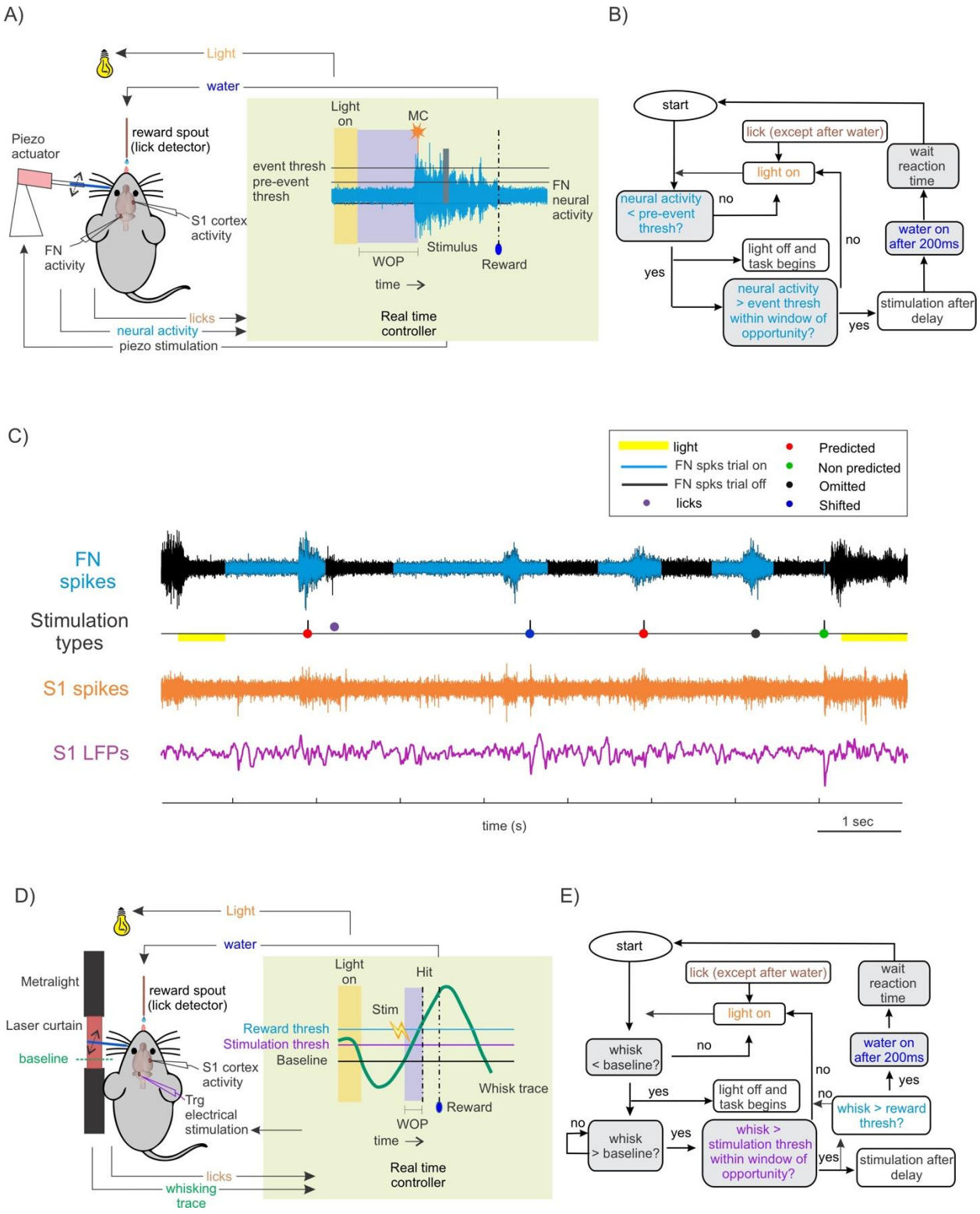
A)
Light
water
Piezo actuator
reward spout (lick detector)
S1 cortex activity
FN activity
licks
neural activity
piezo stimulation
Light on
MC
event thresh
pre-event thresh
FN neural activity
WOP
Stimulus
Reward
time
Real time controller
B)
start
lick (except after water)
light on
wait reaction time
neural activity < pre-event thresh?
no
light off and task begins
yes
neural activity > event thresh within window of opportunity?
yes
no
water on after 200ms
stimulation after delay
C)
light
FN spks trial on
FN spks trial off
licks
Predicted
Non predicted
Omitted
Shifted
FN spikes
Stimulation types
S1 spikes
S1 LFPs
time (s)
1 sec
D)
Light
water
Metralight
reward spout (lick detector)
Laser curtain
baseline
S1 cortex activity
Trg electrical stimulation
licks
whisking trace
Light on
Hit
Stim
Reward thresh
Stimulation thresh
Baseline
Whisk trace
Reward
WOP
time
Real time controller
E)
start
lick (except after water)
wait reaction time
light on
whisk < baseline?
no
water on after 200ms
yes
light off and task begins
no
yes
whisk > reward thresh?
no
whisk > baseline?
yes
whisk > stimulation thresh within window of opportunity?
yes
stimulation after delay

Figure 17. Experimental paradigm for ORL and CRL.

A) Behavioral task for ORL experiment. FN activity that's qualified as the motor command was recorded and used as a trigger for the piezo actuator to stimulate the whisker after a certain delay. Sensory response was recorded in S1 barrel cortex. Water reward was provided after a few milliseconds of stimulation. The task operates under controlled licks. The trigger for the piezo actuator and light & water delivery was controlled by Simulink real-time controller. Licks were checked via a lick sensor that inputs to real-time controller. MC= motor command, WOP= window of opportunity. B) Flowchart of the ORL task controlled by Simulink state engine or state flow. C) A snippet of an example session demonstrating all the stimulus types, their occurrence relative to motor command, and spike & LFP responses to the stimulation. The predicted stimulus was provided 100ms after the motor command, and shifted stimulus was provided 500ms after the motor command. D) Behavioral task for CRL experiment. Whisking was monitored by metralight LOD and used by the real-time controller to detect baseline and threshold crosses. The task initiates when the animal brings the whiskers below the baseline and proceeds when it protracts them simultaneously to cross the stimulation threshold to receive an electrical stimulation in the trigeminal nucleus and cross the reward threshold to get a water reward. Subsequent sensory response is recorded in S1 barrel cortex. All behavioral components like water, light, and electrical stimulation in trigeminal were controlled by Simulink real-time controller. E) Flowchart of the CRL task controlled by Simulink state engine or state flow.

moved from time to time to a different depth using the screw (Schwarz et al., 2010, Haiss et al., 2010) to record responses from different depths of the barrel column.

Closed reafference loop: The 3 trained animals (trained to the motor task) that had electrodes implanted in the trigeminal nucleus of the brainstem performed the CRL experiment. As the animals had intact facial motor nerves, the whisker movements could still be recorded. The whisker stimulation is replaced by the electrical stimulation in the trigeminal nucleus, triggered by the whisker protraction. The electrical stimulation in the trigeminal was in addition to the reafference signal and paired with the whisker protraction. In the experimental state flow (Fig. 17D, E), mice had to do a whisker protraction to get a water reward. Two virtual thresholds were determined in addition to the virtual baseline. The stimulation threshold and reward threshold. The reward threshold is similar to the threshold in motor tasks that needs to be crossed by the animal to get the water reward. The stimulation threshold is lower than the reward threshold to keep the stimulation closer to whisking onset and then include delays accordingly. The trial begins when the water-restricted mouse retracts its whisker below the virtual baseline at a rest position. After the mouse protracted and crossed the stimulation threshold, an electrical

micro-stimulation pulse in the trigeminal nucleus was given after a certain delay (0ms, 100ms, etc.). If the whisk has also crossed the reward threshold in the given opportunity time, a water reward was provided after 200ms. The same 4 stimulus types were presented in ORL and CRL experiments. Also, the recording in S1 was identical in CRL as in the larger part of the ORL experiments using a 2x2 electrode array implanted at a site in S1 that corresponded in terms of whisker represented in the trigeminal nuclei.

Data collection: All the neural and behavioral data were entered into the computer system using the multichannel interface card via analog and digital input ports. Voltage traces and other behavioral signals were watched in real-time and recorded using analog and digital channels of MC rack software. Voltage traces were recorded at a sampling frequency of 40 kHz for non-silicon array animals (n=10), and 20 kHz for silicon array animals (n=5), and a gain of 5000X using preamplifier and bandpass filters for respective spike and LFP traces. 2 sessions were performed each day for each animal. A single session could consist of 400-700 trials.

3.2.5. Histology

After the experiments were completed and the data was collected, animals were deeply anesthetized, and a current of 10 μA for 10 s was passed thrice through electrodes implanted in the facial and trigeminal nucleus in the respective animals and S1 electrodes. This was done to make electrolytic lesions and mark their positions. Afterward, a lethal dosage of sodium pentobarbital (10 mg per kg) was administered to the animal, and it was then subjected to transcardial perfusion using an isotonic saline solution. This was followed by perfusion with 4% paraformaldehyde. Subsequently, the brains were stored in a solution of 4% paraformaldehyde containing 30% sucrose at a temperature of 4 °C for a period of 2–3 days. Once sunk, the brains were sectioned at a thickness of 60 μm using a freezing microtome. Brainstem was prepared by a horizontal cut ventral to the cerebellum and a coronal cut roughly at the anterior-posterior coordinate of visual cortex. Thus, brainstem and neocortex were separated and could be sectioned separately at a thickness of 60 μm. Sections were stored in PBS (phosphate buffer saline) until

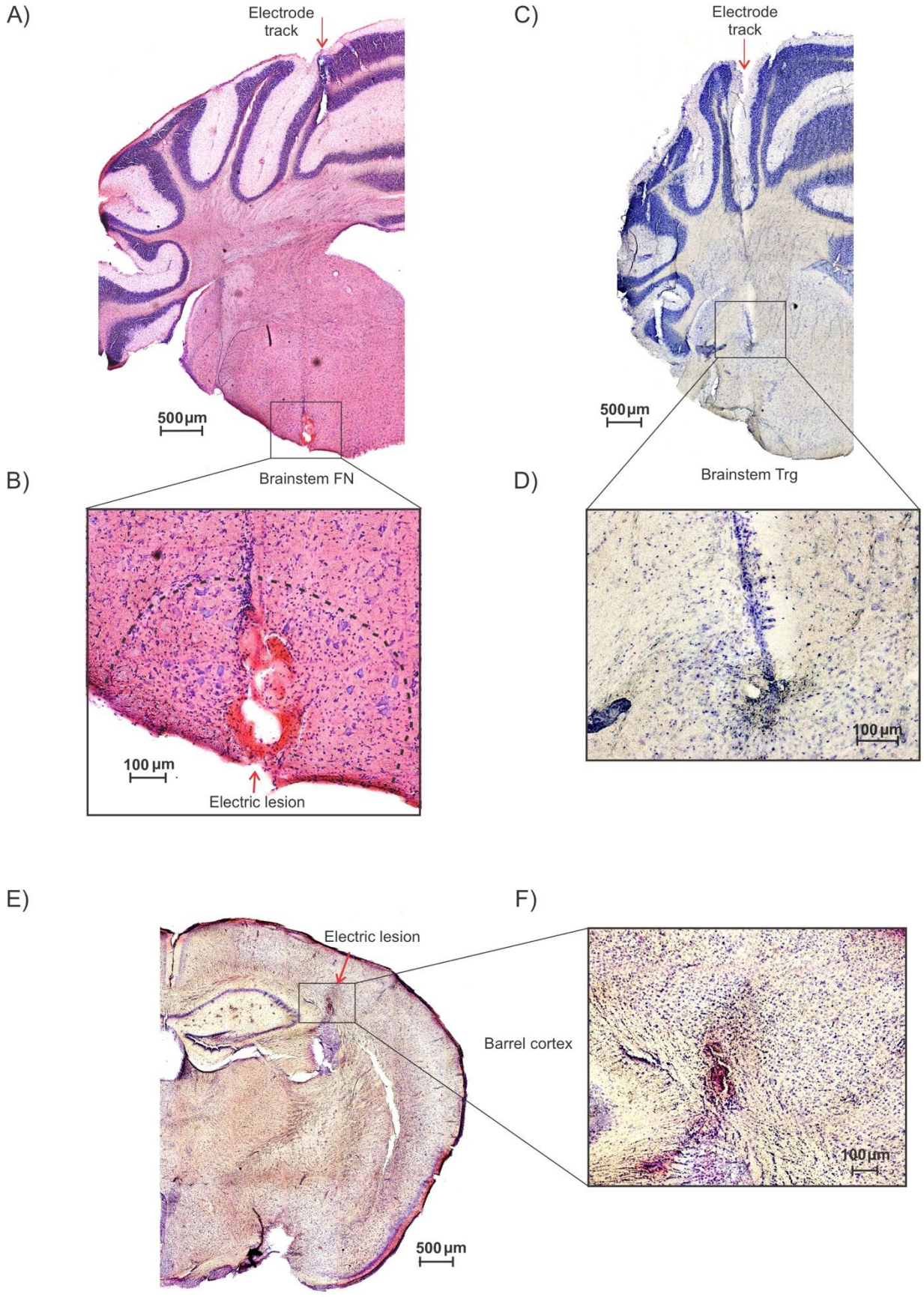
A)
Electrode track
500 µm
B)
Brainstem FN
100 µm
Electric lesion
C)
Electrode track
500 µm
Brainstem Trg
D)
100 µm
E)
Electric lesion
500 µm
F)
Barrel cortex
100 µm

Figure 18. Histology depicting lesions in the implanted brain areas.

A) Ipsilateral brainstem section processed with Nissl staining with eosin counterstain, showing electrode tract and electrolytic lesion. B) Magnified region of the facial nucleus in the brainstem depicting the lesion, evidence of electrode implanted in that area. C) Ipsilateral brainstem section processed with Nissl staining, showing electrolytic lesion in Pr5. D) Magnified trigeminal Pr5 with lesion. E) Contralateral cortex section processed with Nissl staining with eosin counter stain, depicting lesion in barrel cortex. F) Magnified barrel cortex region with a lesion.

processed. The sections for the FN and S1 lesions were processed for Nissl with eosin counter stain. The sections for trigeminal lesions were stained using Nissl stain only. The Cresyl violet staining (Nissl staining) is used to stain Nissl substances in the cytoplasm of neurons. Nissl substance is a basophilic material primarily composed of ribonucleic acid (RNA) and proteins in aggregate with the rough endoplasmic reticulum. The method employs a basic aniline dye that specifically stains RNA blue, serving as a means to emphasize significant structural characteristics of neurons. The Nissl substance, which comprises the rough endoplasmic reticulum, exhibits a dark blue hue owing to the staining of ribosomal RNA. This imparts a mottled appearance to the cytoplasm. DNA within the nucleus is stained similarly in a comparable color.

The sections were placed onto slides coated with gelatin and covered with a coverslip, and mosaic photomicrographs were captured using an Axio Imager Z2 microscope (Carl Zeiss Microscopy, Jena, Germany) equipped with a movable stage. The images of electric lesions for respective brain areas are shown in Fig. 18.

3.3. Data analysis

Data analysis was carried out using custom-built MATLAB scripts. The recorded data files were converted, and all the variables were saved in MATLAB format. Spikes were extracted by manually thresholding the signal and cut out waveforms and timestamps using a custom build MATLAB script. The spikes were sorted by comparing spike waveforms and delineating noise to differentiate single-unit and/or multiunit spike trains. Spike sorting was performed using Moksm Eckert spike sorter (Shan et al., 2017). The spikes responses with sorted spikes were visualized as a raster plot which is a simple

method to visually examine the trial-by-trial variability of the responses. The average of these spikes divided by the number of trials times the bin size is the spike rate. Spike rates were plotted in temporal relation to the external stimulus (also called peri-stimulus-time-histogram, PSTH). Raster plots and PSTHs were plotted for all stimulus types. LFP voltage traces were also plotted in relation to the whisker stimuli and averaged separately for each stimulus type. For population plots, spike rate and LFP - voltage responses for different stimulus types were normalized to the responses to the non-predicted stimulus.

Statistical analysis: The normalized response from all electrodes for a single experiment was averaged for individual stimulus types and plotted using Microsoft excel. The details on data arrangement and compilation can be found in appendix, Table 1 for all experiments and Table 2 for depth wise analysis for all experiments. The responses between non-predicted & shifted stimulus types and shifted & predicted stimulus types were compared for spikes and LFPs, using paired t-test. The paired t-test is a statistical procedure used to determine whether the mean difference between two sets of observations, which are dependent, is zero. GraphPad prism (Boston, USA) was used to perform all t-tests.

Effect sizes: The effect size in this study was quantified as the area under the receiver operating characteristic curve (AUC). This measure represents the probability of a binary classifier accurately classifying data points from two distributions when different thresholds are applied to mitigate observer bias. An AUC value of 0.5 indicates random performance, while values of 0 and 1 indicate complete discrimination. Effect sizes were determined between the non-predicted & shifted stimulus response (indicating sensory gating effect), shifted & predicted stimulus response (indicating state estimation effect), predicted & baseline response (indicating non prediction), and baseline & omitted response (indicating internal prediction).

LFP/CSD analysis: The actual depth of the electrode in the silicon array was determined using the current source density (CSD) analysis (Fig 19B). The LFP signal was processed from the original recordings by down-sampling to a frequency of 2kHz. It was further

refined through a low pass filtering procedure using a Butterworth filter with edge frequencies set at 1 and 200 Hz. The filter had a passband ripple amplitude of less than 0.5 dB and stopband attenuation exceeding 30 dB. The resulting matrix of LFP signals was then transformed into a current source density (CSD) map following the methodology described by (Nicholson and Freeman, 1975) and (Mitzdorf, 1985). CSD reports provided information on the entry and exit points of currents within the extracellular space, allowing me to designate negative CSD values as 'sinks' (colored blue in CSD maps) representing positively charged ions leaving the extracellular space or negatively charged ions entering the cellular compartment. Conversely, positive CSD values were referred to as 'sources' (colored red). I employed the 'kernel-based current source density method' as outlined by (Potworowski et al., 2012), which generated a two-dimensional CSD space spanning the silicon shanks. By incorporating binned trial time and session numbers, I obtained a four-dimensional matrix of CSD values. Subsequently, this matrix was averaged and cropped to produce matrices of reduced dimensionality (refer to Fig. 19). The pattern of sinks and sources in barrel cortex allowed me to locate layer 4 (L4) and the border between layer 5 and 6 (L5/6) and assign the location of my electrodes with respect to layer 4 (Fig 19A).

All the figures were edited and compiled using Corel Draw 2021.

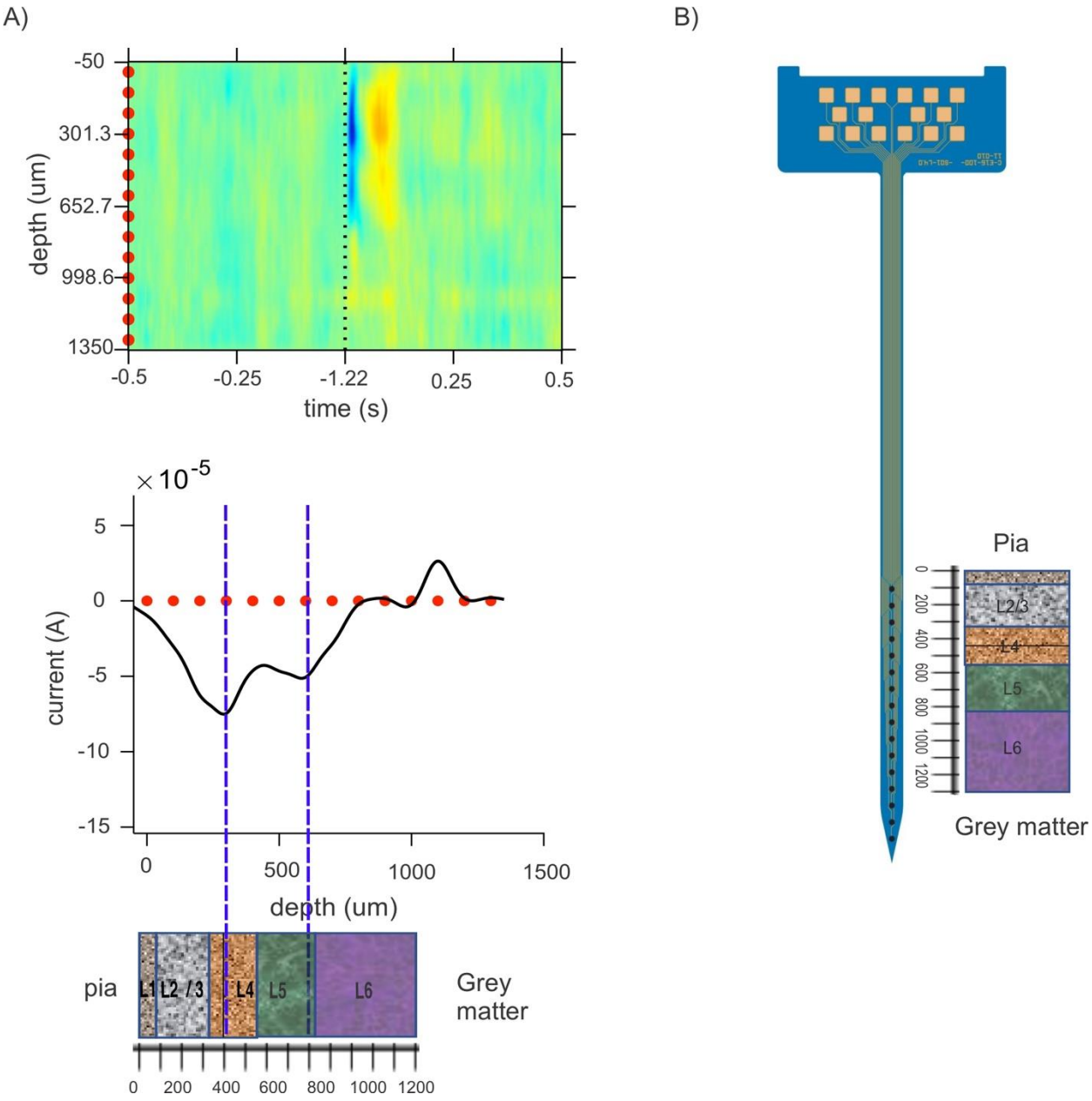

Figure 19. Current source density (CSD) analysis to determine the electrode depth in silicon arrays.

A) Current source density plot in an example session. The first plot depicts the distribution of current across the depth of the layers of the S1 barrel cortex. The second plot can be used to determine the electrode's actual depth. The first peak of the current sink is determined to be a reference point for mid-layer 4, and the second smaller peak could be used as a landmark for the border of layers 5/6. B) Aligning the electrodes in the silicon array to their actual depth along the layers of the S1 barrel cortex.

4. Results

4.1. Existence of two sensory attenuation processes, state estimation (SE) and sensory gating (SG).

The main objective of the study was to show the existence of the two processes that attenuate the sensory signals in the same experimental paradigm and disentangle them. To concur that experiments were performed on mice whisker system, which has a long history of study of sensorimotor integration and has been shown to exhibit reafference signals from whisking movements. Of the two experimental setups, I used an open reafference loop (ORL) setup for all experiments. The closed reafference loop (CRL) experimental setup was used as the control for the nerve cut to only show basic effects.

4.1.1. Basic effects in open reafference loop (ORL) experiment.

Experiments were performed to investigate the existence of the effects of two processes. It was hypothesized that the predicted stimulus would capture both SE and SG effects and the sensory response would be most attenuated, shifted stimulus would capture only the SG effect, and the sensory response will be less attenuated, and non-predicted trials will be free of any attenuating effects (cf. Fig. 10). The results in a total of 12 mice (7 implanted with tungsten electrode and 5 with silicon array) used for ORL experiments (as well as in 3 CRL mice see below) consistently supported this hypothesis, without exception. In figure 20A and B shows spike responses for each stimulus type as a raster plot overlain by the respective firing rate for a representative session (437 trials). In panel C, D the local field potential (LFP) for the same session is plotted. The average neuronal activity obtained on all electrodes, at all depths (80 electrodes, 563 sessions for spikes and 83 electrodes, 574 sessions for LFPs) across all 12 mice, normalized to the non-predicted stimulus are shown in panels E (colored dots) for spikes and LFPs. Each electrode activity (averaged across sessions at particular delay condition) is depicted in different shade of grey. For example, recordings at delay conditions dP=100ms, dSh=300ms; and dP=100ms, dSh= 500ms are depicted as different grey lines.

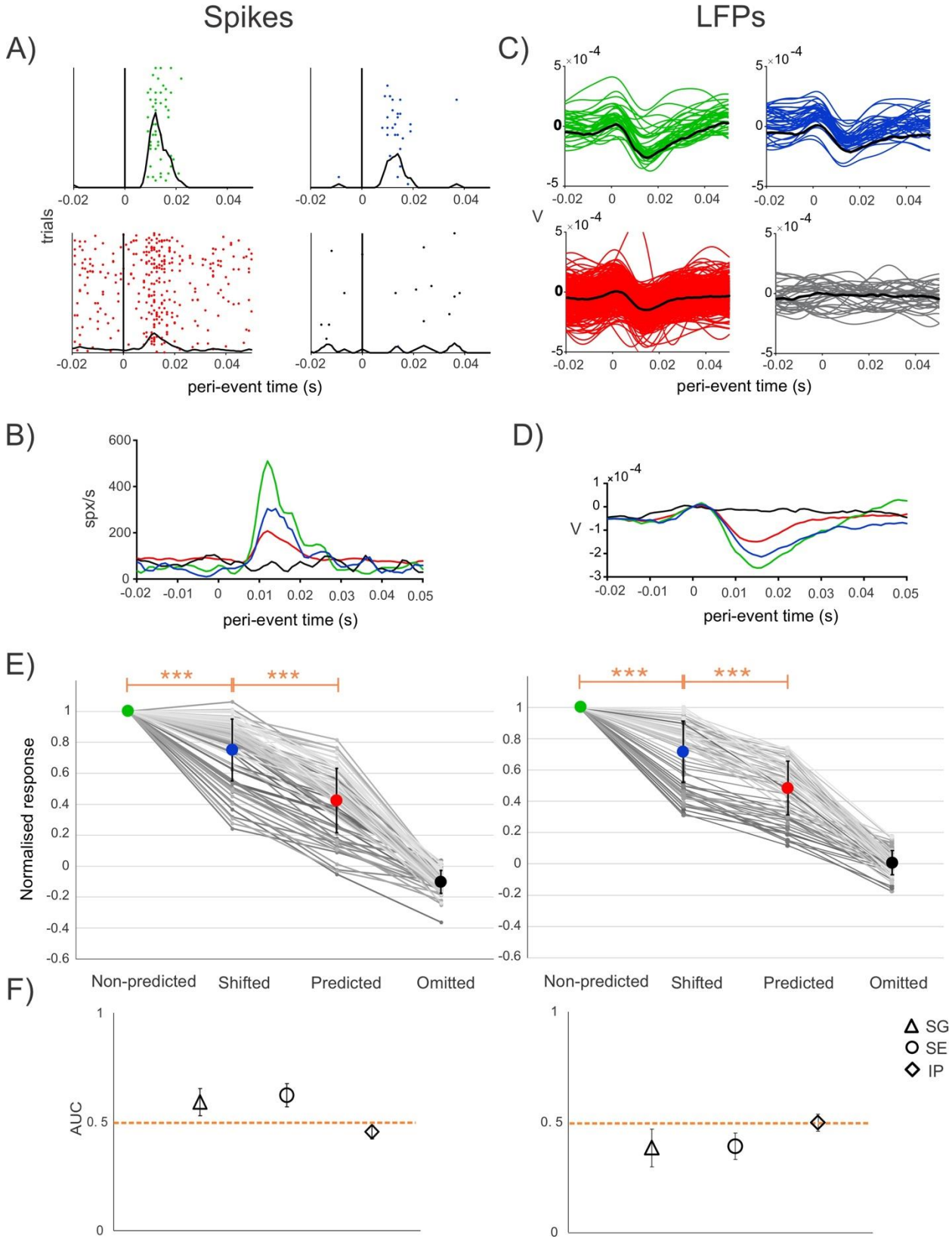
Spikes
LFPs
A)
C)
trials
peri-event time (s)
V
B)
D)
spx/s
E)
Normalised response
***
Non-predicted
Shifted
Predicted
Omitted
F)
AUC
SG
SE
IP

Figure 20. Demonstrating evidence of two sensory attenuation processes: State estimation (SE) and sensory gating (SG) in an open reafference loop (ORL) experiment.

The basic effects of both processes are shown with curves where the green color represents the non-predicted stimulus response, blue is shifted, red is predicted, and black is omitted. dP= prediction delay, time of predicted stimulus from the onset of the motor command. dSh= shifted delay, time of shifted stimulus from the onset of the motor command.
A to D. A representative session, with a total of 437 trials. dP= 100ms, dSh= 500ms. A) Raster plot demonstrating spike responses for all stimulus types in a single session. B) Spike PSTH, averaged across corresponding trials. C) LFP voltage traces for all stimulus types. D) Average LFP across corresponding trials.
E) Spike (left) and LFP (right) response relative to non-predicted stimulus response. All the responses are normalized to non-predicted response. Each grey line depicts each electrode averaged across sessions for a single delay condition. Solid corresponding color dots depict the average response across all electrodes (n=80 for spikes and n=83 for LFPs) from all 12 mice animals. Error bars show standard deviation. Delay conditions: dP=100ms, dSh=multiple (300,400,500ms). Shifted stimulus response is significantly smaller than the non-predicted stimulus response; the difference is extremely statistically significant, determined by one sample, two-tailed t-test with p-value smaller than 0.0001, which signifies the effect of attenuation in shifted response by SG. The predicted stimulus response is significantly smaller than the shifted stimulus response, the difference is extremely statistically significant, determined by paired two-tailed t-test with p-value smaller than 0.0001, which signifies the effect of SE. Statistical results are concurrent in both spikes and LFPs.
F) Comparison of responses in different stimulus types to determine the significance of SE and SG effects in spikes and LFPS. Effect sizes (area under ROC curve; AUC) are quantified between responses in non-predicted vs. shifted (SG), shifted vs. predicted (SE), and baseline vs. omitted (IP). Error bars depict standard deviation. The Orange dotted line depicts AUC=0.5, which signifies random performance where the two conditions are indistinguishable and have no discriminative power.

The difference in responses between non-predicted and shifted signifies the effect of SG, and between shifted and predicted signifies the effect of SE. A negative slope from non-predicted to shifted is shown by 77 of 80 electrodes for spikes and 81 of 83 electrodes for LFPs. All electrodes, 80 spikes and 83 LFPs showed a negative slope from shifted to predicted. The t-test was performed to compare non-predicted and shifted; and shifted and predicted, the two-tailed p-value was less than 0.0001 for both spikes and LFPs. The shifted response was significantly smaller than the non-predicted response and the predicted response was significantly smaller than the shifted response. In other words, the differences that signify SG and SE are highly significant in spike and LFP responses. To quantify the effects of SE and SG, measured effect sizes (MES) were evaluated by computing the area under the curve (AUC) for SG (non-predicted response vs. shifted response), SE (shifted response vs. predicted response), and IP (Baseline response vs

omitted response) (Fig.20F). The effect size is defined as the area under the receive operating characteristic curve (AUC, see Methods, AUC=0.5 signifies random performance, while the AUC values of 0 and 1 signify perfect discrimination). Results in Fig. 25F show that the AUC for SG (0.59, std= ±0.06) and SE (0.62, std= ±0.05) are higher than 0.5 in spikes and AUC for SG (0.38, std= ± 0.08) and SE (0.39, std= ± 0.06) are lower than 0.5 in LFPs (due to the positive sign of spike response and the negative sign of LFP response with neuronal excitation). It is further important to point out that the average spike response was less than zero (one sample t-test, n=80, p<0.0001; mean AUC 0.45) and the LFP response was only slightly positive in the Omitted trials (one sample t-test, n=83, p=0.37; mean AUC 0.49). In summary, neuronal responses show maximally consistent decrements in response strength form non-predicted (green) to shifted (blue) and to predicted (red) stimuli. These results strongly support the hypothesis (cf. Fig. 10) that two movement processes attenuate the sensory signal, one around the predicted stimulus, the other at other times during the stimulus.

4.1.2. Basic effects in closed reafference loop (CRL) experiment.

To support my hypothesis, but with intact reafference loop (intact facial motor nerve), experiments were performed where the physical whisker stimulation was replaced by electrical stimulation in the trigeminal nuclei, triggered by the whisker movement (protraction). This served as a control for brain plasticity and a situation where the animal could be learning different things when the whisker was immobilized. Identical to Fig. 20, an example session is shown in Fig. 21A; the effects of SG and SE were demonstrated using spike rates and LFPs, each electrode averaged across sessions for a delay condition of predicted delay 100ms and shifted delay 300ms. Average responses among electrodes for spikes (n=3, 14 sessions) and LFPs (n=2, 9 sessions), relative to non-predicted stimulus, are shown in different colors corresponding to different stimulus types for all 3 animals (Fig. 21B). The response in shifted trials is attenuated in comparison to the response in non-predicted trials, and the response in predicted trials is attenuated more than shifted trials, as can be seen in the Fig. 21B.

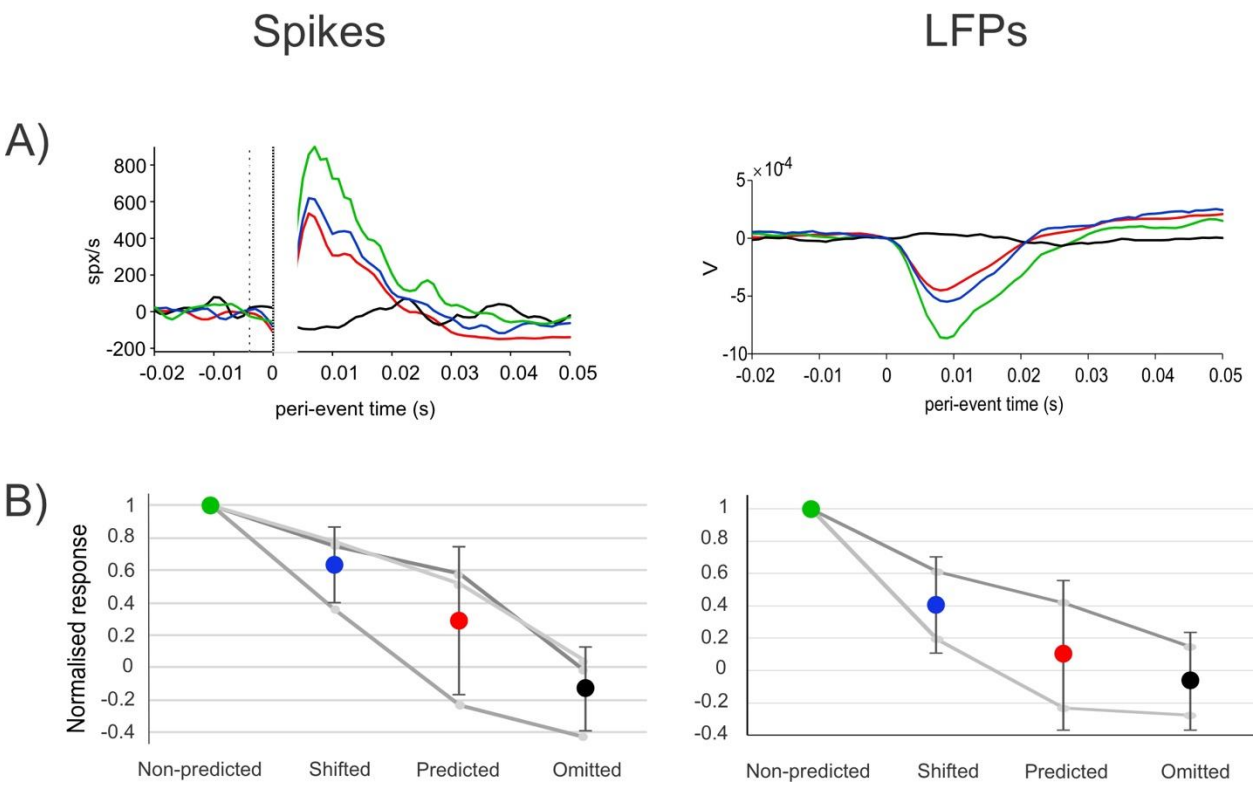

Figure 21. Demonstrating effects in closed reafference loop (CRL) experiment.

The basic effects of both processes are shown with curves where the green color represents the non-predicted stimulus response, blue is shifted, red is predicted, and black is omitted.
A) A representative session with Spike PSTH, averaged across corresponding trials and average LFP across corresponding trials.
B) Spike (left) and LFP (right) response relative to non-predicted stimulus response. Each grey line depicts each electrode averaged across sessions for a delay condition, dp=100ms, dSh=300ms. Solid corresponding color dots depict the average response across all electrodes (n=3, 14 sessions for spikes and n=2, 9 sessions for LFPs) from 3 mice.

4.1.3. Basic effects across layers of S1 barrel cortex.

As the two effects seem similar in their action, there are some characteristics that disentangle the two effects from each other, one of which is the site of origin. As we know from previous studies that sensory gating is a top-down mechanism with cortical origin and is also present in the trigeminal brainstem nucleus. Hence to differentiate the two, it is important to investigate and report the site of origin of State estimation. Since the information from layer 2/3 and layer 4 could be crucial to determine the site of integration, a depth wise analysis was performed from the recordings of silicon array shanks to check

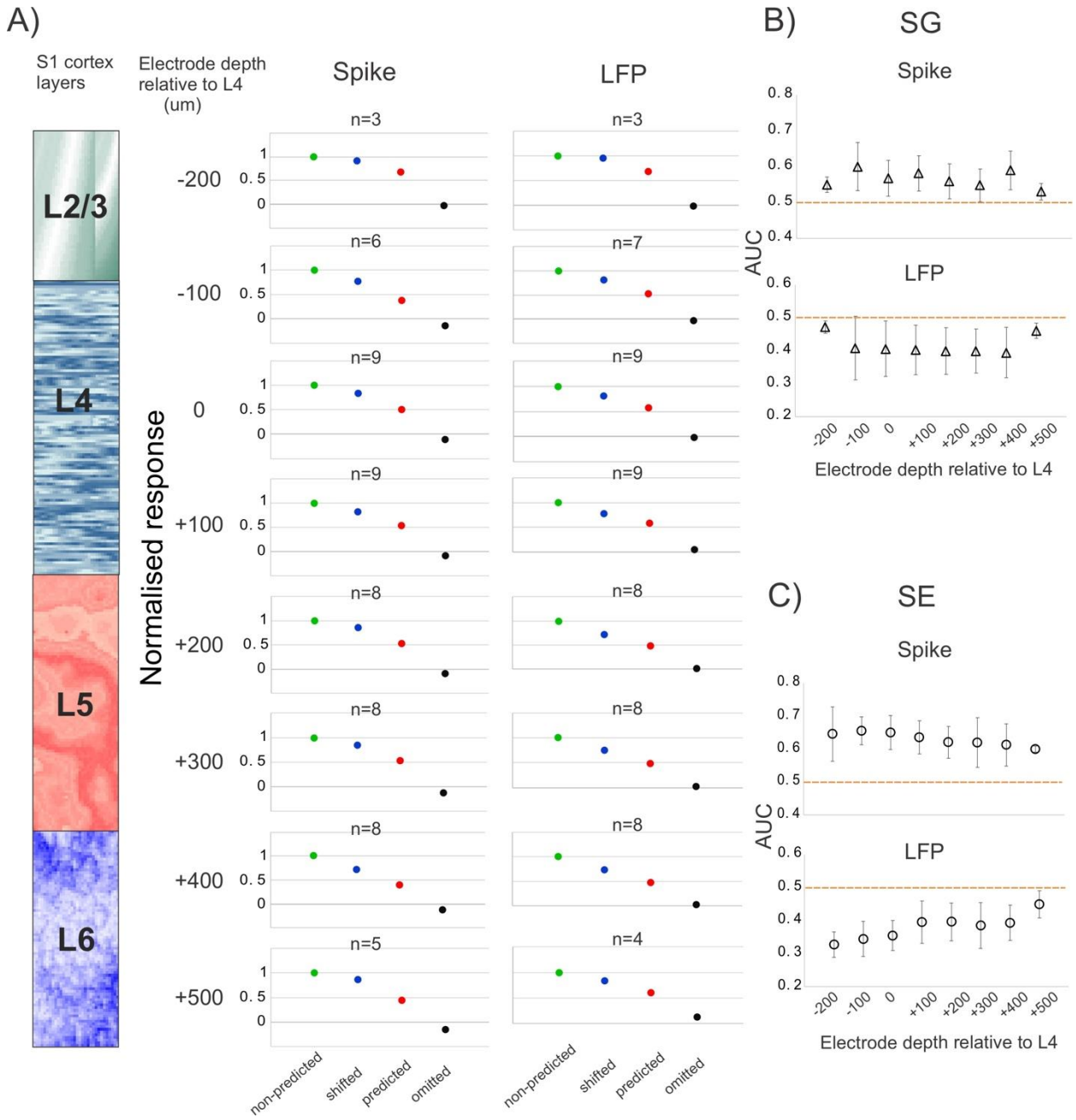

Figure 22. Effects across the layers of the S1 barrel cortex.

A) Spike (left) and LFP (right) responses relative to non-predicted stimulus response. Solid corresponding color dots depict the average response across all electrodes at the same depth from all 5 mice at different delay conditions. Delay conditions: dP=100ms, dSh=multiple (300,400,500ms). Electrodes are arranged relative to layer 4 of the S1 barrel cortex.
B to C: Comparison of responses in different stimulus types to determine the significance of SE and SG effects in spikes and LFPS. Error bars depict standard deviation. The Orange dotted line depicts AUC=0.5, which signifies random performance where the two conditions are indistinguishable and have no discriminative power. B) Effect size of SG (non-predicted vs shifted) across all layers, spikes, and LFPs. C) Effect size of SE (shifted vs. predicted) across all layers, spikes, and LFPs.

the spread of SE and SG effects across all layers of S1 barrel cortex. The recordings from tungsten wire electrodes were only confined to certain depths of barrel column and thus excluded from the analysis.

Silicon array was implanted in 5 mice, and recordings were performed at Layers 2/3 to layer 6 of the S1 barrel cortex, simultaneously. Electrodes were arranged relative to layer 4 by using the CSD (current source density) analysis and averaged across all animals. As shown in Fig. 22, all the electrodes show a significant difference in Non predicted and shifted stimulus response and shifted and predicted stimulus response in both spikes and LFPs, which shows the existence of both SG and SE, respectively. Effect sizes were also measured, and all electrodes demonstrated AUC values of more than 0.5 of both SG (Fig. 22B) and SE (Fig. 22C) in spikes and less than 0.5 in LFPs (due to the opposite sign of LFP). This shows that the effects are spread across all layers of the S1 barrel cortex.

Having disentangled SE and SG and studied their spatial distribution across layers in S1 the following sections deal with their precision or temporal extent.

4.2. Precision of the effect of State estimation (SE).

To check the precision in the working range of state estimation around the learned stimulus delay, an experimental paradigm was designed where the shifted stimulus trials, capturing only the SG effect, were moved in session-wise fashion towards the predicted stimulus trials, reducing the difference in the time delay between them, as depicted in the hypothesis in Figure 23A. Predicted stimulus trials were most attenuated with SG and SE effects, and the predicted delay was kept fixed. The aim was to investigate the time delay at which the shifted stimulus trials as well started to capture the effect of SE. The experiment was performed at 3 different shifted delays with the difference between shifted and predicted stimulus delay (Δ) of: Δ= 100ms, 50ms, and 10ms. The responses were averaged from individual electrodes from 5 animals for each delay, dP=200ms (spikes n=16, LFPs n=17), dP=150ms (spikes n=16, LFPs n=17) and dP= 110ms (spikes n=16, LFPs n=17). As demonstrated in Fig. 23B, the difference in shifted and predicted stimulus response is significant with Δ= 100ms and Δ= 50ms. At Δ= 10ms, however, the difference

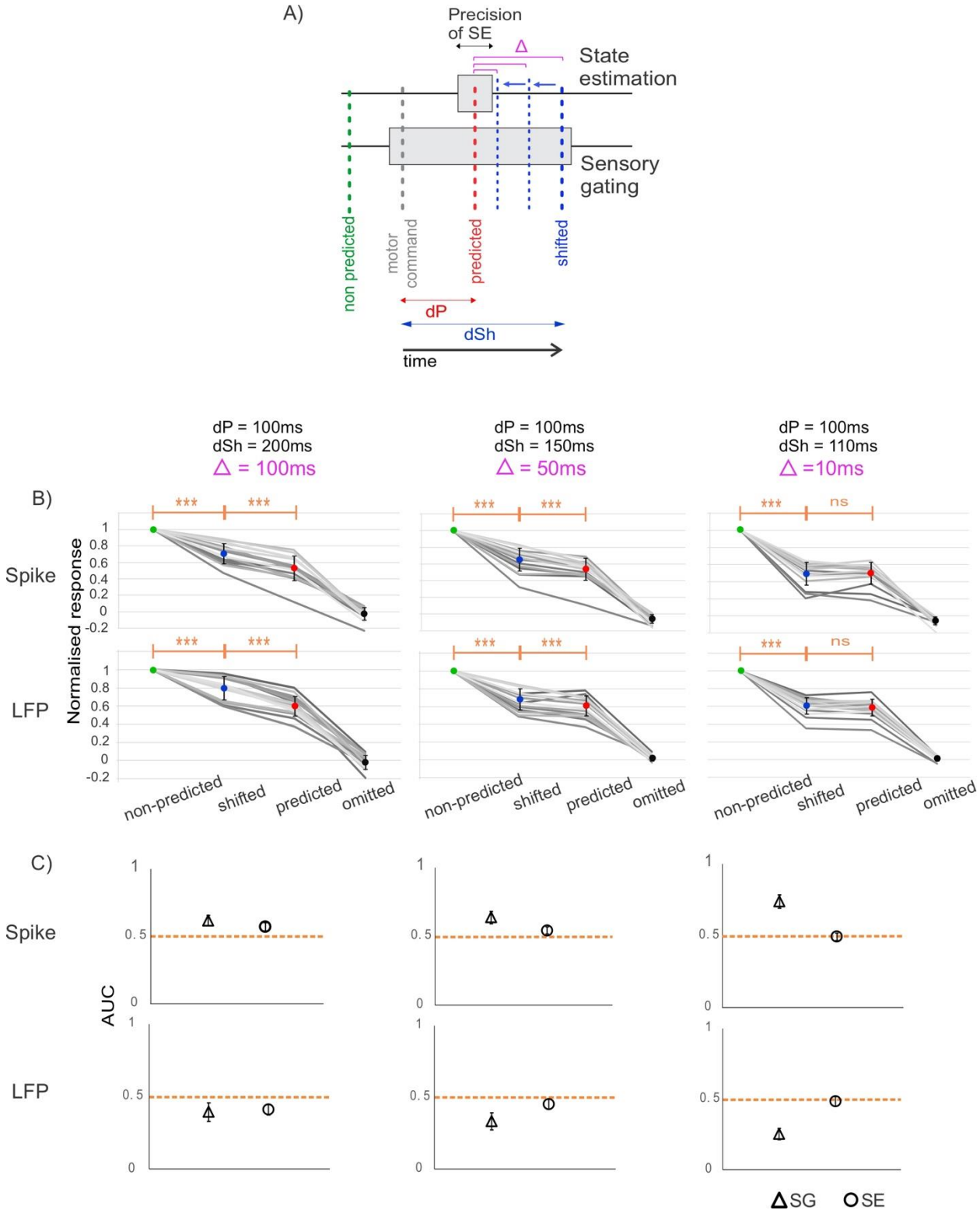
A)
Precision of SE
Δ
State estimation
Sensory gating
non predicted
motor command
predicted
shifted
dP
dSh
time
dP = 100ms
dSh = 200ms
Δ = 100ms
dP = 100ms
dSh = 150ms
Δ = 50ms
dP = 100ms
dSh = 110ms
Δ =10ms
B)
Spike
LFP
Normalised response
***
ns
non-predicted
shifted
predicted
omitted
C)
Spike
LFP
AUC
SG
SE

Figure 23. The precision of the effect of State estimation.

A) Hypothesis figure. dP= prediction delay, time of predicted stimulus from the onset of the motor command. dSh= shifted delay, time of shifted stimulus from the onset of the motor command. ∆= time difference between predicted and shifted stimulus. Shifted stimulus moves towards the predicted stimulus, and the difference goes to 10ms from 100ms.
B) Spike and LFP responses relative to non-predicted stimulus-response. Each grey line depicts each electrode averaged across sessions for a single delay condition. Solid corresponding color dots depict the average response across all electrodes (n=16 for spikes and n=17 for LFPs) from all animals (n=5). Error bars show standard deviation. Delay conditions: dP=100ms, dSh= 200,150,110ms.
At ∆=100ms, the predicted stimulus response is significantly smaller than the shifted stimulus response, the difference is extremely statistically significant, determined by paired two-tailed t-test with a p-value smaller than 0.0001 in both spikes and LFPs.
At ∆=50ms, the predicted stimulus response is significantly smaller than the shifted stimulus response, the difference is extremely statistically significant, determined by paired two-tailed t-test with a p-value smaller than 0.0001 in spikes and p=0.0004 in LFPs.
At ∆=10ms, the predicted stimulus response is not significantly smaller than the shifted stimulus response, the difference is not statistically significant, determined by paired two-tailed t-test with a p-value equal to 0.663 in spikes and p=0.090 in LFPs.
C) Comparison of responses in shifted and predicted stimulus type in spikes and LFPs to determine the significance of the difference between the two. Effect sizes (area under ROC curve; AUC) are quantified at ∆=100ms, 50ms, and 10ms. Error bars depict standard deviation. The Orange dotted line depicts AUC=0.5, which signifies random performance where the two conditions are indistinguishable and have no discriminative power. At ∆=100ms and 50ms, AUC≠0.5 in both spikes and LFPs, which signifies the shifted and predicted response to be different; but at ∆=10ms, AUC~0.5, the two conditions are similar or indistinguishable.

becomes non-significant, indicating that the shifted and predicted stimulus trials are equally attenuated, showing the presence of both SG and SE in both shifted and predicted stimulus trials. The effect size (Fig. 23C) between shifted vs. predicted reduced when moving from ∆= 100ms to ∆= 50ms. And at ∆= 10ms, the two conditions were inferred as inseparable, or the latter is larger with AUC 0.5 and less, respectively. The result was concurrent in both spikes and LFPs.

The response in different layers is shown in Fig 24. The effect size between shifted vs. predicted reduced when moving from ∆= 100ms to ∆= 50ms, and at ∆= 10ms the two conditions were inferred as inseparable. The result is concurrent in both spikes and LFPs.

These results strongly suggest that the SE is effective within a time interval less than 50ms around the delay of the predicted stimulus after motor command onset.

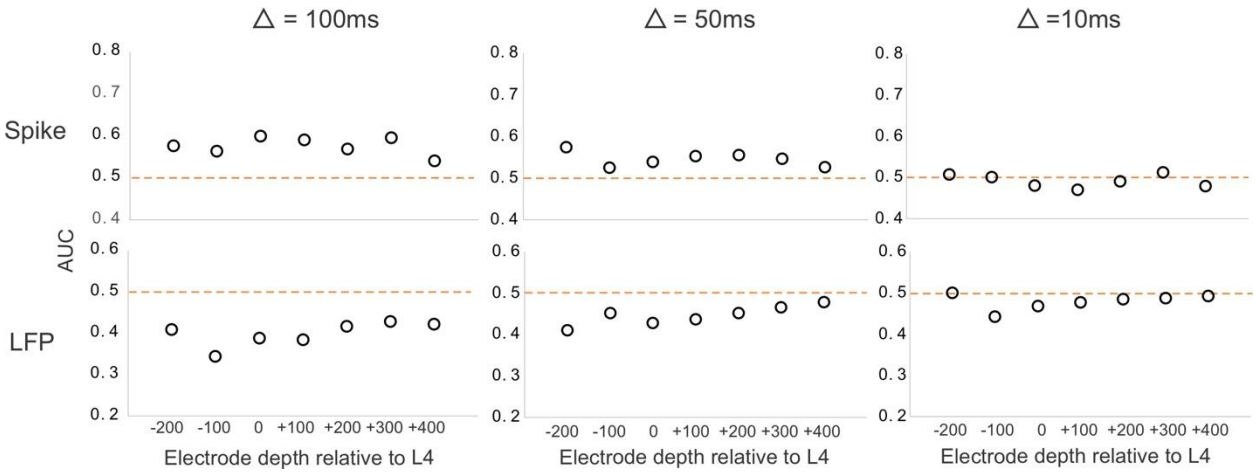

Figure 24. Precision of the effect of SE across the layers of S1 barrel cortex.

Effect sizes (area under ROC curve; AUC) across layers of S1 barrel cortex, between shifted & predicted response in spikes and LFPs. AUC is computed at ∆=100ms, 50ms, and 10ms. The response across all electrodes is averaged at the same depth from 2 mice. Delay conditions: dP=100ms, dSh=200,150,110ms. Electrodes are arranged relative to layer 4 of the S1 barrel cortex. The Orange dotted line depicts AUC=0.5, which signifies random performance where the two conditions are indistinguishable and have no discriminative power. At ∆=100ms and 50ms, AUC≠0.5 in both spikes and LFPs, which signifies the shifted and predicted response to be different; but at ∆=10ms, AUC=0.5, the two conditions are similar or indistinguishable. The results were concurrent across all layers of the S1 barrel cortex.

4.3. Adaptive features of State estimation (SE).

4.3.1. Learning the effect of SE at different delays.

In weakly electric fish Bell (1982) demonstrated that SE related attenuation is a learning process. Here I attempted to estimate an upper bound of repetitions of stimulus presentations needed to learn SE in mice. Mice were first trained to the predicted delay of 100ms until they successfully showed a significant difference between SE and SG (i.e., significantly different attenuation of the tactile signal to the predicted and shifted stimuli). Next, they were re-trained to a predicted delay of 200ms. I then compared the last session that displayed both the effects before the switch with the first session after the switch (termed “pre-switch” and “post-switch” sessions). Figure 25 (format as in Fig. 23) shows highly significant presence of SE and SG type of attenuation in the normalized responses

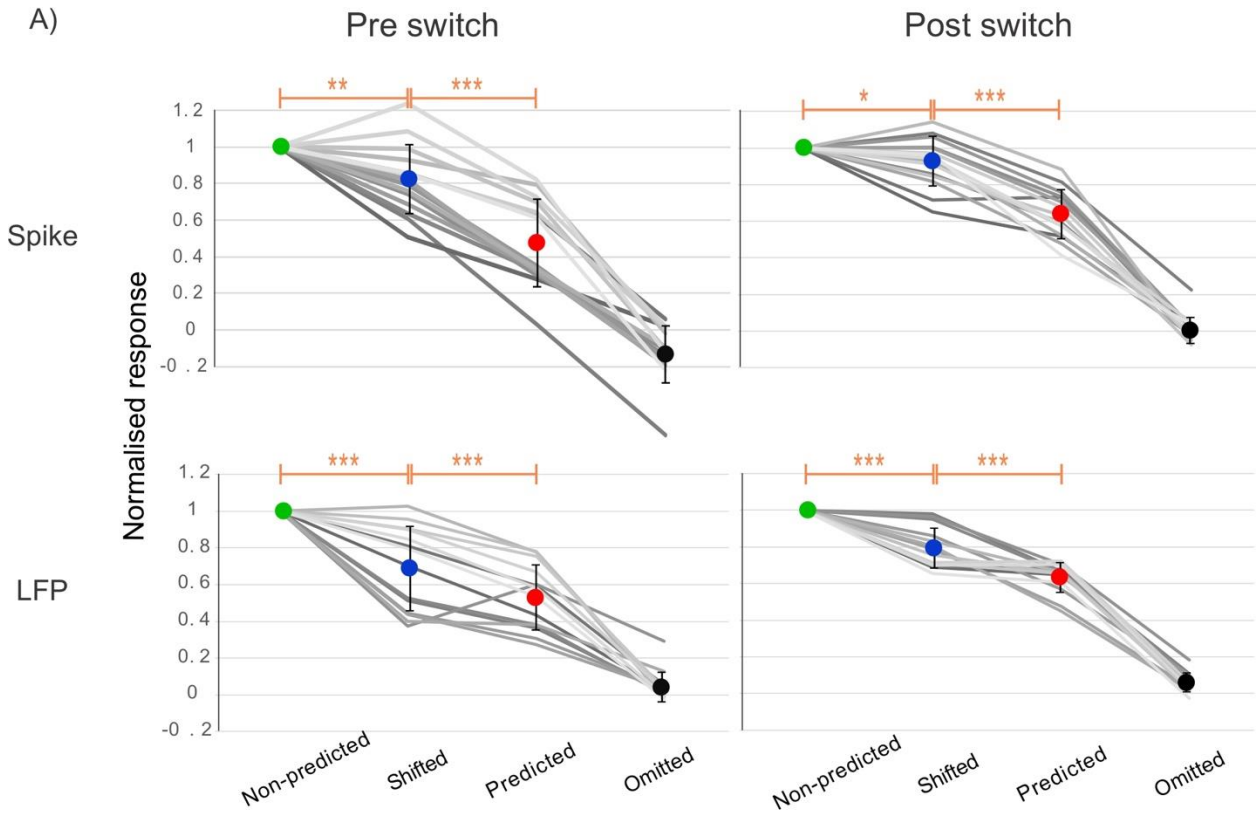
A)
Pre switch
Post switch
Spike
LFP
Normalised response
**
***
*
***
1.2
1
0.8
0.6
0.4
0.2
0
-0.2
Non-predicted
Shifted
Predicted
Omitted

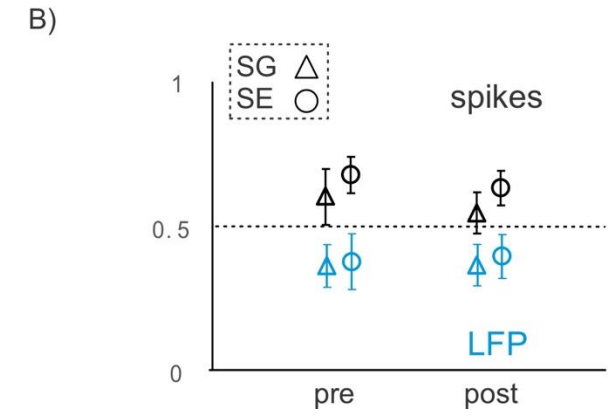
B)
SG △
SE ○
spikes
LFP
1
0.5
0
pre
post

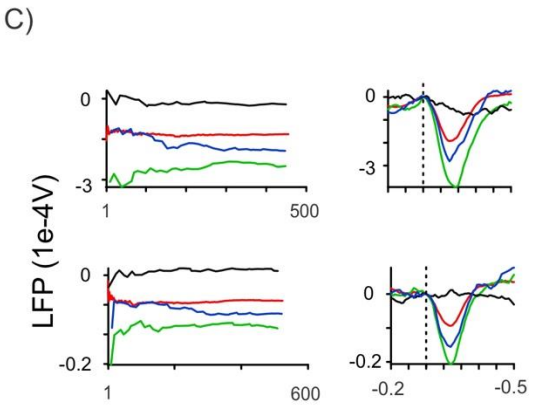
C)
LFP (1e-4V)
0
-3
1
500
-0.2
600
-0.5

Figure 25. Latency of learning to a different predicted delay.

A) Spike and LFP responses relative to non-predicted stimulus-response. Each grey line depicts each electrode for respective pre-switch or post switch session. Solid corresponding color dots depict the average response across all electrodes (n=15 for spikes and n=14 for LFPs) from 4 mice. Error bars show standard deviation. Delay conditions: dSh= multiple (300,400,500ms); for pre switch, dP= 100ms and for post switch dP= 200ms. In both pre-switch and post-switch conditions, the predicted stimulus response is significantly smaller than the shifted stimulus response, the difference is extremely statistically significant, determined by paired t-test, two-tailed with p-value < 0.001, which signifies the effect of SE. Statistical results are concurrent for both spikes and LFPs. In spikes responses, the shifted stimulus response is also significantly smaller than the non-predicted stimulus response; the difference is statistically significant, determined by one sample, two-tailed t-test with p=0.002 and p=0.05 in pre and post conditions, respectively, which signifies the effect of attenuation in shifted response by SG. LFPs show extremely significant SG.
B) Comparison of responses in different stimulus types to determine the significance of SE and SG effects in spikes and LFPS for pre-switch and post-switch conditions. Effect sizes (area under ROC curve; AUC) are quantified between responses in non-predicted vs. shifted (SG), shifted vs. predicted (SE). Error bars depict standard deviation. The Orange dotted line depicts AUC=0.5, which signifies random performance where the two conditions are indistinguishable and have no discriminative power.
C: Averages of LFP responses cumulatively averaged across trials. Data from two mice are shown (top and bottom graphs). The split of responses to Predicted and to Shifted occurs within the first 150-200 trials.

already in the post-switch session (Fig. 25A), as well as corresponding effect sizes (Fig. 25B). The results thus suggest that the latency of learning SE in response to a newly timed stimulus delay is within one session which was between (300-550 trials). To find out when during the post-switch session, the attenuation started to appear, I calculated a cumulative mean of the stimulus responses across the trials in this session in two mice (Fig. 25C). The LFPs clearly show that in the beginning SE and SG attenuations coalesced, and separated again after some 100-200 trials, indicating that a new stimulus can be learned within a few hundred trials.

4.3.2. Range of the effect of State estimation (SE) from the onset of motor command.

Next, the pairing of predicted stimuli with the motor command was provided at different time points to investigate at which stimulus delays with respect to motor command onset SE can be learned. Delays of predicted stimulus at 0ms, 200ms, and 400ms were trained. At 0ms and 200ms predicted delay SG and SE was readily observed and significant in

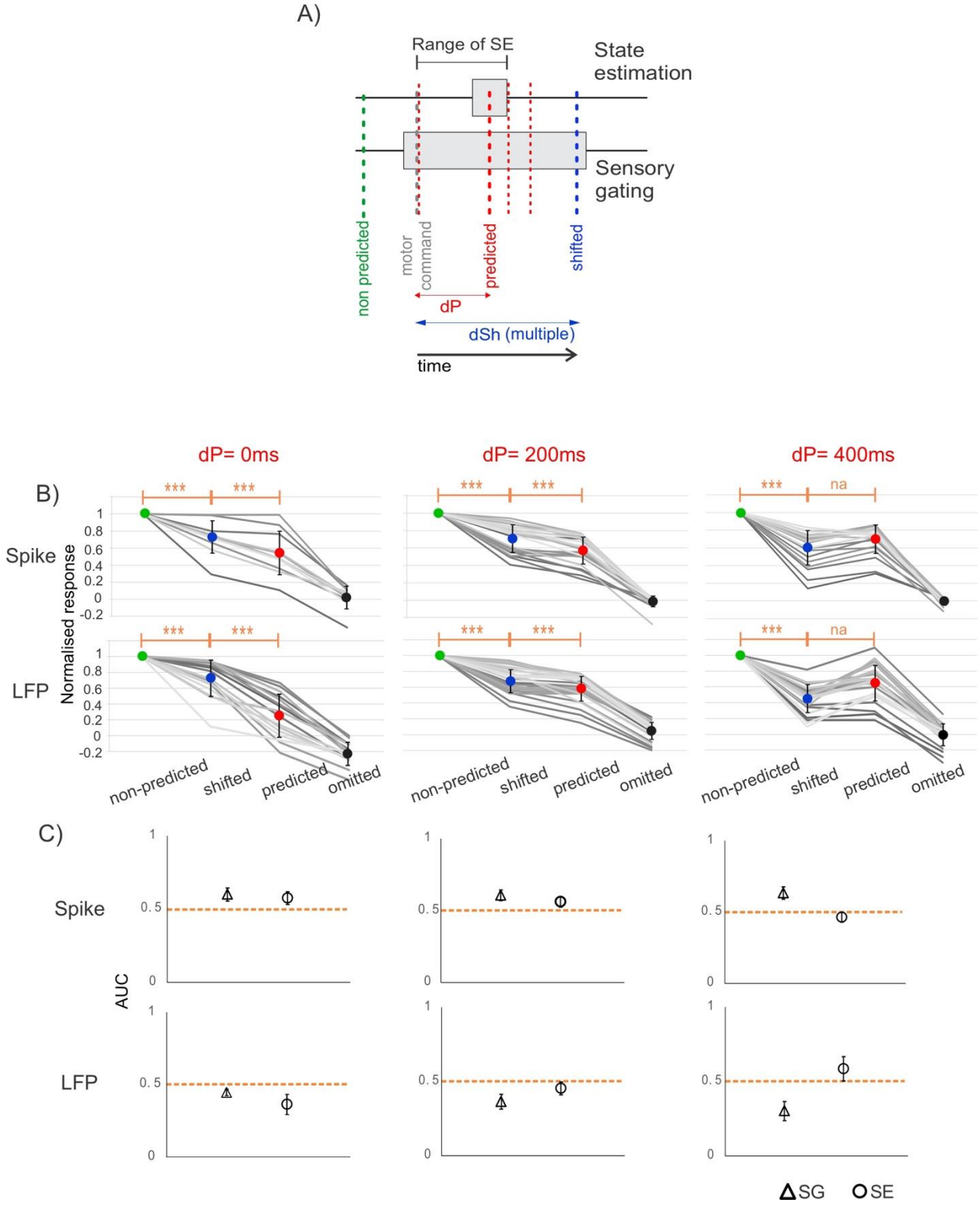
A)
Range of SE
State estimation
Sensory gating
non predicted
motor command
predicted
shifted
dP
dSh (multiple)
time
dP= 0ms
dP= 200ms
dP= 400ms
B)
Spike
LFP
Normalised response
***
na
non-predicted
shifted
predicted
omitted
C)
AUC
SG
SE

Figure 26. Range of the effect of SE from motor command and adaptation at different delays.

A) Hypothesis figure. dP= prediction delay, time of predicted stimulus from the onset of the motor command. dSh= shifted delay, time of shifted stimulus from the onset of the motor command. Predicted stimulus moved to different delays from movement onset or motor command.
B) Spike and LFP responses relative to non-predicted stimulus response. Each grey line depicts each electrode averaged across sessions for a single delay condition. Solid corresponding color dots depict average response across all electrodes for dP=0ms, 200ms, and 400ms and dSh= multiple (300,400,500ms). Error bars show standard deviation.
At dP=0ms, responses from electrodes (n=11 for spikes and n=16 for LFPs) are averaged from 4 mice. At dP=200ms, responses from electrodes (n=23 for spikes and n=30 for LFPs) are averaged from 6 mice. At dP=400ms, responses from electrodes (n=20 for spikes and n=24 for LFPs) are averaged from 4 mice.
At dP=0ms and 200ms, the predicted stimulus response is significantly smaller than the shifted stimulus response, the difference is extremely statistically significant, determined by paired t-test, two-tailed with a p-value smaller than 0.0001, which signifies the effect of SE. Statistical results are concurrent in both spikes and LFPs.
At dP=400ms, the predicted stimulus response is not significantly smaller than the shifted stimulus response, but larger. SE effect is not significant. The difference is still significant, determined by paired two-tailed t-test with a p-value smaller than 0.0001. Statistical results are concurrent in both spikes and LFPs.
C) Comparison of responses in shifted and predicted stimulus type to determine the significance of SE effect in spikes and LFPs. Effect sizes (area under ROC curve; AUC) for shifted vs. predicted are quantified at dP=0ms, 200ms, and 400ms. Error bars depict standard deviation. The Orange dotted line depicts AUC=0.5, which signifies random performance where the two conditions are indistinguishable and have no discriminative power. At dP=0ms and 200ms, AUC≠0.5 in both spikes and LFPs, which signifies the difference in two conditions and the presence of SE effect; but at dP=400ms, AUC=0.5, or opposite sign the two conditions are similar or indistinguishable and the effect of SE is absent.

spike and LFP responses (Fig. 26, format as Fig. 23; for dP= 0ms, the plot contains response from 4 animals, and for dP=200ms, the responses were obtained from 6 animals). Also, the effect size of SG and SE related attenuations, was higher than 0.5, indicating the presence of SG and SE effects in both spike and LFP responses (Fig. 26C). However, at a delay of 400ms, the difference between shifted and predicted response became non- significant, indicating the absence of SE-related attenuation, and AUC were close to 0.5.

These findings indicate that the state estimation can be learned for delays up to 200-400ms after the onset of the motor command. The adaptive properties of the effect of SE were also investigated across the layers of the S1 barrel cortex (Fig. 27). The responses from electrodes located at the same depth relative to L4 were averaged from 3 animals.

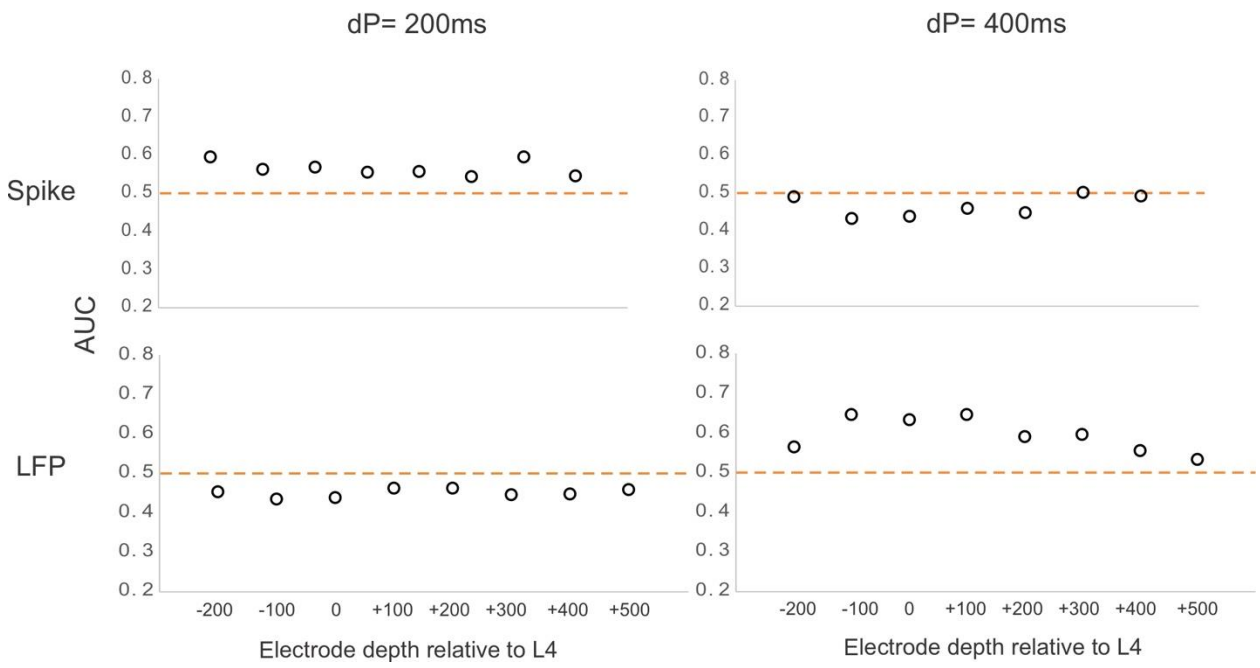

Figure 27. Range of the effect of SE and adaptation at different delays across the layers of the S1 barrel cortex.

Effect sizes (area under ROC curve; AUC) across layers of S1 barrel cortex, between shifted & predicted response in spikes and LFPs. AUC is computed at dP= 200ms and 400ms. The response across all electrodes is averaged at the same depth from 3 mice. Electrodes are arranged relative to layer 4 of the S1 barrel cortex. The Orange dotted line depicts AUC=0.5, which signifies random performance where the two conditions are indistinguishable and have no discriminative power. At dP= 200ms, AUC≠0.5 in both spikes and LFPs, which signifies the presence of SE effect; but at dP=400ms, AUC=0.5, or the opposite sign the two conditions are similar or indistinguishable, and the effect of SE is absent. The results were concurrent across all layers of the S1 barrel cortex.

All electrodes show the effect of SE across all layers at 200ms predicted delay. At 400ms, the effect of SE (difference between shifted and predicted) is shown to be either 0 (at AUC 0.5) or negative at AUC<0.5 in spikes and AUC>0.5 in LFPs.

4.4. Range of Sensory gating (SG) from the onset of motor command.

Having determined the range of SE-related attenuation, I aimed at assessing the range of SG as well. To do this, the delay of the shifted stimulus from motor command onset was varied between 500ms, 700ms, and 1000ms in subsequent training sessions, while keeping the predicted delay constant (Fig. 28 format as in Fig. 23). The responses at

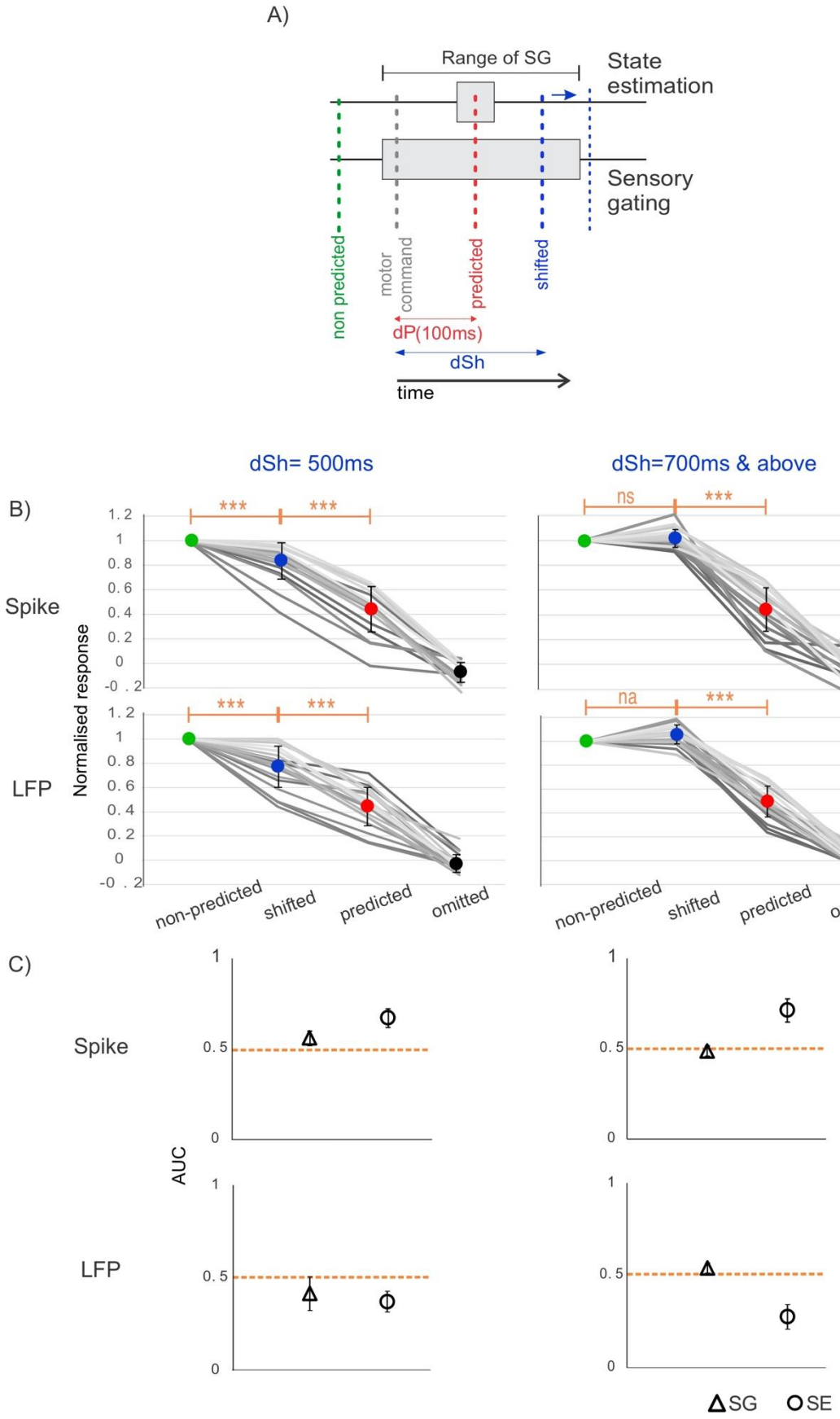
A)
Range of SG
State estimation
Sensory gating
non predicted
motor command
predicted
shifted
dP(100ms)
dSh
time
dSh= 500ms
dSh=700ms & above
B)
Spike
LFP
Normalised response
***
ns
na
non-predicted
shifted
predicted
omitted
C)
AUC
SG
SE

Figure 28. Range of the effect of sensory gating (SG) from the onset of motor command.

A) Hypothesis figure. dP= prediction delay, time of predicted stimulus from the onset of the motor command. dSh= shifted delay, time of shifted stimulus from the onset of the motor command. Shifted stimulus moved to different delays from movement onset or motor command.
B) Spike and LFP responses relative to non-predicted stimulus response. Each grey line depicts each electrode averaged across sessions for a single delay condition. Solid corresponding color dots depict average response across all electrodes for dSh=500ms and 700ms & above and dP=100ms. Error bars show standard deviation.
At dSh=500ms, responses from electrodes (n=19 for spikes and n=20 for LFPs) are averaged from 6 mice. Shifted stimulus response is significantly smaller than the non-predicted stimulus response; the difference is extremely statistically significant; one sample, a two-tailed t-test with a p-value smaller than 0.0001, signifies the effect of attenuation in shifted response by SG. Statistical results are concurrent in both spikes and LFPs.
At dSh=700ms & above, responses from electrodes (n=21 for spikes and n=23 for LFPs) are averaged from 4 mice. Shifted stimulus response is not significantly smaller than the non-predicted stimulus response; the difference is not statistically significant, determined by one sample, two-tailed t-test with p value=0.19 in spikes. Statistical results are concurrent in both spikes and LFPs, with the difference being significant in LFPs, but shifted response is higher than non-predicted response.
C) Comparison of responses in non-predicted and shifted stimulus types to determine the significance of the effect of SG in spikes and LFPs. Effect sizes (area under ROC curve; AUC) are quantified at dSh=500ms and 700ms & above. Error bars depict standard deviation. The Orange dotted line depicts AUC=0.5, which signifies random performance where the two conditions are indistinguishable and have no discriminative power. At dSh=500ms, AUC≠0.5 in both spikes and LFPs, which signifies the difference in two conditions and the presence of SG effect; but at dSh=700ms & above, AUC=0.5, the two conditions are similar or indistinguishable, and the effect of SG is absent.

shifted delay 700ms and 1000ms are averaged and shown together as both the conditions displayed concurrent results. The spike and LFP responses normalized to non-predicted stimulus responses show significant differences in non-predicted and shifted stimulus responses, indicating the presence of the effect of sensory gating at a shifted delay of 500ms (panel B). When the stimulus moved to 700ms and 1000ms, the difference computed is not significant (spike and LFP response were measured as mean responses from electrode with similar location from 6 animals at dSh= 500ms, and 4 animals at dSh= 700ms & above. The effect sizes (panel C) accordingly show a value approaching 0.5 at 700ms and above.

This effect is consistently obtained as well across layers of S1 (Fig. 29). The effect size of SG, which is the difference between non-predicted stimulus response and shifted response, was quantified for electrodes averaged across animals (2 mice for dSh=500ms

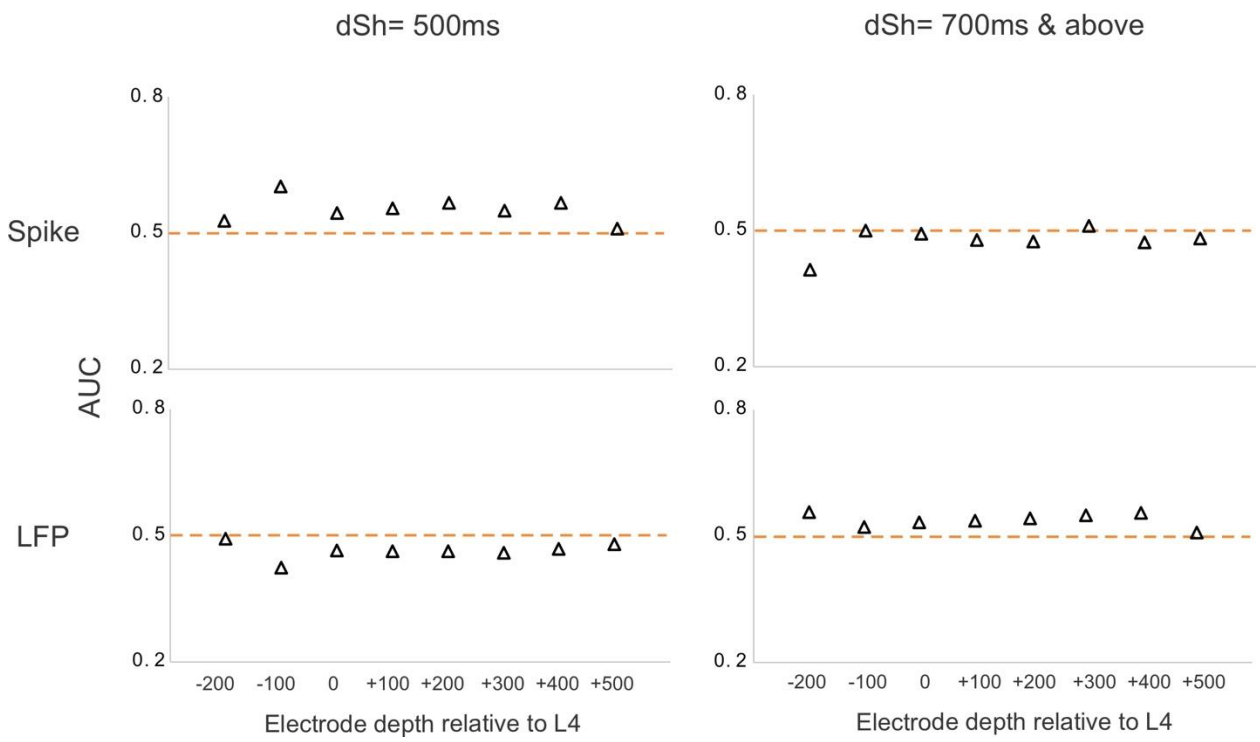

Figure 29. Range of the effect of SG across the layers of S1 barrel cortex.

Effect sizes (area under ROC curve; AUC) across layers of S1 barrel cortex, between non-predicted and shifted response in spikes and LFPs. AUC is computed at dSh= 500ms (2 mice) and 700ms & above (3 mice). Electrodes are arranged relative to layer 4 of the S1 barrel cortex. The triangles depict AUC for spike and LFP response averaged across all electrodes at the same depth and arranged relative to layer 4 of the S1 cortex. The Orange dotted line depicts AUC=0.5, which signifies random performance where the two conditions are indistinguishable and have no discriminative power. At dP= 500ms, AUC≠0.5 in both spikes and LFPs, which signifies the presence of SE effect; but at dP=700ms & above, AUC=0.5, or opposite sign the two conditions are similar or indistinguishable, and the effect of SE is absent. The results were concurrent across all layers of the S1 barrel cortex.

and 3 mice for dSh=700ms &above). Together these results point to an interval of 500 to 700ms after motor command onset, in which SG effects are present, a range thus different form the range in which SE could be trained (200-400ms).

5. Discussion

In the present study, I established an experimental methodology to provide evidence of the existence of two phenomena that attenuate the somatosensory signals, those predicting the consequences of the body's own movements (SE) and those generated in the external environment during movements (SG). I have shown both phenomena, SE and SG, in the same experiment, and dissociated them using the fact that they are active in different intervals after motor command onset. A further distinction was that it turned out that they can be invoked in different intervals after motor command onset, and that their dependency on the predicted stimulus is different, SE tracks it, while SG is independent from it. The experimental methodology included open and closed-loop approaches, which have their own pros and cons.

5.1. Open or closed loop approach?

My motivation to open the reafference loop was to have a clean sensory feedback signal, which is not contaminated by the natural reafference signals: This lack of reafference signals in open loop conditions serves to securely excluded the possibility that the observed SE-related attenuation could be caused by the very sensory feedback evoked by movement, rather than by an internal motor command or efference copy. My demonstration of attenuation of the sensory signal in open loop, therefore, is a necessary prerequisite to be able to state with confidence that internal predicative processes, based on internal motor commands/efference copies must have played a part in generating the observed attenuation. Another way how one can show that SE is based on internal predictive signals, is to demonstrate that SE can be invoked before the movement starts. This demonstration was enabled as well by recording the motor command (rather than the movement) in this study: When triggering the artificial sensory consequence with zero delay (see Fig. 26) at the onset of the motor command, the SE-based attenuation could be readily observed. This attenuation thus occurred at a point in time, at which under natural circumstance whisker movements would take some 30-50 ms more to commence (shown in Fig. 15D). There are many experiments in the literature that showed predictive

effects on sensory signals (Singla et al., 2017, Roy and Cullen, 2004, Bays et al., 2006, Schneider et al., 2018). They all, often implicitly, assumed that efference copy-based mechanisms are at work. Following the seminal open loop experiments of Bell (1982) in weakly electric fish, the present experiments however, are, to the best of my knowledge, the only ones that realized the open loop conditions in mammals, thus directly indicating an internal origin of SE-based predictive signaling.

Nevertheless, the open-loop approach also has limitations. Most importantly, the facial motor nerve cut used here could have led to unwanted brain plasticity. For instance, experimentally uncontrolled variation of facial nucleus activity could develop over the weeks of experimentation following the nerve cut, as well as instabilities due to regeneration of the nerve, bridging the nerve stumps with concomitant recovery of whisker movements. Further, the nature or origin of the inputs driving neuronal activity in the facial nucleus could change in nature, unbeknownst of the experimenter. These limitations were the motivation to perform some control experiments as well in closed loop conditions. To this end we left natural reafference signals and whisker movement intact, and added the artificial stimulation of feedback signals using electrical activation of the ascending tactile pathway in the trigeminal nucleus. The results were highly comparable to the main findings in open loop conditions. Together, the similarity of results under open and closed loop conditions supports the claim that the open loop approach was adequate and provided stable conditions to study internal signal-based (motor command) predictive attenuation of the sensory signal flow. On the other hand, these controls help to validate many studies, cited above, that assumed to study the action of internal motor-related mechanisms in the presence of movement-evoked sensory feedback.

The same arguments are also valid for the study of SG. The presence of SG in open loop conditions, as demonstrated here, argue that SG-attenuating signals are independent of sensory feedback as well. For whisker movements the internal origin of SG has been demonstrated before in a whisker reaching task by observing that attenuation survived the severing of primary afferents in the infraorbital nerve (Hentschke et al., 2006). However, in the literature of SG in primate arm movements, it has been reported that SG

attenuation is observable also in the case of passive movements, i.e., moving a limb with a motor, which excludes a specific motor command, but leaves the proprioceptive feedback (Rushton et al., 1981, Chapman et al., 1987a, Chapman et al., 1988). These results appear discrepant with those obtained in the whisker system and need further study. However, one needs to keep in mind that they were not obtained with nerve deafferentation (as in the whisker system), but with the behavioral instruction “to do nothing”. So, the presence of some unobserved, hidden activity, internal motor commands that e.g., served postural corrections or resisted the passive displacement, cannot securely excluded in the experiments in the primate arm motor system. Further, central signals originating from higher hierarchy cognitive centers related to e.g., attention, motor planning etc. cannot be excluded to have played a role.

5.2. Dissociating state estimation from sensory gating.

One of the computational frameworks suggest that the brain generates motor commands through an inverse model (Kawato, 1999) or controller (Todorov, 2004). A copy of the motor command, known as the "efference copy," is utilized by a forward model to predict the sensory feedback resulting from the movement. This prediction is then integrated by the comparator or state estimator with actual sensory input to estimate the body's state (Kawato, 1999, McNamee and Wolpert, 2019, Todorov, 2004, Ghahramani, 2000). Regarding the attenuation of sensory reafference, it has been proposed that the prediction signal from the forward model is employed to "cancel out" the sensory reafference (Bays and Wolpert, 2007, Blakemore et al., 2000, McNamee and Wolpert, 2019, Wolpert and Flanagan, 2001). In other words, central motor processes are thought to play a more significant role in somatosensory attenuation than actual sensory feedback. This notion is supported by studies demonstrating that conditions involving highly predictable touches without movement do not result in attenuation (Bays et al., 2005, Kilteni et al., 2020). The dependence of attenuation on action prediction was further demonstrated when participants attenuated touches applied to one hand, which were anticipated based on the movement of their other hand, even when the two hands unexpectedly failed to make contact (Bays et al., 2006). As discussed above, the present

results using the open loop approach add strong and most direct support for the idea that it is internal motor commands that bring about the SE-related attenuation.

Neuroimaging studies on somatosensory attenuation consistently reveal activation of the cerebellum (Blakemore et al., 1998, Blakemore et al., 1999, Kilteni and Ehrsson, 2020, Shergill et al., 2013), a structure associated with motor prediction (Wolpert, 1996, Shadmehr and Krakauer, 2008, Shadmehr et al., 2010, Daniel M. Wolpert, 1998, Therrien and Bastian, 2019). The present results add critical evidence to such forward model-based mechanisms, as my results show sensory attenuation in response to the predicted sensory stimuli mimicking reafference signals generated by (or tightly correlated to) the brain's own motor command, and further show that this attenuation cannot be explained by SG-related attenuation, as it was found to be separable from SE-based effects.

In fact, focusing now on SG-mediated effects, the present results do not support the notion that SG is based on predictions of sensory consequences by a forward model. The main argument is that shifting the stimulus to an unpredicted time point leaves SG entirely intact. It thus appears completely independent from the (artificial) sensory consequence presented systematically in the training sessions in this study. The literature on SG with primate arm movements further states that it is even active several hundreds of milliseconds before movement onset, or even with passive movements, opening the possibility that it is active before (or independent of) a top-down motor command that arrives at the spinal motoneurons (Chapman, 1994, Williams et al., 1998, Williams and Chapman, 2000, Williams and Chapman, 2002). The internal signals driving SG may therefore be different from an efference copy and forward models and may be driven by higher cognitive signals about attention, motor planning etc., that occur even earlier. This notion, at present, remains purely speculative and needs to be investigated by future experimentation attempting to separate SG-based attenuation from movement and motor command.

Although these fundamental processes likely coexist and cooperate during voluntary motor control, my study strongly suggests that they are distinct processes. Interestingly,

when both phenomena were present at the same time (in predicted trials), or when only SG was present (shifted trials), my results demonstrated an additive effect of the state estimation and gating condition on the stimulus response.

My findings have the potential to reconcile various previously isolated observations on sensory gating and state estimation that have been investigated independently in recent decades, and have produced apparent contradictory results, based on the ignorance on whether SE and SG are structurally and functionally independent functional systems. For instance, it has been shown that the self-generated tactile signals are attenuated when presented at the anticipated timing of the action (Bays et al., 2005, Blakemore et al., 1999, Kilteni et al., 2019). Even a 100ms delay between the movement and its tactile feedback substantially reduces the attenuation, which is consistent with my result that the precision of SE is better than the 50 ms interval around the stimulus. On the other hand, there is evidence that externally generated stimuli are gated with less temporal sensitivity. For instance, gating is observed for stimuli presented at various unpredictable times during movement (Rushton et al., 1981), at movement onset (Colino and Binsted, 2016), and notably, even hundreds of milliseconds before movement onset (Chapman and Beauchamp, 2006, Colino et al., 2014, Colino and Binsted, 2016, Williams et al., 1998). This set of results can be explained as well by my results, this time by the relative independence of SG-effects on the delay after motor command onset. I showed the presence of SG-related attenuation at delays ranging from zero to 500ms after the onset of the motor command.

My study is the first to distinguish neural processes between state estimation and sensory gating and aligns with previous behavioral experiments on the same whisker/limb and different limbs. Bays and Wolpert (2008) found that self-generated force on the left index finger did not alter the perception of an electrical stimulus. However, their study only assessed touch perception on a resting limb, which doesn't evoke gating effects (Papakostopoulos, Cooper et al. 1975, Rushton, Rothwell et al. 1981, Chapman, Bushnell et al. 1987, Colino, Buckingham et al. 2014). In contrast, my study evaluates both phenomena on the same whisker. Similarly, Palmer et al. (2016) measured

somatosensory evoked potentials during self-generated force on both wrists but did not explore perception during movement (sensory gating), focusing solely on resting touches (state estimation). Their setting, therefore, was not able to behaviorally differentiate these phenomena.

The most relevant study to this thesis is a recent behavioral study in humans, which aimed at directly testing the hypothesis of two attenuating functional systems. The perceptual effect of self-generated vs. external touch was tested during movement of the touching finger as well as the touched arm/hand (Kilteni and Ehrsson, 2022). The authors demonstrated that self-generated touch consistently reduced (attenuated) perceived touch intensity, but that arm movement adds to the reduction of the perceived intensity (Kilteni and Ehrsson, 2022). These results on the perceptual level bear evident resemblance to my present results in that they show independence and additivity of perceptual attenuation of two systems. They may well represent the reflection of SE and SG neuronal effects as found here on the behavioral level. If SE relates to self-generated sensory consequences as it is precisely predictable in time, and SG relates to sensory consequences generated by external factors that is less predictable in time, then my results in the whisker system would qualitatively support their behavioral analysis and complement it by additionally revealing matching neural signatures of the two separable mechanisms.

5.3. Neuronal bases of SE and SG.

In terms of the neural mechanisms underlying these two phenomena, research has demonstrated that sensory attenuation in state estimation is associated with reduced activity in the secondary somatosensory cortex (Blakemore et al., 1998, Kilteni and Ehrsson, 2020, Shergill et al., 2013) and the cerebellum (Blakemore et al., 1998, Kilteni and Ehrsson, 2020), along with increased functional connectivity between these regions (Blakemore et al., 1999, Kilteni and Ehrsson, 2020). Consequently, the cerebellum is proposed to predict the sensory consequences of an action based on the efference copy and subsequently attenuate somatosensory activity (Blakemore et al., 1998, Kilteni and

Ehrsson, 2020). In contrast, studies on SG in primates have revealed suppression effects at early stages of the somatosensory pathway, including the spinal cord (Seki et al., 2003), the cuneate nucleus (Suresh et al., 2021), and the thalamus (Fahy et al., 1993), and the trigeminal nucleus (Chakrabarti and Schwarz, 2018).

In a study performed by Kilteni et al. (Kilteni and Ehrsson, 2020), fMRI in conjunction with the traditional force-matching task was employed to examine the neural mechanisms underlying the predictive attenuation of self-generated touch. The results revealed that self-generated touch is linked to reduced activation in the bilateral secondary somatosensory cortex. Additionally, they observed decreased activation within the cerebellum during touch when presented alongside self-generated movement. Furthermore, it was observed that the functional connectivity between the ipsilateral cerebellum and the contralateral primary and bilateral secondary somatosensory areas increased during self-generated touch. Notably, this increase in functional connectivity exhibited a linear scaling across participants, corresponding to the extent of somatosensory attenuation measured in the force-matching task. These findings highlight the pivotal role of the cerebellum in predicting and canceling self-generated somatosensory input and suggest that the functional connectivity between the cerebellum and the somatosensory cortex underlies the phenomenon of somatosensory attenuation.

Kilteni et al. (Kilteni and Ehrsson, 2020), discussed that it is important to note that functional connectivity between two brain regions does not necessarily indicate a causal relationship (Eickhoff and Müller, 2015). However, one possible hypothesis is that this observed connectivity represents the prediction signal sent from the cerebellum to the somatosensory cortices, effectively suppressing their activity. Alternatively, the observed functional connectivity could reflect the conveyance of somatosensory input from the cortex to the cerebellum. According to this interpretation, somatosensory areas project to the cerebellum to transmit received tactile feedback, which could be utilized to compute prediction errors by contrasting the received feedback with the predicted feedback.

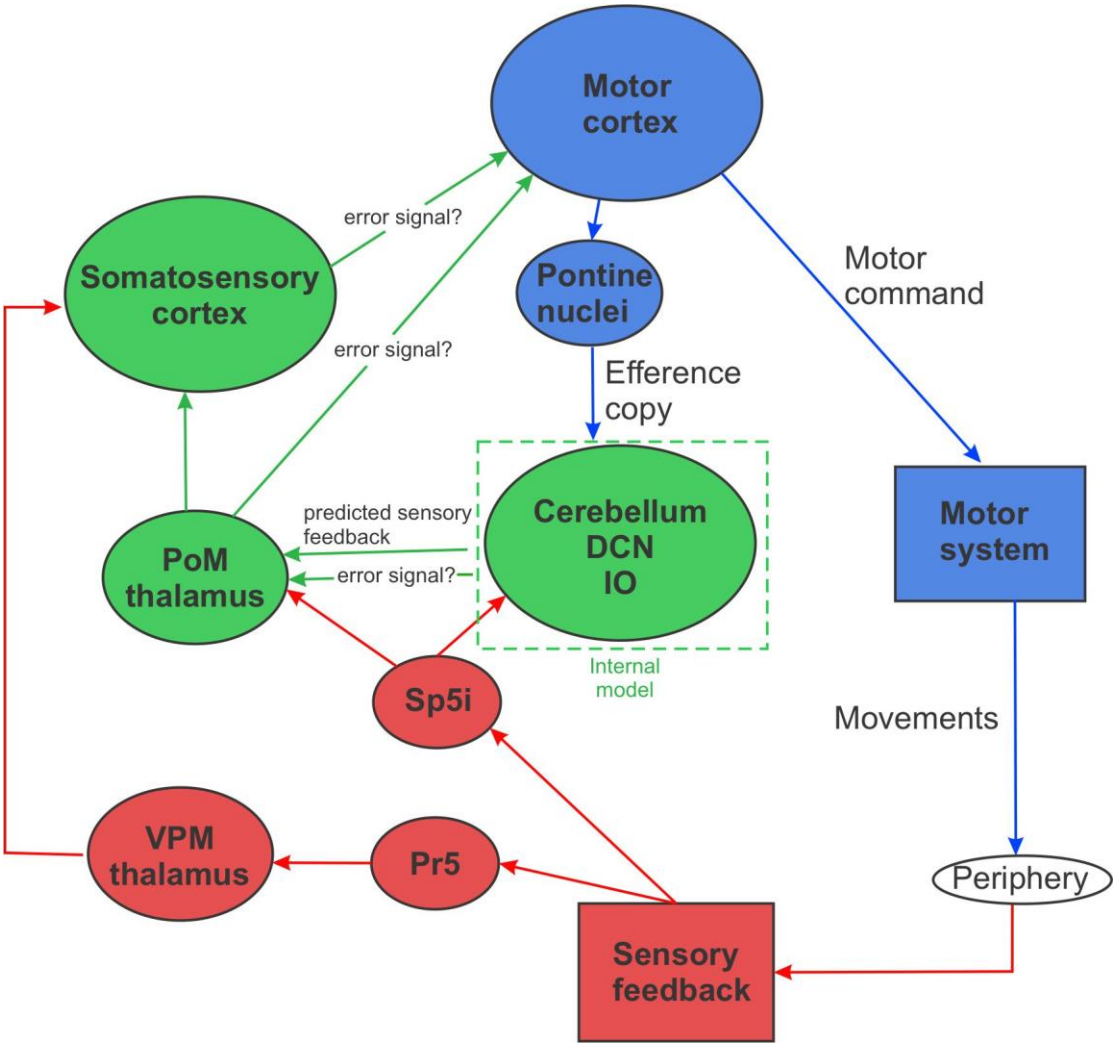

Figure 30. Hypothetical cerebrocerebellar circuits and structures involved in sensory prediction and state estimation.

Structures in red are involved in sensory processing. The principal trigeminal nucleus (Pr5) and spinal trigeminal nuclei pars interpolaris (Sp5i) are brainstem nuclei. Red arrows depict sensory flow. Blue-shaded structures are involved in motor pathways, and the structures in green are hypothesized to be involved in sensory prediction and state estimation.

Another interpretation, inspired by influential animal tracing studies (Aoki et al., 2019), suggests a reciprocal exchange of information between the cerebellum and the cortex. In this scenario, the functional connectivity observed in the study by Kilteni et.al (2020), could indicate a closed loop between the cerebellum and the sensory cortex, where the cerebellum sends a cancellation signal to the somatosensory areas, while the

somatosensory areas provide tactile feedback for updating the internal forward models in a proper manner. It is worth considering these various interpretations, as they offer different perspectives on the functional connectivity observed in my study, each suggesting a potential mechanism underlying the interactions between the cerebellum and the somatosensory cortex.

Fig 30. depict the structures that are potential candidates for state estimation. According to the above interpretations, the somatosensory cortex could be a potential candidate for being the comparator as it receives the prediction signals from the cerebellum that serves as an internal forward model and receives direct inputs of actual sensory feedback. Also, it has been suggested that optogenetic inhibition of S1 cortex abolished the ability to update the motor command in a mouse model indicating a role of S1 in forelimb motor adaptation (Mathis et al., 2017). This further supports the hypothesis of S1 having direct (being a comparator) or indirect involvement in generating sensory prediction error signals and sending them to the motor system. In a recent study on the distribution of prediction neurons across different layers of the auditory cortex, it was investigated how movement and sound signals are distributed among individual neurons (Audette et al., 2022). The authors of this study reported that prediction-based suppression neurons and prediction error neurons, which indicate the presence of predictive processes, were concentrated in L2/3 and L5. In contrast, neurons in L6 exhibited general movement-related signals (Audette et al., 2022). My results do not tally with their findings. In contrast, I was able to see the sensory attenuation based on predictions in all layers of the S1 barrel cortex. This indicates that the primary somatosensory cortex is less likely to be a site for the comparison or integration of prediction signals or state estimation.

It is suggested by previous studies (Miall and King, 2008) that the predictive internal model and state estimator presumably lies in the cerebellar Purkinje cells which are said to form the internal forward model of the brain (Daniel M. Wolpert, 1998, Izawa et al., 2012, Lisberger, 2009, Miall et al., 2007, Nowak et al., 2007, Yavari et al., 2016, Streng et al., 2022). The output structure DCN receives the presumptive prediction signals of PCs as well as the sensory inputs from the brainstem (Sp5i) via mossy fiber collaterals

(Llinas and Muhlethaler, 1988) Thus DCN is a second candidate to play the role of the comparator.

Since S1 cortex is unlikely to contain the site for comparative integration (from current results) but has been shown to involve in sending prediction error signals to update the motor command, it could be serving as an intermediate. Another potential candidate for that reason could be thalamus PoM, which inputs to S1. PoM receives direct inputs from the cerebellum (Nakamura et al., 2014, Kuramoto et al., 2011) and brainstem Sp5i. Thus, it may well in the position to integrate prediction with signals about sensory consequences. PoM also projects to the motor cortex, which could be an alternate pathway for error signals to the motor cortex to correct the motor command. In future studies, the location of the comparator must be tracked by investigating the entire cerebello-cerebral pathway from DCN via thalamus to S1.

6. Appendix

Table 1. Data compilation details all experiments.

Experiment	Delay conditions		No. of animals	Spikes		LFPs	
	Pred Delay (ms)	Shifted Delay (ms)		No. of electrodes (n)	No. of sessions averaged	No. of electrodes (n)	No. of sessions averaged
Basic effect (ORL)	100	0,300,400, 500, random	12	80	563	83	574
Basic effect (CRL)	100	300	3	3	14	2	9
SE Precision	100	110	5	16	65	17	71
	100	150	5	16	74	17	25
	100	200	5	16	75	17	83
SE Adaptation and range	0	100,250, 300,500	4	11	71	16	109
	200	300,400, random	6	23	158	30	222
	400	0, random	4	20	99	24	130
Learning latency	100	300,400, 500	4	15	15	14	14
	200	300,400	4	15	15	14	14
SG range	100	500	6	19	88	20	92
	100	700, 1000	4	21	84	23	92

Table 2. Data compilation details depth wise analysis.

Experiment	Delay conditions		No. of animals	Electrode depth (relative to L4)	Spikes		LFPs	
	Pred Delay (ms)	Shifted Delay (ms)			No. of electrodes (n)	No. of sessions averaged	No. of electrodes (n)	No. of sessions averaged
Basic effect (ORL)	100	300, 400, 500, random	5	-200	3	20	3	20
				-100	6	45	7	49
				0	9	59	9	59
				100	9	59	9	59
				200	8	55	8	55
				300	8	55	8	55
				400	8	55	8	55
				500	5	28	4	18
SE Precision	100	110, 150, 200 (each have same number of electrodes and sessions)	2	-200	1	4	1	4
				-100	1	4	1	4
				0	2	8	2	8
				100	2	8	2	8
				200	2	8	2	8
				300	2	8	2	8
				400	2	8	2	8
SE Adaptation and range	200	random, 400	3	-200	1	4	2	19
				-100	2	19	2	19
				0	3	23	3	23
				100	3	23	3	23
				200	3	23	3	23
				300	3	23	3	23
				400	2	8	3	23
				500	1	4	2	19
	400	random, 0	3	-200	1	3	2	9
				-100	2	8	2	8
				0	3	11	3	11
				100	3	11	3	11
				200	3	11	3	11
				300	3	11	3	11
				400	2	5	3	11
				500			1	6

SG range	100	500	2	-200	1	4	1	4
				-100	1	4	1	4
				0	2	8	2	8
				100	2	8	2	8
				200	2	8	2	8
				300	2	8	2	8
				400	2	8	2	8
				500	2	8	2	8
	100	700, 1000	3	-200	1	4	1	4
				-100	2	8	2	8
				0	3	12	3	12
				100	3	12	3	12
				200	3	12	3	12
				300	3	12	3	12
				400	3	12	3	12
				500	1	4	1	4

7. References

1. Adibi, M. 2019. Whisker-mediated touch system in rodents: from neuron to behavior. Frontiers in systems neuroscience, 13.
2. Ahissar, E. & Kleinfeld, D. 2003. Closed-loop neuronal computations: focus on vibrissa somatosensation in rat. Cereb cortex, 13, 53-62.
3. Aoki, S., Coulon, P. & Ruigrok, T. J. H. 2019. Multizonal cerebellar influence over sensorimotor areas of the rat cerebral cortex. Cereb cortex, 29, 598-614.
4. Audette, N. J., Zhou, W., La Chioma, A. & Schneider, D. M. 2022. Precise movement-based predictions in the mouse auditory cortex. Curr biol, 32, 4925-4940 e6.
5. Azim, E. & Seki, K. 2019. Gain control in the sensorimotor system. Current opinion in physiology, 8, 177-187.
6. Baizer, J. S., Kralj-Hans, I. & Glickstein, M. 1999. Cerebellar lesions and prism adaptation in macaque monkeys. Journal of neurophysiology, 81, 1960-1965.
7. Bays, P. M., Flanagan, J. R. & Wolpert, D. M. 2006. Attenuation of self-generated tactile sensations is predictive, not postdictive. Plos biol, 4, e28.
8. Bays, P. M. & Wolpert, D. M. 2007. Computational principles of sensorimotor control that minimize uncertainty and variability. J physiol, 578, 387-96.
9. Bays, P. M., Wolpert, D. M. & Flanagan, J. R. 2005. Perception of the consequences of self-action is temporally tuned and event driven. Curr biol, 15, 1125-8.
10. Bell, C. C. 1982. Properties of a modifiable efference copy in an electric fish. Journal of neurophysiology.
11. Blakemore, S. J., Frith, C. D. & Wolpert, D. M. 1999. Spatio-temporal prediction modulates the perception of self-produced stimuli. J cogn neurosci, 11, 551-9.
12. Blakemore, S. J., Wolpert, D. & Frith, C. 2000. Why can't you tickle yourself? Neuroreport, 11, r11-6.
13. Blakemore, S. J., Wolpert, D. M. & Frith, C. D. 1998. Central cancellation of self-produced tickle sensation. Nat neurosci, 1, 635-40.
14. Brooks, J. X., Carriot, J. & Cullen, K. E. 2015. Learning to expect the unexpected: rapid updating in primate cerebellum during voluntary self-motion. Nat neurosci, 18, 1310-7.
15. Brooks, J. X. & Cullen, K. E. 2013. The primate cerebellum selectively encodes unexpected self-motion. Curr biol, 23, 947-55.

16. Brooks, J. X. & Cullen, K. E. 2019. Predictive sensing: the role of motor signals in sensory processing. Biological psychiatry: cognitive neuroscience and neuroimaging, 4, 842-850.

17. Cano-De-La-Cuerda, R., Molero-Sanchez, A., Carratala-Tejada, M., Alguacil-Diego, I. M., Molina-Rueda, F., Miangolarra-Page, J. C. & Torricelli, D. 2015. Theories and control models and motor learning: clinical applications in neuro-rehabilitation. Neurologia, 30, 32-41.

18. Chakrabarti, S., Nambiar, J. & Schwarz, C. 2021. Adaptive whisking in mice. Front syst neurosci, 15, 813311.

19. Chakrabarti, S. & Schwarz, C. 2018. Cortical modulation of sensory flow during active touch in the rat whisker system. Nat commun, 9, 3907.

20. Chapman, C. E. 1994. Active versus passive touch: factors influencing the transmission of somatosensory signals to primary somatosensory cortex. Canadian journal of physiology and pharmacology, 72, 558-570.

21. Chapman, C. E. & Beauchamp, E. 2006. Differential controls over tactile detection in humans by motor commands and peripheral reafference. Journal of neurophysiology, 96, 1664-1675.

22. Chapman, C. E., Bushnell, M. C., Miron, D., Duncan, G. H. & Lund, J. P. 1987a. Sensory perception during movement in man. Experimental brain research, 68, 516-524.

23. Chapman, C. E., Jiang, W. & Lamarre, Y. 1988. Modulation of lemniscal input during conditioned arm movements in the monkey. Exp brain res, 72, 316-34.

24. Claxton, G. 1975. Why can't we tickle ourselves? Perceptual and motor skills, 41, 335-338.

25. Colino, F. L. & Binsted, G. 2016. Time course of tactile gating in a reach-to-grasp and lift task. J mot behav, 48, 390-400.

26. Colino, F. L., Buckingham, G., Cheng, D. T., Van Donkelaar, P. & Binsted, G. 2014. Tactile gating in a reaching and grasping task. Physiol rep, 2, e00267.

27. Collins, D. F., Cameron, T., Gillard, D. M. & Prochazka, A. 1998. Muscular sense is attenuated when humans move. The journal of physiology, 508, 635-643.

28. Cox, R. T. 1946. Probability, frequency and reasonable expectation. American journal of physics, 14.

29. Crapse, T. B. & Sommer, M. A. 2008. Corollary discharge across the animal kingdom. Nat rev neurosci, 9, 587-600.

30. Cullen, K. E. 2012. The vestibular system: multimodal integration and encoding of self-motion for motor control. Trends neurosci, 35, 185-96.

31. Cybulska-Klosowicz, A., Meftah El, M., Raby, M., Lemieux, M. L. & Chapman, C. E. 2011. A critical speed for gating of tactile detection during voluntary movement. Exp brain res, 210, 291-301.

32. Dale, A. & Cullen, K. E. 2019. The ventral posterior lateral thalamus preferentially encodes externally applied versus active movement: implications for self-motion perception. Cereb cortex, 29, 305-318.

33. Daniel M. Wolpert, R. C. M. A. M. K. 1998. Internal models in the cerebellum. Trends in cognitive sciences, (1998), 338-347, 2(9).

34. Davidson, P. R. & Wolpert, D. M. 2005. Widespread access to predictive models in the motor system: a short review. J neural eng, 2, s313-9.

35. Dayan, P., Hinton, G. E., Neal, R. M. & Zemel, R. S. 1995. The helmholtz machine. Neural comput, 7, 889-904.

36. Diamond, M. E., Von Heimendahl, M., Knutsen, P. M., Kleinfeld, D. & Ahissar, E. 2008. 'Where' and 'what' in the whisker sensorimotor system. Nat rev neurosci, 9, 601-12.

37. Dorfl, J. 1982. The musculature of the mystacial vibrissae of the white mouse. J anat, 135, 147-54.

38. Eickhoff, S. B. & Müller, V. I. 2015. Functional connectivity.

39. Fahy, F. L., Riches, I. P. & Brown, M. W. 1993. Neuronal signals of importance to the performance of visual recognition memory tasks: evidence from recordings of single neurones in the medial thalamus of primates. Prog brain res, 95, 401-16.

40. Fee, M. S., Mitra, P. P. & Kleinfeld, D. 1997. Central versus peripheral determinants of patterned spike activity in rat vibrissa cortex during whisking. J neurophysiol, 78, 1144-9.

41. Feinberg, I. 1978. Efference copy and corollary discharge: implications for thinking and its disorders. Schizophr bull, 4, 636-40.

42. Ferezou, I., Haiss, F., Gentet, L. J., Aronoff, R., Weber, B. & Petersen, C. C. 2007. Spatiotemporal dynamics of cortical sensorimotor integration in behaving mice. Neuron, 56, 907-23.

43. Flanagan, J. R. & Wing, A. M. 1997. The role of internal models in motion planning and control: evidence from grip force adjustments during movements of hand-held loads. J neurosci, 17, 1519-28.

44. Franklin, D. W. & Wolpert, D. M. 2011. Computational mechanisms of sensorimotor control. Neuron, 72, 425-42.

45. Fraser, L. E. & Fiehler, K. 2018. Predicted reach consequences drive time course of tactile suppression. Behav brain res, 350, 54-64.

46. Friauf, E. 1986. Morphology of motoneurons in different subdivisions of the rat facial nucleus stained intracellularly with horseradish peroxidase. J comp neurol, 253, 231-41.

47. Friston, K. 2010. The free-energy principle: a unified brain theory? Nat rev neurosci, 11, 127-38.

48. Frith, C. D. 1992. The cognitive neuropsychology of schizophrenia, hillsdale, nj, us, lawrence erlbaum associates, inc.

49. Frith, C. D., Blakemore, S. & Wolpert, D. M. 2000. Explaining the symptoms of schizophrenia: abnormalities in the awareness of action. Brain res brain res rev, 31, 357-63.

50. Gahery, Y., Ioffe, M. E., Massion, J. & Polit, A. 1981. [postural support for local movements in cats and dogs]. Zh vyssh nerv deiat im i p pavlova, 31, 232-41.

51. Gao, Z., Van Beugen, B. J. & De Zeeuw, C. I. 2012. Distributed synergistic plasticity and cerebellar learning. Nat rev neurosci, 13, 619-35.

52. Gerdjikov, T. V., Haiss, F., Rodriguez-Sierra, O. E. & Schwarz, C. 2013. Rhythmic whisking area (rw) in rat primary motor cortex: an internal monitor of movement-related signals? J neurosci, 33, 14193-204.

53. Gertz, H., Voudouris, D. & Fiehler, K. 2017. Reach-relevant somatosensory signals modulate tactile suppression. J neurophysiol, 117, 2262-2268.

54. Ghahramani, D. M. W. Z. 2000. Computational principles of movement neuroscience. Nature neuroscience, 3, 1212-1217.

55. Ghez, C. & Lenzi, G. L. 1971. Modulation of lemniscal transmission during voluntary movement. Boll soc ital biol sper, 47, 76-7.

56. Ghez, C. & Pisa, M. 1972. Inhibition of afferent transmission in cuneate nucleus during voluntary movement in the cat. Brain res, 40, 145-55.

57. Grinevich, V., Brecht, M. & Osten, P. 2005. Monosynaptic pathway from rat vibrissa motor cortex to facial motor neurons revealed by lentivirus-based axonal tracing. J neurosci, 25, 8250-8.

58. Haarmeier, T., Thier, P., Repnow, M. & Petersen, D. 1997. False perception of motion in a patient who cannot compensate for eye movements. Nature, 389, 849-52.

59. Haidarliu, S., Simony, E., Golomb, D. & Ahissar, E. 2010. Muscle architecture in the mystacial pad of the rat. Anat rec (hoboken), 293, 1192-206.

60. Haiss, F., Butovas, S. & Schwarz, C. 2010. A miniaturized chronic microelectrode drive for awake behaving head restrained mice and rats. J neurosci methods, 187, 67-72.

61. Heaton, J. T., Sheu, S. H., Hohman, M. H., Knox, C. J., Weinberg, J. S., Kleiss, I. J. & Hadlock, T. A. 2014. Rat whisker movement after facial nerve lesion: evidence for autonomic contraction of skeletal muscle. Neuroscience, 265, 9-20.

62. Heiligenberg, W. 1969. The effect of stimulus chirps on a cricket's chirping (acheta domesticus). Zeitschrift für vergleichende physiologie, 65, 70-97.

63. Hentschke, H., Haiss, F. & Schwarz, C. 2006. Central signals rapidly switch tactile processing in rat barrel cortex during whisker movements. Cereb cortex, 16, 1142-56.

64. Hillis, J. M., Ernst, M. O., Banks, M. S. & Landy, M. S. 2002. Combining sensory information: mandatory fusion within, but not between, senses. Science, 298, 1627-30.

65. Hillman, E. M. 2007. Optical brain imaging in vivo: techniques and applications from animal to man. J biomed opt, 12, 051402.

66. Izawa, J., Criscimagna-Hemminger, S. E. & Shadmehr, R. 2012. Cerebellar contributions to reach adaptation and learning sensory consequences of action. J neurosci, 32, 4230-9.

67. Jiang, W., Chapman, C. E. & Lamarre, Y. 1991. Modulation of the cutaneous responsiveness of neurones in the primary somatosensory cortex during conditioned arm movements in the monkey. Exp brain res, 84, 342-54.

68. Jiang, W., Lamarre, Y. & Chapman, C. E. 1990. Modulation of cutaneous cortical evoked potentials during isometric and isotonic contractions in the monkey. Brain res, 536, 69-78.

69. Joachimsthaler, B., Brugger, D., Skodras, A. & Schwarz, C. 2015. Spine loss in primary somatosensory cortex during trace eyeblink conditioning. J neurosci, 35, 3772-81.

70. Johansson, R. S. & Cole, K. J. 1992. Sensory-motor coordination during grasping and manipulative actions. Curr opin neurobiol, 2, 815-23.

71. Jordan, M. I. & Rumelhart, D. E. 1992. Forward models: supervised learning with a distal teacher. Cognitive science, 16, 307-354.

72. Juavinett, A. L., Nauhaus, I., Garrett, M. E., Zhuang, J. & Callaway, E. M. 2017. Automated identification of mouse visual areas with intrinsic signal imaging. Nat protoc, 12, 32-43.

73. Kawato, M. 1999. Internal models for motor control and trajectory planning. Curr opin neurobiol, 9, 718-27.

74. Kilteni, K. & Ehrsson, H. H. 2020. Functional connectivity between the cerebellum and somatosensory areas implements the attenuation of self-generated touch. J neurosci, 40, 894-906.

75. Kilteni, K. & Ehrsson, H. H. 2022. Predictive attenuation of touch and tactile gating are distinct perceptual phenomena. Iscience, 25, 104077.

76. Kilteni, K., Engeler, P. & Ehrsson, H. H. 2020. Efference copy is necessary for the attenuation of self-generated touch. Iscience, 23, 100843.

77. Kilteni, K., Houborg, C. & Ehrsson, H. H. 2019. Rapid learning and unlearning of predicted sensory delays in self-generated touch. Elife, 8.

78. Kleinfeld, D. & Deschênes, M. 2011. Neuronal basis for object location in the vibrissa scanning sensorimotor system. Neuron, 72, 455-468.

79. Körding, K. P. & Wolpert, D. M. 2004. Bayesian integration in sensorimotor learning. Nature, 427, 244-247.

80. Krakauer, J. W., Ghilardi, M. F. & Ghez, C. 1999. Independent learning of internal models for kinematic and dynamic control of reaching. Nat neurosci, 2, 1026-31.

81. Krakauer, J. W., Pine, Z. M., Ghilardi, M.-F. & Ghez, C. 2000. Learning of visuomotor transformations for vectorial planning of reaching trajectories. The journal of neuroscience, 20, 8916-8924.

82. Kuramoto, E., Fujiyama, F., Nakamura, K. C., Tanaka, Y., Hioki, H. & Kaneko, T. 2011. Complementary distribution of glutamatergic cerebellar and gabaergic basal ganglia afferents to the rat motor thalamic nuclei. Eur j neurosci, 33, 95-109.

83. Langer, D., Van 'T Hoff, M., Keller, A. J., Nagaraja, C., Pfaffli, O. A., Goldi, M., Kasper, H. & Helmchen, F. 2013. Helioscan: a software framework for controlling in vivo microscopy setups with high hardware flexibility, functional diversity and extendibility. J neurosci methods, 215, 38-52.

84. Lindner, A., Haarmeier, T., Erb, M., Grodd, W. & Thier, P. 2006. Cerebrocerebellar circuits for the perceptual cancellation of eye-movement-induced retinal image motion. J cogn neurosci, 18, 1899-912.

85. Lisberger, S. G. 2009. Internal models of eye movement in the floccular complex of the monkey cerebellum. Neuroscience, 162, 763-76.

86. Llinas, R. & Muhlethaler, M. 1988. An electrophysiological study of the in vitro, perfused brain stem-cerebellum of adult guinea-pig. J physiol, 404, 215-40.

87. Malenka, R. C., Angel, R. W., Hampton, B. & Berger, P. A. 1982. Impaired central error-correcting behavior in schizophrenia. Arch gen psychiatry, 39, 101-7.

88. Martin, A., Wiggs, C. L., Ungerleider, L. G. & Haxby, J. V. 1996. Neural correlates of category-specific knowledge. Nature, 379, 649-652.

89. Massion, J. 1992. Movement, posture and equilibrium: interaction and coordination. Prog neurobiol, 38, 35-56.

90. Mathis, M. W., Mathis, A. & Uchida, N. 2017. Somatosensory cortex plays an essential role in forelimb motor adaptation in mice. Neuron, 93, 1493-1503 e6.

91. Matyas, F., Sreenivasan, V., Marbach, F., Wacongne, C., Barsy, B., Mateo, C., Aronoff, R. & Petersen, C. C. 2010. Motor control by sensory cortex. Science, 330, 1240-3.

92. Mclaughlin, S. C. 1967. Parametric adjustment in saccadic eye movements. Perception & psychophysics 2, 359-362.

93. Mcnamee, D. & Wolpert, D. M. 2019. Internal models in biological control. Annu rev control robot auton syst, 2, 339-364.

94. Miall, R. C., Christensen, L. O., Cain, O. & Stanley, J. 2007. Disruption of state estimation in the human lateral cerebellum. Plos biol, 5, e316.

95. Miall, R. C. & King, D. 2008. State estimation in the cerebellum. Cerebellum, 7, 572-6.

96. Mitzdorf, U. 1985. Current source-density method and application in cat cerebral cortex: investigation of evoked potentials and eeg phenomena. Physiol rev, 65, 37-100.

97. Morone, K. A., Neimat, J. S., Roe, A. W. & Friedman, R. M. 2017. Review of functional and clinical relevance of intrinsic signal optical imaging in human brain mapping. Neurophotonics, 4, 031220.

98. Nakamura, K. C., Sharott, A. & Magill, P. J. 2014. Temporal coupling with cortex distinguishes spontaneous neuronal activities in identified basal ganglia-recipient and cerebellar-recipient zones of the motor thalamus. Cereb cortex, 24, 81-97.

99. Nicholson, C. & Freeman, J. A. 1975. Theory of current source-density analysis and determination of conductivity tensor for anuran cerebellum. J neurophysiol, 38, 356-68.

100. Nowak, D. A., Topka, H., Timmann, D., Boecker, H. & Hermsdorfer, J. 2007. The role of the cerebellum for predictive control of grasping. Cerebellum, 6, 7-17.

101. Papakostopoulos, D., Cooper, R. & Crow, H. J. 1975. Inhibition of cortical evoked potentials and sensation by self-initiated movement in man. Nature, 258, 321-4.

102. Petersen, C. C. 2014. Cortical control of whisker movement. Annu rev neurosci, 37, 183-203.

103. Potworowski, J., Jakuczun, W., Leski, S. & Wojcik, D. 2012. Kernel current source density method. Neural comput, 24, 541-75.

104. Powers, W. T. 2022. The reafference principle and control theory.

105. Raymond, J. L., Lisberger, S. G. & Mauk, M. D. 1996. The cerebellum: a neuronal learning machine? Science, 272, 1126-31.

106. Requarth, T. & Sawtell, N. B. 2011. Neural mechanisms for filtering self-generated sensory signals in cerebellum-like circuits. Curr opin neurobiol, 21, 602-8.

107. Roy, J. E. & Cullen, K. E. 2004. Dissociating self-generated from passively applied head motion: neural mechanisms in the vestibular nuclei. J neurosci, 24, 2102-11.

108. Rushton, D. N., Rothwell, J. C. & Craggs, M. D. 1981. Gating of somatosensory evoked potentials during different kinds of movement in man. Brain, 104, 465-91.

109. Sawtell, N. B. 2017. Neural mechanisms for predicting the sensory consequences of behavior: insights from electrosensory systems. Annu rev physiol, 79, 381-399.

110. Schneider, D. M., Sundararajan, J. & Mooney, R. 2018. A cortical filter that learns to suppress the acoustic consequences of movement. Nature, 561, 391-395.

111. Schneider, K. 1959. Clinical psychopathology, grune & stratton.

112. Schwarz, C. & Chakrabarti, S. 2015. Whisking control by motor cortex. Scholarpedia, 10(3): 7466.

113. Schwarz, C., Hentschke, H., Butovas, S., Haiss, F., Stuttgen, M. C., Gerdjikov, T. V., Bergner, C. G. & Waiblinger, C. 2010. The head-fixed behaving rat--procedures and pitfalls. Somatosens mot res, 27, 131-48.

114. Seki, K. & Fetz, E. E. 2012. Gating of sensory input at spinal and cortical levels during preparation and execution of voluntary movement. J neurosci, 32, 890-902.

115. Seki, K., Perlmutter, S. I. & Fetz, E. E. 2003. Sensory input to primate spinal cord is presynaptically inhibited during voluntary movement. Nat neurosci, 6, 1309-16.

116. Shadmehr & Mussa-Ivaldi 2012. Biological learning and control.

117. Shadmehr, R. & Krakauer, J. W. 2008. A computational neuroanatomy for motor control. Exp brain res, 185, 359-81.

118. Shadmehr, R., Smith, M. A. & Krakauer, J. W. 2010. Error correction, sensory prediction, and adaptation in motor control. Annu rev neurosci, 33, 89-108.

119. Shan, K. Q., Lubenov, E. V. & Siapas, A. G. 2017. Model-based spike sorting with a mixture of drifting t-distributions. J neurosci methods, 288, 82-98.

120. Shergill, S. S., Bays, P. M., Frith, C. D. & Wolpert, D. M. 2003. Two eyes for an eye: the neuroscience of force escalation. Science, 301, 187.

121. Shergill, S. S., White, T. P., Joyce, D. W., Bays, P. M., Wolpert, D. M. & Frith, C. D. 2013. Modulation of somatosensory processing by action. Neuroimage, 70, 356-62.

122. Singla, S., Dempsey, C., Warren, R., Enikolopov, A. G. & Sawtell, N. B. 2017. A cerebellum-like circuit in the auditory system cancels responses to self-generated sounds. Nat neurosci, 20, 943-950.

123. Sperry, R. W. 1950. Neural basis of the spontaneous optokinetic response produced by visual inversion.

124. Sreenivasan, V., Karmakar, K., Rijli, F. M. & Petersen, C. C. 2015. Parallel pathways from motor and somatosensory cortex for controlling whisker movements in mice. Eur j neurosci, 41, 354-67.

125. Streng, M. L., Popa, L. S. & Ebner, T. J. 2022. Cerebellar representations of errors and internal models. Cerebellum, 21, 814-820.

126. Suresh, A. K., Greenspon, C. M., He, Q., Rosenow, J. M., Miller, L. E. & Bensmaia, S. J. 2021. Sensory computations in the cuneate nucleus of macaques. Proceedings of the national academy of sciences, 118, e2115772118.

127. Szwed, M., Bagdasarian, K. & Ahissar, E. 2003. Encoding of vibrissal active touch. Neuron, 40, 621-630.

128. Takatoh, J., Nelson, A., Zhou, X., Bolton, M. M., Ehlers, M. D., Arenkiel, B. R., Mooney, R. & Wang, F. 2013. New modules are added to vibrissal premotor circuitry with the emergence of exploratory whisking. Neuron, 77, 346-60.

129. Teune, T. M., Van Der Burg, J., Van Der Moer, J., Voogd, J. & Ruigrok, T. J. 2000. Topography of cerebellar nuclear projections to the brain stem in the rat. Prog brain res, 124, 141-72.

130. Therrien, A. S. & Bastian, A. J. 2019. The cerebellum as a movement sensor. Neurosci lett, 688, 37-40.

131. Todorov, E. 2004. Optimality principles in sensorimotor control. Nat neurosci, 7, 907-15.

132. Von Holst, E. & Mittelstaedt, H. 1950. The principle of reafference: interactions between the central nervous system and the peripheral organs.

133. Voudouris, D., Broda, M. D. & Fiehler, K. 2019. Anticipatory grasping control modulates somatosensory perception. J vis, 19, 4.

134. Weiskrantz, L., Elliott, J. & Darlington, C. 1971. Preliminary observations on tickling oneself. Nature, 230, 598-599.

135. Welsh, J. P. 1998. Systemic harmaline blocks associative and motor learning by the actions of the inferior olive. Eur j neurosci, 10, 3307-20.

136. Wiersma, C. A. 1947. Giant nerve fiber system of the crayfish; a contribution to comparative physiology of synapse. J neurophysiol, 10, 23-38.

137. Williams, M. V., Baker, D. W., Parker, R. M. & Nurss, J. R. 1998. Relationship of functional health literacy to patients' knowledge of their chronic disease. A study of patients with hypertension and diabetes. Arch intern med, 158, 166-72.

138. Williams, S. R. & Chapman, C. E. 2000. Time course and magnitude of movement-related gating of tactile detection in humans. Ii. Effects of stimulus intensity. Journal of neurophysiology, 84, 863-875.

139. Williams, S. R. & Chapman, C. E. 2002. Time course and magnitude of movement-related gating of tactile detection in humans. Iii. Effect of motor tasks. Journal of neurophysiology, 88, 1968-1979.

140. Wolpert, D. M. & Flanagan, J. R. 2001. Motor prediction. Curr biol, 11, r729-32.

141. Wolpert, R. C. M. A. D. M. 1996. Forward models for physiological motor control.

142. Yavari, F., Mahdavi, S., Towhidkhah, F., Ahmadi-Pajouh, M. A., Ekhtiari, H. & Darainy, M. 2016. Cerebellum as a forward but not inverse model in visuomotor adaptation task: a tdcs-based and modeling study. Exp brain res, 234, 997-1012.

8. Statement of Contributions

The open loop experiments, the main part of the study conducted in 12 mice, were done exclusively by me. I designed, established, and optimized major methodological requirements for these experiments. I performed all experiments, along with the required data analysis. For the control experiment employing closed-loop control, conducted in 3 mice, I implanted all 3 animals with electrodes and head screws, trained Ms. Ritu Roy Chowdhury on all experimental procedures, and prepared figures related to the closed-loop approach presented in the thesis. Ms. Roy Chowdhury was responsible for data acquisition in these 3 mice, performed the data analysis, and provided the histology image illustrating the lesion in the trigeminal brainstem area.

9. Acknowledgements

I wish to express my heartfelt gratitude to all those who contributed their knowledge, effort, and time to the completion of my PhD thesis. Prof. Dr. Cornelius Schwarz, I am incredibly thankful to you for granting me the opportunity to work on this exciting project by welcoming me into your group and for consistently providing the guidance, support, valuable suggestions, and constructive feedback. Your encouragement to explore new avenues of learning and pursue excellence, have been invaluable.

I extend my sincere appreciation to Dr. Shubhodeep Chakrabarti for providing co-guidance and support during my initial days of PhD. Your contribution to my project also extends to providing invaluable support in designing the tasks and MATLAB scripts for data analysis. Your expertise and support in this aspect have been greatly appreciated.

Prof. Dr. Jan Benda and Prof. Dr. Ziad Hafed, I am grateful for your contributions as part of my advisory board committee and for providing constructive feedback time to time that strengthened my research.

Ritu Roy Chowdhury, thank you for your contributions to the control experiment in the study. I highly appreciated working with you while exchanging the knowledge and skills. I have always enjoyed our valuable discussions in your cabin and kitchen.

Ursula Pascht, I extend my gratitude for your technical assistance. I am very much thankful to you for providing electrodes for many of my experiments and helping me with histology. You were always my go-to person in the need. From the very first day and throughout these years, your help and support have been indispensable in my smooth settling down in Tübingen.

To all the members of the Schwarz lab, thank you for warmly welcoming me and creating a positive atmosphere in the lab. Your helpful discussions, feedback, and technical

assistance have been invaluable. May-Li Silva-Prieto, special thanks to you for teaching and guiding me on mice surgical and head fixation procedures. You were the person who always motivated me during my failures. I will always cherish our discussions inside and outside science. I would like to extend my thanks to Dr. Alia Benali, for providing refined suggestions and guidance during my PhD journey. Dr. Arindam Bhattacharjee, I am thankful to you for our enjoyable talks, I have always admired your ideas and friendly suggestions.

Lastly, I would like to extend my thanks to my parents, family and husband for their unwavering love, support, and encouragement. Abhishek Kumar Verma, your inspiration and guidance have been instrumental in my journey. I thank you for sharing all the emotions during my achievements and failures and for standing by my side during the best and toughest times. Prerna Srivastava, I am grateful for your guidance and support when I arrived here in Tübingen and after. Your company made my stay and my PhD journey more enjoyable and enriching. Meera Srikrishna, thank you so much for making timely visits that provided me much needed break from work that helped me to further focus on my research and keep things going.